Neutrino-nucleon DIS from holographic QCD: PDFs of sea and valence quarks, form factors, and structure functions of the proton

Kiminad A. Mamo[*]

Physics Division, Argonne National Laboratory, Argonne, Illinois 60439, USA

Ismail Zahed[†]

Center for Nuclear Theory, Department of Physics and Astronomy, Stony Brook University, Stony Brook, New York 11794-3800, USA

(Received 16 March 2021; accepted 24 June 2021; published 8 September 2021)

We discuss unpolarized neutrino- and anti-neutrino-nucleon deep inelastic scattering using a chiral doublet of baryonic sources with explicit symmetry breaking, in a slice of AdS_5 with both a hard and soft wall. We explicitly derive the direct and transition form factors for the vector and axial-vector currents for the holographic dual of a proton and neutron. We use them to derive the s-channel structure functions for neutrino and antineutrino scattering on a proton and neutron in bulk. The t-channel contributions stemming from the Pomeron and Reggeon exchanges are also evaluated explicitly. The pertinent even and odd structure functions in the limit of large and small parton momentum fraction x are given. The results allow for the extraction of the nonperturbative parton distribution functions carried by the sea and valence quarks both at large-x and small-x regimes. Our holographic parton distribution function (PDF) sets compare well with the Les Houches accord PDF (LHAPDF) and the coordinated theoretical-experiment project on QCD (CTEQ) PDF sets in the large-x and small-x regimes in the intermediate range of $Q^2 < 10$ GeV^2.

DOI: 10.1103/PhysRevD.104.066010

I. INTRODUCTION

At extremely low x, the measured nucleon structure functions on unpolarized nucleon targets, show a rapid growth of sea quarks and gluons at low x [1,2]. Phenomenological arguments suggest that the growth saturates [3], a point supported by perturbative QCD arguments [4]. A central question is then this: what is the primary mechanism for the growth of the sea quarks at low x?

Deep inelastic scattering (DIS) in holography at moderate x is different from weak coupling as it involves hadronic and not partonic constituents [5]. The large gauge coupling at the low renormalization point, causes the color charges to rapidly deplete their energy and momentum, making them visible to hard probes only through double trace operators. However, because the holographic limit enjoys approximate conformal symmetry, the structure functions and form factors exhibit various scaling laws including the parton-counting rules [6]. DIS scattering at low x is partonic and fully saturated [7]. Recently, we have extended the notion of DIS scattering to nuclei as extremal Reisner-Nordstrom (RN)-AdS (anti–de Sitter) black holes with an emerging Fermi surface [8].

In this paper we consider neutrino and antineutrino DIS scattering on an unpolarized nucleon described by a Dirac chiral doublet using holographic QCD. The scattering is chiefly due to neutral and charge exchanges. In QCD the charge exchange currents discriminate between partons and antipartons. When combined with antineutrino DIS scattering, it allows for the separation between sea and valence partons. In holography, the partonic description holds only for very large x and very small x in the Regge limit. The purpose of the present study is to construct the even and odd parity leptonic structure functions for neutrino and antineutrino scattering, and use them to extract the sea parton distribution of the nucleon as a Dirac fermion in bulk.

The organization of the paper is as follows: in Sec. II we briefly review the setting for the model with bulk chiral gauge fields and a doublet of Dirac fermions in a slice of AdS_5, for both the soft and hard wall. The explicit breaking of chiral symmetry is enforced by the boundary value of a scalar bulk field in the bifundamental representation. In Sec. III we derive the direct and transition form factors for the vector and axial-vector form factors for both the proton and neutron. In Sec. IV, we briefly review the essentials of neutrino and antineutrino DIS scattering on unpolarized

[*]kmamo@anl.gov
[†]ismail.zahed@stonybrook.edu

nucleon targets, and show how the valence and sea up and down parton distribution functions are related to the structure functions of $W^{\pm}$ exchanges. The s-channel contributions to these structure functions are derived using the direct and transition form factors in holographic QCD. The t-channel contributions are also derived using the Pomeron and Reggeon exchanges in bulk. In Sec. V, all the results are combined to extract the valence and sea partonic distributions at large and small x, with a detailed comparison to the LHAPDF and CTEQ PDFs. Our conclusions are in Sec. V. A number of Appendixes are added to support some of the derivations.

II. HOLOGRAPHIC MODEL

AdS/CFT duality maps a conformal and strongly coupled gauge theory in $1+3$ dimensions at the boundary to a weakly coupled type-II supergravity in $1+9$ dimensions in bulk, with a dilaton, an antisymmetric tensor field, and additional odd (IIA) or even (IIB) forms. $AdS_5 \times S^5$ geometry emerges from solitonic and Bogomolnyi-Prasad-Sommerfield (BPS) charged D-brane supergravity solutions in bulk with the graviton and dilaton excitations dual to glueballs. The dual of the flavor excitations at the boundary, are obtained through probe Dp-branes and described by DBI and Chern-Simons effective actions.

A simple way to capture AdS/CFT duality in the non-conformal limit is to model it using a slice of AdS_5 with various bulk fields with assigned anomalous dimensions and pertinent boundary values, in the so-called bottom-up approach which we will follow here. We consider AdS_5 both with a soft and hard wall, with a background metric $g_{MN} = (\eta_{\mu\nu}, -1)R^2/z^2$ with the flat metric $\eta_{\mu\nu} = (1,-1,-1,-1)$ at the boundary. Confinement will be described by a background dilaton $\phi = \kappa^2 z^2$ for mesons and $\phi = \tilde{\kappa}^2 z^2$ for nucleons in the soft wall model. In the hard wall model, $\phi = 0$ and confinement is enforced at $z = z_0$.

A. Bulk vector mesons

The vector mesons fields in bulk are denoted by L_μ, R_μ. They are U(2) valued and described by the effective action [9,10]

$$S_M = -\frac{1}{4g_5^2}\int d^5x e^{-\phi(z)}\sqrt{g}g^{MP}g^{NQ}\mathrm{Tr}(\mathcal{F}^L_{MN}\mathcal{F}^L_{PQ} + \mathcal{F}^R_{MN}\mathcal{F}^R_{PQ}) + \int d^5x(\omega_5^L(\mathcal{A}) - \omega_5^R(\mathcal{A})), \tag{2.1}$$

with $\mathcal{F} = d\mathcal{A} - i\mathcal{A}^2$ in form notations and $\mathcal{A} = \mathcal{A}^a T^a$ with $T^0 = \frac{3}{2}\mathbf{1_2}$ and $T^i = \frac{1}{2}\tau^i$. Note that the generators T^a are fixed in such a way that the electromagnetic charge of the proton is 1, while that of the neutron is 0. The bulk U(2) vector field $V = (R+L)/2$ and axial-vector field $A = (R-L)/2$ reduce to the QCD flavor source fields at the boundary. The Chern-Simons contributions in (2.1) are

$$\omega_5(\mathcal{A}) = \frac{N_c}{24\pi^2}\int d^5x \mathrm{Tr}\left(\mathcal{A}F^2 + \frac{1}{2}\mathcal{A}^3\mathcal{F} - \frac{1}{10}\mathcal{A}^5\right) = \frac{N_c}{24\pi^2}\int d^5x \mathrm{Tr}\left(\mathcal{A}(d\mathcal{A})^2 - \frac{3i}{2}\mathcal{A}^3 d\mathcal{A} - \frac{3}{5}\mathcal{A}^5\right). \tag{2.2}$$

The equation of motions for the bulk gauge fields follow by variation ($\mathcal{D} = d - i\mathcal{A}$)

$$\frac{1}{\sqrt{g}}[\mathcal{D}_M, (\sqrt{g}e^{-\phi}\mathcal{A}^{MN})] = 0. \tag{2.3}$$

The coupling g_5 in (2.1) is fixed by the brane embeddings in bulk, with $1/g_5^2 \equiv 3N_c/(12\pi^2)$ (D7-branes), and $1/g_5^2 \equiv (3\sqrt{\lambda}/2^{5/2}\pi)N_c/(12\pi^2)$ (D9-branes). When ignoring these embedding, the standard assignment is $1/g_5^2 \equiv N_c/(12\pi^2)$ to match the vector 2-point correlation functions of QCD in the UV [11].

B. Bulk fermionic doublet

The bulk Dirac fermion action in curved AdS_5 with minimal coupling to the left U(2) gauge fields is

$$S_F = \frac{1}{2g_5^2}\int d^5x e^{-\phi(z)}\sqrt{g}(\mathcal{L}_{F1} + \mathcal{L}_{F2}) + \frac{1}{2g_5^2}\int d^4x\sqrt{-g^{(4)}}(\mathcal{L}_{UV1} + \mathcal{L}_{UV2}), \tag{2.4}$$

with $\mathcal{L}_{UV1,2} = (\bar{\Psi}_{1,2}\Psi_{1,2})_{z=\varepsilon}$. This extra UV contribution is needed to maintain the bulk to boundary correspondence. The Dirac and Pauli fermionic contributions $\mathcal{L}_{F1,2} = \mathcal{L}_{\mathrm{Dirac}1,2} + \mathcal{L}_{\mathrm{Pauli}1,2}$ are explicitly

$$\begin{aligned}\mathcal{L}_{\mathrm{Dirac}1,2} &= \left(\frac{i}{2}\bar{\Psi}_{1,2}e_A^N\Gamma^A(\vec{D}_N^{L,R} - \overleftarrow{D}_N^{L,R})\Psi_{1,2} - (\pm M + V(z))\bar{\Psi}_{1,2}\Psi_{1,2}\right),\\ \mathcal{L}_{\mathrm{Pauli}1,2} &= \pm 2g_5^2 \times \eta\bar{\Psi}_{1,2}e_A^M e_B^N\sigma^{AB}\mathcal{F}^{L,R}_{MN}\Psi_{1,2},\end{aligned} \tag{2.5}$$

with $\sigma^{AB}=\frac{i}{2}[\Gamma^A,\Gamma^B]$, and the left and right covariant derivatives

$$\begin{aligned}\vec{D}^L_N&=\vec{\partial}_N+\frac{1}{8}\omega_{NAB}[\Gamma^A,\Gamma^B]-iL^a_N T^a\equiv\vec{\mathcal{D}}_N-iL^a_N T^a,\\ \overleftarrow{D}^L_N&=\overleftarrow{\partial}_N+\frac{1}{8}\omega_{NAB}[\Gamma^A,\Gamma^B]+iL^a_N T^a\equiv\overleftarrow{\mathcal{D}}_N+iL^a_N T^a,\\ \vec{D}^R_N&=\vec{\partial}_N+\frac{1}{8}\omega_{NAB}[\Gamma^A,\Gamma^B]-iR^a_N T^a\equiv\vec{\mathcal{D}}_N-iR^a_N T^a,\\ \overleftarrow{D}^R_N&=\overleftarrow{\partial}_N+\frac{1}{8}\omega_{NAB}[\Gamma^A,\Gamma^B]+iR^a_N T^a\equiv\overleftarrow{\mathcal{D}}_N+iR^a_N T^a.\end{aligned}\tag{2.6}$$

The left and right flavor field strengths are set to $\mathcal{A}^L_{MN}=L_{MN}$, $\mathcal{A}^R_{MN}=R_{MN}$. The Dirac or minimal fermionic coupling is standard, but the Pauli coupling is not. It can be shown to follow from the Supergravity (SUGRA) action by reduction from the top-down approach. Without it, the neutron form factor vanishes. The nucleon doublet refers to

$$\Psi_{1,2}\equiv\begin{pmatrix}\Psi_{p1,2}\\ \Psi_{n1,2}\end{pmatrix}.\tag{2.7}$$

The nucleon fields in bulk form an isodoublet p, n with 1,2 referring to their $\pm=R$, L chirality at the *boundary* [12]. They are dual to a boundary chiral doublet of baryonic sources with $\Psi_{p1,2}\leftrightarrow\mathcal{O}_{p,\pm}$ and $\Psi_{n1,2}\leftrightarrow\mathcal{O}_{n,\pm}$ with anomalous dimensions $\pm M=\pm(\Delta-2)=\pm(\tau-3/2)$. They map onto a non-normalizable solution or source, plus a normalizable or expectation value of the corresponding source at the boundary. This doubling is best seen in the top-down approach using a left and a right bulk filling brane.

The fermionic potential $V(z)=\tilde{\kappa}^2z^2$ will be used for both the soft and hard wall. Here $e^N_A=z\delta^N_A$ is the inverse vielbein. The components of the spin connection are $\omega_{\mu z\nu}=-\omega_{\mu\nu z}=\frac{1}{z}\eta_{\mu\nu}$, the Dirac gamma matrices $\Gamma^A=(\gamma^\mu,-i\gamma^5)$ are chosen in the chiral representation, and satisfy the flat anticommutation relation $\{\Gamma^A,\Gamma^B\}=2\eta^{AB}$. The equation of motions for the bulk Dirac chiral doublet follows by variation

$$\left(ie^N_A\Gamma^A D^{L,R}_N-\frac{i}{2}(\partial_N\phi)e^N_A\Gamma^A-(\pm M+V(z))\right)\Psi_{1,2}=0,\tag{2.8}$$

with $1,2=R,L=\pm$. The inclusion of a fermionic potential which is set to the dilaton profile for simplicity, breaks conformal symmetry and guarantees the Reggeization of the nucleon spectrum in bulk. Equation (2.8) is supplemented with confining boundary conditions for the hard wall, and vanishing fields asymptotically for the soft wall. The solutions to (2.8) are briefly discussed in Appendix B. In short, for the soft wall and in the absence of a tachyon coupling in bulk, the spectrum Reggeizes with $M_n^2=4\tilde{\kappa}^2(n+\tau-1)$ and the ground state proton, neutron states with $n=0$ are degenerate. They follow from the mixed representation

$$\Psi_1(p,z)=\psi_R(z)\Psi^0_R(p)+\psi_L(z)\Psi^0_L(p)\tag{2.9}$$

for $n=0$, with $\psi_R(z\approx0)\approx z^{\tau+1/2}$ and $\psi_L(z\approx0)\approx z^{\tau+3/2}$ for the positive parity states $1\equiv+$ at the boundary. Similar relations follow for the negative parity states $2\equiv-$ at the boundary through the substitution $\psi_{R,L}\leftrightarrow\mp\psi_{L,R}$ by parity.

Note that the canonical dimension for the QCD baryonic sources is $\Delta=9/2$ which would suggest a twist $\tau=4$. However, we expect nonvanishing anomalous dimensions to develop at strong coupling. We do not know of any reliable calculational scheme to assess them. We will assume Δ and thus τ as a parameter with a twist $\tau=3$ to recover the hard scattering rules. The inclusion of additional twist contributions is discussed in [13].

C. Fermionic currents

For later use, it will be useful to define the bulk U(2) Dirac 1-form currents

$$\begin{aligned}J^{aN}_L&=\frac{\partial\mathcal{L}_{\text{Dirac1}}}{\partial L^a_N}=\bar{\Psi}_1e^N_A\Gamma^AT^a\Psi_1,\\ J^{aN}_R&=\frac{\partial\mathcal{L}_{\text{Dirac2}}}{\partial R^a_N}=\bar{\Psi}_2e^N_A\Gamma^AT^a\Psi_2,\end{aligned}\tag{2.10}$$

and the bulk U(2) Pauli 2-form currents

$$\begin{aligned}J^{aMN}_L&=\frac{\partial\mathcal{L}_{\text{Pauli1}}}{\partial L^a_{MN}}=+2g_5^2\times\eta\bar{\Psi}_1e^M_Ae^N_B\sigma^{AB}T^a\Psi_1,\\ J^{aMN}_R&=\frac{\partial\mathcal{L}_{\text{Pauli2}}}{\partial R^a_{MN}}=-2g_5^2\times\eta\bar{\Psi}_2e^M_Ae^N_B\sigma^{AB}T^a\Psi_2,\end{aligned}\tag{2.11}$$

in terms of which the pertinent 1- and 2-form charged currents read, respectively,

$$\begin{aligned}J^{+N}_{L,R}&=J^{1N}_{L,R}-iJ^{2N}_{L,R}=\bar{\Psi}_{n1,2}e^N_A\Gamma^A\Psi_{p1,2},\\ J^{-N}_{L,R}&=J^{1N}_{L,R}+iJ^{2N}_{L,R}=\bar{\Psi}_{p1,2}e^N_A\Gamma^A\Psi_{n1,2},\end{aligned}\tag{2.12}$$

and

$$
\begin{aligned}
J_L^{+MN} &= J_L^{1MN} - iJ_L^{2MN} = +2g_5^2 \times \eta\bar{\Psi}_{n1} e_A^M e_B^N \sigma^{AB} \Psi_{p1}, \\
J_L^{-MN} &= J_L^{1MN} + iJ_L^{2MN} = +2g_5^2 \times \eta\bar{\Psi}_{p1} e_A^M e_B^N \sigma^{AB} \Psi_{n1}, \\
J_R^{+MN} &= J_R^{1MN} - iJ_R^{2MN} = -2g_5^2 \times \eta\bar{\Psi}_{n2} e_A^M e_B^N \sigma^{AB} \Psi_{p2}, \\
J_R^{-MN} &= J_R^{1MN} + iJ_R^{2MN} = -2g_5^2 \times \eta\bar{\Psi}_{p2} e_A^M e_B^N \sigma^{AB} \Psi_{n2}.
\end{aligned} \tag{2.13}
$$

D. Bulk effective action

In terms of the charged and left 1-form gauge fields $L_N^{\pm} \equiv \frac{1}{\sqrt{2}}(L_N^1 \mp iL_N^2)$, the bulk meson effective action (2.1) can be recast in the following form

$$
\begin{aligned}
S_M \supset \frac{1}{g_5^2} \int d^5x e^{-\phi(z)} \sqrt{g} \Big(& -\partial^M L^{-N} \partial_M L_N^+ + \partial^M L^{-N} \partial_N L_M^+ - \frac{1}{4} L^{0MN} L_{MN}^0 - \frac{1}{4} L^{3MN} L_{MN}^3 + L \to R \Big) \\
& + \frac{N_c}{48\pi^2} \int d^5x \epsilon^{\mu\nu\rho\sigma} (\mathcal{L}_{\mu\nu\rho\sigma}^{CS}(L) - \mathcal{L}_{\mu\nu\rho\sigma}^{CS}(R)),
\end{aligned} \tag{2.14}
$$

with the Chern-Simons contribution restricted to the charged left currents through a neutral

$$
\mathcal{L}_{\mu\nu\rho\sigma}^{CS}(L) = \partial_z L_\mu^+ \partial_\nu L_\rho^0 L_\sigma^- + \partial_z L_\mu^- \partial_\nu L_\rho^0 L_\sigma^+ - \partial_z L_\mu^+ L_\rho^0 \partial_\nu L_\sigma^- - \partial_z L_\mu^- L_\rho^0 \partial_\nu L_\sigma^+ + \partial_z L_\mu^0 \partial_\nu L_\rho^- L_\sigma^+ + \partial_z L_\mu^0 \partial_\nu L_\rho^+ L_\sigma^-, \tag{2.15}
$$

where we made use of the Abelian field strengths

$$
\begin{aligned}
L_{MN}^{\pm} &= \partial_M L_N^{\pm} - \partial_N L_M^{\pm}, \\
L_{MN}^{0,3} &= \partial_M L_N^{0,3} - \partial_N L_M^{0,3}.
\end{aligned} \tag{2.16}
$$

In terms of the 1- and 2-form currents, the bulk fermion effective action (2.5) now reads

$$
\begin{aligned}
\mathcal{L}_{F1} + \mathcal{L}_{F2} \supset & \frac{i}{2} \bar{\Psi}_1 e_A^N \Gamma^A (\vec{\mathcal{D}}_N - \overleftarrow{\mathcal{D}}_N) \Psi_1 - (M + V(z)) \bar{\Psi}_1 \Psi_1 + \frac{1}{\sqrt{2}} L_N^+ J_L^{-N} + \frac{1}{\sqrt{2}} L_N^- J_L^{+N} + L_N^0 J_L^{0N} + L_N^3 J_L^{3N} \\
& + L_{MN}^+ J_L^{-MN} + L_{MN}^- J_L^{+MN} + L_{MN}^0 J_L^{0MN} + L_{MN}^3 J_L^{3MN} + (1 \leftrightarrow 2, L \leftrightarrow R, M \leftrightarrow -M) \\
= & \frac{i}{2} \bar{\Psi}_1 e_A^N \Gamma^A (\vec{\mathcal{D}}_N - \overleftarrow{\mathcal{D}}_N) \Psi_1 - (M + V(z)) \bar{\Psi}_1 \Psi_1 + \frac{i}{2} \bar{\Psi}_2 e_A^N \Gamma^A (\vec{\mathcal{D}}_N - \overleftarrow{\mathcal{D}}_N) \Psi_2 - (-M + V(z)) \bar{\Psi}_2 \Psi_2 \\
& + \frac{1}{\sqrt{2}} V_N^+ J_V^{-N} + \frac{1}{\sqrt{2}} A_N^+ J_A^{-N} + \frac{1}{\sqrt{2}} V_N^- J_V^{+N} + \frac{1}{\sqrt{2}} A_N^- J_A^{+N} + V_N^0 J_V^{0N} + A_N^0 J_A^{0N} + V_N^3 J_V^{3N} + A_N^3 J_A^{3N} \\
& + \frac{1}{\sqrt{2}} V_{MN}^+ J_V^{-MN} + \frac{1}{\sqrt{2}} A_{MN}^+ J_A^{-MN} + \frac{1}{\sqrt{2}} V_{MN}^- J_V^{+MN} + \frac{1}{\sqrt{2}} A_{MN}^- J_A^{+MN} \\
& + V_{MN}^0 J_V^{0MN} + A_{MN}^0 J_A^{0MN} + V_{MN}^3 J_V^{3MN} + A_{MN}^3 J_A^{3MN},
\end{aligned} \tag{2.17}
$$

where we defined

$$
J_{V,A}^{\bar{\alpha}N} = J_L^{\bar{\alpha}N} \pm J_R^{\bar{\alpha}N}, \qquad J_{V,A}^{\bar{\alpha}MN} = J_L^{\bar{\alpha}MN} \mp J_R^{\bar{\alpha}MN}, \tag{2.18}
$$

with $\bar{\alpha} \equiv -, +, 0, 3$, and $V_N, A_N \equiv (L_N \pm R_N)/2$.

E. Hard and soft wall models

We now detail the specifics of the hard and soft wall model with chiral symmetry breaking through the use of a flavor scalar in the bifundamental representation in a slab of AdS spacetime. These well motivated bottom-up models capture the essentials of the top-down approaches and make more transparent the essential aspects of holography. Their parameters are fixed by the brane embeddings and reduction in higher dimensions.

1. Hard wall with bifundamentals

To distinguish vector and axial-vector spectra and introduce a scalar $\tilde{X}$ in the bifundamental representation of $U(N_f)_L \times U(N_f)_R$ with a scaling dimension $\Delta = 3$ and bulk action

$$\mathcal{S}[\tilde{X}] = \frac{1}{2g_5^2}\int d^5x\sqrt{g}\mathrm{Tr}(|D\tilde{X}|^2 + 3|\tilde{X}|^2) \tag{2.19}$$

using the 1-form $D\tilde{X} = d\tilde{X} - i\mathcal{A}^L\tilde{X} + i\tilde{X}\mathcal{A}^R$. Note by replacing $X \to \sqrt{2g_5^2}\times\tilde{X}$, we can rewrite (2.19), in a form similar to [14], as

$$\mathcal{S}[X] = \int d^5x\sqrt{g}\mathrm{Tr}(|DX|^2 + 3|X|^2). \tag{2.20}$$

The equation of motion derived from the above action (2.20), for $\mathcal{A} = 0$, has a background solution for the bifundamental scalar near the UV boundary ($z \to 0$) given by

$$X_0(x, z\to 0) \approx \frac{1}{\sqrt{2g_5^2}}\left(\frac{1}{2}M_q z + \frac{1}{2}\Sigma z^3\right) \equiv \frac{1}{\sqrt{2g_5^2}}v(z). \tag{2.21}$$

Both the current mass matrix and the quark bilinear are diagonal, $M_q = m_q\mathbf{1}$ and $\Sigma = \sigma\mathbf{1}$, with $\Sigma^{ij} = 2g_5^2\langle\bar{q}_R^i q_L^j\rangle$ where $i, j = 1, 2\ldots N_f$ are the flavor indices. For the hard wall, the boundary condition for the $U(N_f)$ gauge fields is $\mathcal{F}^{R,L}(x, z_0) = 0$.

Vectors.—The bulk vector field $V_M = (V_\mu, V_5)$ splits into a μ transverse, μ longitudinal, and 5-contribution. The 5-longitudinal components of the vector field mix through a Higgs-type effect. They can be decoupled by a pertinent choice of gauge. The transverse part of the vector field decouples, and its mode decomposition in terms of $\psi_n(z)$ yields the bulk equation

$$\partial_z\left(\frac{1}{z}\partial_z\psi_n(z)\right) + \frac{1}{z}m_n^2\psi_n(z) = 0 \tag{2.22}$$

subject to the confining conditions $\psi_n(0) = \psi_n'(z_0) = 0$. The solutions are readily found as $\psi_n(z) \sim zJ_1(m_n z)$ with the vector spectrum m_n fixed by the zeros $\gamma_{0,n}$ of the Bessel function $J_0(\gamma_{0,n}) = 0$, with normalization

$$\int_0^{z_0} dz\sqrt{g_{xx}}\psi_n(z)\psi_m(z) = \delta_{nm} \tag{2.23}$$

and the completeness relation

$$\sum_{n=1}^{\infty}\psi_n(z)\psi_n(z') = \sqrt{g^{xx}}\delta(z - z'). \tag{2.24}$$

The first zero of J_0 or $\gamma_{0,1} = 2.40483$, is identified with the rho meson state $m_{1=\rho} = \gamma_{0,1}/z_0 = 0.775$ GeV which fixes the IR scale $z_0 = 3.103/\mathrm{GeV}$. Note that asymptotically $\gamma_{0,n} \approx n\pi$ with $m_n \approx n\pi/z_0$.

The bulk-to-boundary vector propagator follows from (2.22) through the substitution $m_n^2 \to -Q^2$ with the boundary conditions $\mathcal{V}(Q, 0) = 1$ and $\partial_z\mathcal{V}(Q, z_0) = 0$ (confining). The solution can be obtained in closed form

$$\begin{aligned}\mathcal{V}(Q, z) &= \sum_n \frac{g_5F_n\psi_n(z)}{Q^2 + m_n^2},\\ &= Qz\left(K_1(Qz) + \frac{K_0(Qz_0)}{I_0(Qz_0)}I_1(Qz)\right),\end{aligned} \tag{2.25}$$

where we have also shown its mode decomposition with the decay constants $g_5F_n = (-\partial_z\psi_n(z)/z)_0$.

Axials.—Similarly the bulk axial-vector field $A_M = (A_\mu, A_5)$ splits into a μ transverse, μ longitudinal, and 5-contribution. The 5-longitudinal components of the axial-vector field, mix through a Higgs-type effect. They can be decoupled by a pertinent choice of gauge, at the expense of more coupling of the A_5 field with the tachyon field. For instance in the R gauge, the A_5 field is identified with the pion field. These contributions will not be followed except when discussing the pion contribution to the direct and transitional axial-vector form factors below.

The μ-transverse part of A_μ is always decoupled. Its mode decomposition in terms of $\tilde{\psi}_n(z)$ yields the bulk equation

$$\partial_z\left(\frac{1}{z}\partial_z\tilde{\psi}_n(z)\right) - \frac{1}{2}\frac{v^2(z)}{z^3}\tilde{\psi}_n(z) + \frac{1}{z}\tilde{m}_n^2\tilde{\psi}_n(z) = 0. \tag{2.26}$$

Upon taking the chiral limit before the near-boundary limit (i.e., $m_q \to 0$ before $z \to 0$), (2.26) reduces to

$$\partial_z\left(\frac{1}{z}\partial_z\tilde{\psi}_n(z)\right) - \frac{1}{2}\sigma^2z^3\tilde{\psi}_n(z) + \frac{1}{z}\tilde{m}_n^2\tilde{\psi}_n(z) = 0 \tag{2.27}$$

with the same confining boundary conditions $\tilde{\psi}_n(0) = \tilde{\psi}_n'(z_0) = 0$ and a similar normalization (2.23) and completeness relation (2.24). Note that (2.27) can only be solved numerically.

However, we can find an equation that can be solved analytically, if we take the near-boundary limit first without taking the chiral limit (i.e., $z \to 0$ with $m_q \neq 0$) of (2.26) which reduces to

$$\partial_z\left(\frac{1}{z}\partial_z\tilde{\psi}_n(z)\right) - \frac{1}{2z}m_q^2\tilde{\psi}_n(z) + \frac{1}{z}\tilde{m}_n^2\tilde{\psi}_n(z) = 0. \tag{2.28}$$

Defining $\tilde{m}_n^2 = m_n^2 + \frac{1}{2}m_q^2$, we can recast (2.28) in the form

$$\partial_z\left(\frac{1}{z}\partial_z\tilde{\psi}_n(z)\right)+\frac{1}{z}m_n^2\tilde{\psi}_n(z)=0, \tag{2.29}$$

which maps onto the vector equation (2.22) with the replacement of $\tilde{\psi}_n(z)\leftrightarrow\psi_n(z)$, and $\tilde{m}_n\leftrightarrow m_n$.

In the near boundary or UV limit, the differences between the axial-vector and vector masses are only due to the explicit symmetry breaking effect with $m_q\neq 0$, and vanishes in the chiral limit. In general however, the difference is largely due to the spontaneous breaking of chiral symmetry through $\Sigma=\sigma\mathbf{1}$, as a numerical solution to (2.27) shows. For $\sigma z_0^3\ll 1$, a simple parametric estimate can be obtained using first order perturbation theory in (2.27)

$$\tilde{m}_n^2\approx m_n^2+\frac{1}{2}\int_0^{z_0}dz\sqrt{g_{xx}}|\psi_n(z)|^2(\sigma z^2+m_q)^2, \tag{2.30}$$

which reduces to the near boundary or UV limit result for $\sigma z_0^3\to 0$. In the chiral limit (2.30) yields a chiral splitting between the axials and vectors

$$\tilde{m}_n^2\approx m_n^2+0.38\left(\frac{1}{2}\sigma^2 z_0^4\right) \tag{2.31}$$

solely due to the chiral condensate. Note that asymptotically, the *linear* mass splitting in the hard wall model vanishes, i.e., $\tilde{m}_n-m_n\approx\sigma^2 z_0^5/n\to 0$ for $n\gg 1$. Below and for simplicity, we will carry the analytical analysis using the near boundary limit, using the substitution

$$\frac{1}{2}m_q^2\to\tilde{m}_n^2-m_n^2. \tag{2.32}$$

The bulk-to-boundary axial-vector propagator follows from (2.29) through the substitution $m_n^2\to-\tilde{Q}^2=-(Q^2+\frac{1}{2}m_q^2)$ with the boundary conditions $\mathcal{A}(Q,0)=1$ and $\partial_z\mathcal{A}(Q,z_0)=0$ (confining). Note that $\mathcal{A}(Q,0)\neq\mathcal{A}(0,z)$ since $\mathcal{A}(0,z)\neq 1$. The solution can be obtained in closed form as

$$\begin{aligned}\tilde{\mathcal{V}}(Q,z)&\approx\sum_n\frac{g_5\tilde{F}_n\tilde{\psi}_n(z)}{\tilde{Q}^2+m_n^2}=\sum_n\frac{g_5\tilde{F}_n\tilde{\psi}_n(z)}{Q^2+\tilde{m}_n^2},\\&=\tilde{Q}z\left(K_1(\tilde{Q}z)+\frac{K_0(\tilde{Q}z_0)}{I_0(\tilde{Q}z_0)}I_1(\tilde{Q}z)\right),\end{aligned} \tag{2.33}$$

where we have also shown its mode decomposition with the decay constants $g_5\tilde{F}_n=(-\partial_z\tilde{\psi}_n(z)/z)_{z=0}$.

2. Hard wall without bifundamentals

Both the bulk-to-boundary vector and axial-vector propagators can be obtained in closed form in a variant of the Sakai-Sugimoto construction [15] using a hard wall model without the use of the bifundamental scalar field in bulk but with modified boundary conditions.

Vectors.—The vector fields are still given with the same hard wall boundary conditions $\psi_n(0)=\psi_n'(z_0)=0$, but the axial-vector fields satisfy $\tilde{\psi}_n(0)=\tilde{\psi}_n(z_0)=0$ and $\tilde{\psi}_n'(z_0)\neq 0$. The solutions are again readily found in the form $\psi_n(z)\sim zJ_1(m_n z)$ with $m_n=\gamma_{0,n}/z_0$.

Axials.—Similarly, the axial vector spectrum follows with $\tilde{\psi}_n(z)\sim zJ_1(\tilde{m}_n z)$ with $\tilde{m}_n=\gamma_{1,n}/z_0$. If z_0 is fixed by the rho mass then the ratio of the axial-to-rho meson mass is $\tilde{m}_1/M_1=\gamma_{1,1}/\gamma_{0,1}=1.593$, which is consistent with the empirical ratio $m_A/m_\rho=1.587$ as in the Sakai-Sugimoto construction. The higher excited modes fare less better empirically in both formulations.

The bulk-to-boundary axial-vector propagator follows a similar reasoning as the vector analog, through the substitution $\tilde{m}_n^2\to-Q^2$ with the boundary conditions $\tilde{\mathcal{V}}(Q,0)=\tilde{\mathcal{V}}(0,z)=1$ and $\tilde{\mathcal{V}}(Q,z_0)=0$ (confining). The solution follows as

$$\begin{aligned}\tilde{\mathcal{V}}(Q,z)&\approx\sum_n\frac{g_5\tilde{F}_n\tilde{\psi}_n(z)}{Q^2+\tilde{m}_n^2}\\&=\tilde{Q}z\left(K_1(\tilde{Q}z)-\frac{K_1(\tilde{Q}z_0)}{I_1(\tilde{Q}z_0)}I_1(\tilde{Q}z)\right).\end{aligned} \tag{2.34}$$

3. Soft wall with bifundamentals

In the soft wall model with scalar bifundamentals, we replace (2.20) by [14]

$$\mathcal{S}[X]=\int d^5x e^{-\phi(z)}\sqrt{g}\mathrm{Tr}(|DX|^2+3|X|^2) \tag{2.35}$$

with again the same background solution and boundary identification for the bifundamentals.

Vectors.—In this model, the bulk vector gauge field in terms of $\psi_n(z)$ yields the bulk equation

$$\partial_z\left(\frac{e^{-\phi(z)}}{z}\partial_z\psi_n(z)\right)+\frac{e^{-\phi(z)}}{z}m_n^2\psi_n(z)=0. \tag{2.36}$$

The solutions are readily found as $\psi_n(z)=c_n\tilde{\kappa}^2z^2L_n^1(\tilde{\kappa}^2z^2)$, and $m_n^2=4\tilde{\kappa}^2(n+1)$ for $n=0,1,\ldots$ with normalization coefficients $c_n=\sqrt{2/n+1}$ determined from the normalization condition (for the soft wall model with background dilaton $\phi=\tilde{\kappa}^2z^2$)

$$\int dz\sqrt{g}e^{-\phi}(g^{xx})^2\psi_n(z)\psi_m(z)=\delta_{nm}. \tag{2.37}$$

For the soft wall model, the bulk-to-boundary vector propagator follows from (2.36) through the substitution $m_n^2\to-Q^2$ with the boundary conditions $\mathcal{V}(Q,0)=1$. The solution can be obtained in closed form as

$$\mathcal{V}(Q,z) = \sum_n \frac{g_5 F_n \psi_n(z)}{Q^2+m_n^2}, \\ = \tilde{\kappa}^2 z^2 \Gamma\left(1+\frac{Q^2}{4\tilde{\kappa}^2}\right)\mathcal{U}\left(1+\frac{Q^2}{4\tilde{\kappa}^2};2;\tilde{\kappa}^2 z^2\right), \\ = \tilde{\kappa}^2 z^2 \int_0^1 \frac{dx}{(1-x)^2} x^a \exp\left[-\frac{x}{1-x}\tilde{\kappa}^2 z^2\right], \quad (2.38)$$

where we have also shown its mode decomposition with the decay constants $g_5 F_n = (-\partial_z \psi_n(z)/z)_0$, and defined $a \equiv Q^2/4\tilde{\kappa}^2$.

Axials.—For the soft wall model, the mode decomposition of the axial-vector gauge field in terms of $\tilde{\psi}_n(z)$ yields the bulk equation

$$\partial_z\left(\frac{e^{-\phi(z)}}{z}\partial_z\tilde{\psi}_n(z)\right) - \frac{e^{-\phi(z)}\frac{1}{2}v(z)^2}{z^3}\tilde{\psi}_n(z) \\ + \frac{e^{-\phi(z)}}{z}\tilde{m}_n^2\tilde{\psi}_n(z) = 0, \quad (2.39)$$

which, upon taking the chiral limit before the near-the-boundary one (i.e., taking $m_q \to 0$ before $z \to 0$), reduces to

$$\partial_z\left(\frac{e^{-\phi(z)}}{z}\partial_z\tilde{\psi}_n(z)\right) - e^{-\phi(z)}\frac{1}{2}\sigma^2 z^3\tilde{\psi}_n(z) \\ + \frac{e^{-\phi(z)}}{z}\tilde{m}_n^2\tilde{\psi}_n(z) = 0, \quad (2.40)$$

with a similar normalization (2.37). Again, note that (2.40) can only be solved numerically.

But, similar to the hard wall case, we can find an equation that can be solved analytically, for the soft wall model, if we take the near-boundary limit first without taking the chiral one (i.e., $z \to 0$ with $m_q \neq 0$) of (2.39) which reduces to

$$\partial_z\left(\frac{e^{-\phi(z)}}{z}\partial_z\tilde{\psi}_n(z)\right) - \frac{e^{-\phi(z)}}{z}\frac{1}{2}m_q^2\tilde{\psi}_n(z) \\ + \frac{e^{-\phi(z)}}{z}\tilde{m}_n^2\tilde{\psi}_n(z) = 0. \quad (2.41)$$

Defining $m_n^2 = \tilde{m}_n^2 - \frac{1}{2}m_q^2$, we can rewrite (2.41) as

$$\partial_z\left(\frac{e^{-\phi(z)}}{z}\partial_z\tilde{\psi}_n(z)\right) + \frac{e^{-\phi(z)}}{z}m_n^2\tilde{\psi}_n(z) = 0, \quad (2.42)$$

which is essentially the same equation as the vector one (2.36) with the replacement of $\tilde{\psi}_n(z) \leftrightarrow \psi_n(z)$, and $M_n \leftrightarrow m_n$.

For the soft wall model, the bulk-to-boundary axial-vector propagator follows from (2.42) through the substitution $m_n^2 \to -\tilde{Q}^2 = -(Q^2+\frac{1}{2}m_q^2)$ with the boundary conditions $\tilde{\mathcal{V}}(Q,0) = 1$. Note that $\tilde{\mathcal{V}}(Q,0) \neq \tilde{\mathcal{V}}(0,z)$ since $\tilde{\mathcal{V}}(0,z) \neq 1$. The approximate solution follows as

$$\tilde{\mathcal{V}}(Q,z) \approx \sum_n \frac{g_5\tilde{F}_n\tilde{\psi}_n(z)}{\tilde{Q}^2+m_n^2} = \sum_n \frac{g_5\tilde{F}_n\tilde{\psi}_n(z)}{Q^2+\tilde{m}_n^2} \\ = \tilde{\kappa}^2 z^2 \Gamma\left(1+\frac{\tilde{Q}^2}{4\tilde{\kappa}^2}\right)\mathcal{U}\left(1+\frac{\tilde{Q}^2}{4\tilde{\kappa}^2};2;\tilde{\kappa}^2 z^2\right) = \tilde{\kappa}^2 z^2 \int_0^1 \frac{dx}{(1-x)^2} x^{\tilde{a}} \exp\left[-\frac{x}{1-x}\tilde{\kappa}^2 z^2\right] \quad (2.43)$$

where we have also shown its mode decomposition with the decay constants $g_5\tilde{F}_n = (-\partial_z\tilde{\psi}_n(z)/z)_0$, and defined $\tilde{a} \equiv \tilde{Q}^2/4\tilde{\kappa}^2$.

We emphasize that the exact form of (2.43) requires solving numerically (2.39) for the normalizable modes and using the mode decomposition (first line). Alternatively, one can solve (2.39) also numerically for the non-normalizable modes, after the substitution $\tilde{m}_n^2 \to -Q^2$. However, for DIS scattering which is the main thrust of this paper, this is not needed. Indeed, in the DIS regime with $Qz_0 \gg 1$, the near-boundary approximation giving (2.43) (second line) is sufficient. This will be assumed throughout.

III. DIRECT AND TRANSITION FORM FACTORS

The vector and axial-vector couplings to the Dirac fermion in bulk follow from the Witten diagrams. They involve both the Dirac and Pauli form factors. We note that neutrino scattering through the charged currents involve solely the charged left currents. Here we construct both the direct and transition form factors needed for the vector and axial-vector currents and compare the direct ones to the most current data on the proton and neutron. We will use these form factors to construct the s-channel contributions for neutrino DIS scattering on nucleon targets.

A. Direct vector and axial form factors

The direct vector and axial form factors for the proton and neutron $V, A + N(p) \to N(p')$, can be extracted from the boundary to bulk three point functions with pertinent Lehmann-Symanzic-Zimmermann (LSZ) reduction using

$$C_{NN}^{(0,3)}(p,p',q) = \lim_{p'^2,p^2\to m_N^2}(p'^2-m_N^2)(p^2-m_N^2)\int d^4x d^4y e^{i(p'\cdot x - p\cdot y - q\cdot z)}\langle 0|T(\mathcal{O}_N(x)\tilde{J}_{V,A}^{(0,3)\mu}(z)\mathcal{O}_N(y))|0\rangle \tag{3.1}$$

through the ratio

$$W_{V,A}^{(0,3)\mu}(Q^2) = \langle N(p')|\tilde{J}_{V,A}^{(0,3)\mu}(0)|N(p)\rangle = \frac{C_{NN}^{(0,3)}(p,p',q)}{F_N(p')F_N(p)} \tag{3.2}$$

for the chargeless form factor, and similarly for the charged currents

$$W_{V,A}^{\pm\mu}(Q^2) = \langle N(p')|\frac{1}{\sqrt{2}}\tilde{J}_{V,A}^{\pm\mu}(0)|N(p)\rangle \tag{3.3}$$

and the electomagnetic currents

$$W_{\rm EM}^{\mu}(Q^2) = \langle N(p')|\tilde{J}_{\rm EM}^{\mu}(0)|N(p)\rangle = \langle N(p')|\frac{1}{3}\tilde{J}_V^{0\mu}(0) + \tilde{J}_V^{3\mu}(0)|N(p)\rangle, \tag{3.4}$$

with $q^2 = (p'-p)^2 = -Q^2$. Here $N(p)$ refers to the U(2) proton-neutron doublet

$$N(p) \equiv \begin{pmatrix} N_p(p) \\ N_n(p) \end{pmatrix}, \tag{3.5}$$

and the baryonic decay constant $F_N(p)$ is canonically defined as the

$$\langle 0|\mathcal{O}_N(x)|N(p)\rangle = F_N(p)e^{-ip\cdot x} \tag{3.6}$$

modulo the spin-flavor structure of the nucleon source $\mathcal{O}_N$. These definitions are commensurate with the lattice definitions for the three point functions and form factors [16], with the baryonic decay constants defined and evaluated in [17] (and references therein). In our case they are tied to the bulk wave functions and given in (B14)–(B15).

The chargeless currents $\tilde{J}_{V,A}^{(0,3)\mu}$ at the boundary are identified with the quark (partonic) currents, with the quarks in the fundamental representation of $\mathrm{U}(N_f = 2)$. They are sourced by the dual bulk vector fields $V_\mu^0(Q, z\to 0)$ and $V_\mu^3(Q, z\to 0)$ at the boundary, respectively. Similarly, the dual bulk axial vector fields $A_\mu^{(0,3)}(Q, z\to 0)$ and $\frac{1}{2}\times\frac{1}{\sqrt{2}}\times A_\mu^{\pm}(Q, z\to 0)$ at the boundary, are the dual of the quark currents $\tilde{J}_A^{(0,3)\mu}(0)$ and $2\tilde{J}_A^{\pm\mu}(0)$, respectively.

We now proceed to evaluate the Abelian part, $U(1)_{V,A}^{\tilde{\alpha}} \subset U(2)$ of the Dirac and Pauli contributions to the direct vector or axial form factors of the proton and neutron (3.2). We will give a detailed account of the Dirac contribution to the direct parts of the ectromagnetic and axial-vector currents, setting up this way the various definitions and normalizations. The Pauli contributions will follow a similar reasoning and will be only quoted.

1. Direct vector form factor: Dirac

The Dirac contribution to the direct part of the electromagnetic current can be extracted from the bulk Dirac part of the action in (2.17) in the soft wall model

$$S_{\rm Dirac}^{\rm EM}[i,X] = \frac{1}{2g_5^2}\int dz d^4y\sqrt{g}e^{-\tilde{\kappa}^2z^2}\left(\frac{1}{3}V_N^0 J_V^{0N} + V_N^3 J_V^{3N}\right) \tag{3.7}$$

or more explicitly

$$\begin{aligned} S_{\rm Dirac}^{\rm EM}[i,X] &= \frac{1}{2g_5^2}\int dz d^4y\sqrt{g}e^{-\tilde{\kappa}^2z^2}\frac{z}{R}\left(\bar{\Psi}_{1X}\gamma^N\left(\frac{1}{3}V_N^0T^0 + V_N^3T^3\right)\Psi_{1i} + \bar{\Psi}_{2X}\gamma^N\left(\frac{1}{3}V_N^0T^0 + V_N^3T^3\right)\Psi_{2i}\right), \\ &= (2\pi)^4\delta^4(P_X - p - q)\times F_X(P_X)\times F_N(p)\frac{1}{2g_5^2}\times 2g_5^2\times e_{\rm nucleon}\times\bar{u}_{s_X}(P_X)\not{\epsilon}(q)u_{s_i}(p) \\ &\quad\times\frac{1}{2}[\mathcal{I}_L(n_X,Q^2) + \mathcal{I}_R(n_X,Q^2)], \end{aligned} \tag{3.8}$$

following the conventions for the interaction action used in [18]. Here $\epsilon^\mu(q)$ is the polarization of the EM probe. In the last equality in (3.8) we substituted the bulk gauge fields by (A4), and the bulk fermionic currents in terms of the fermionic fields (B15). The charge assignments are $e_{\text{nucleon}} = 1$ for the proton, and $e_{\text{nucleon}} = 0$ for the neutron. We have also defined

$$\mathcal{I}_L(n_X, Q^2) \equiv \mathcal{I}(M + 5/2, n_X, Q^2), \qquad \mathcal{I}_R(n_x, Q^2) \equiv \mathcal{I}(M + 3/2, n_X, Q^2), \tag{3.9}$$

with ($w = \tilde{\kappa}^2 z^2$)

$$\begin{aligned}\mathcal{I}(\bar{m}, n_X, Q^2) &= C(\bar{m}, n_X)\Gamma\left(1 + \frac{Q^2}{4\tilde{\kappa}^2}\right)\int_0^\infty dw w^{\bar{m}-1} e^{-w}\mathcal{U}\left(1 + \frac{Q^2}{4\tilde{\kappa}^2}; 2; w\right)L_{n_X}^{\bar{m}-2}(w), \\ &= \frac{\Gamma(\bar{m})(\frac{\Gamma(\bar{m}-1)\Gamma(n_X+\bar{m}-1)}{\Gamma(n_X+1)})^{\frac{1}{2}}}{\Gamma(\bar{m}-1)}\frac{\frac{Q^2}{4\tilde{\kappa}^2}\Gamma(\frac{Q^2}{4\tilde{\kappa}^2} + n_X)}{\Gamma(\frac{Q^2}{4\tilde{\kappa}^2} + n_X + \bar{m})}\end{aligned} \tag{3.10}$$

and the normalization

$$C(\bar{m}, n_X) = \left(\frac{\Gamma(n_X + 1)}{\Gamma(\bar{m} - 1)\Gamma(n_X + \bar{m} - 1)}\right)^{\frac{1}{2}}. \tag{3.11}$$

Here we have set $Q^2 = -q^2$ (spacelike), and used the final state mass shell condition

$$P_X^2 = (p + q)^2 = M_0^2 + Q^2\left(\frac{1}{x} - 1\right) \equiv M_X^2 = 4\tilde{\kappa}^2\left(n_X + M + \frac{1}{2}\right) \tag{3.12}$$

to identify $n_X = Q^2(1/x - 1)/4\tilde{\kappa}^2$, with $p^2 = M_0^2 = 4\tilde{\kappa}^2(M + \frac{1}{2}) = 8\tilde{\kappa}^2$ for the initial nucleon state.

The Dirac part of the electromagnetic current (3.4) can be extracted from (3.8) using

$$W^\mu_{EM(\text{Dirac})}(Q^2) = \bar{u}_{s'}(p')\gamma^\mu u_s(p) \times F_1^{EM(\text{Dirac})}(Q) \equiv \frac{1}{F_N(p')F_N(p)}\frac{\delta S^{\text{EM}}_{\text{Dirac}}}{\delta\epsilon_\mu(q)} + \mathcal{O}(N_c^{-2}), \tag{3.13}$$

which amounts to the Dirac or minimal contribution to the electromagnetic form factor ($Q^2 < 0$)

$$F_1^{EM(\text{Dirac})}(Q^2) = \frac{1}{2g_5^2} \times 2g_5^2 \times e_{\text{nucleon}} \times \frac{1}{2}[\mathcal{I}_L(n_X = 0, Q^2) + \mathcal{I}_R(n_X = 0, Q^2)] + \mathcal{O}(N_c^{-2}), \tag{3.14}$$

or more explicitly in the soft wall model

$$\begin{aligned}F_1^{EM(\text{Dirac})}(Q) &= e_{\text{nucleon}}\left(\frac{1}{(\frac{Q^2}{4\tilde{\kappa}^2} + 1)(\frac{Q^2}{4\tilde{\kappa}^2} + 2)} + \frac{3}{(\frac{Q^2}{4\tilde{\kappa}^2} + 1)(\frac{Q^2}{4\tilde{\kappa}^2} + 2)(\frac{Q^2}{4\tilde{\kappa}^2} + 3)}\right) + \mathcal{O}(N_c^{-2}), \\ &= e_{\text{nucleon}}\left(\frac{m_0^4}{(Q^2 + m_0^2)(Q^2 + m_1^2)} + \frac{3m_0^6}{(Q^2 + m_0^2)(Q^2 + m_1^2)(Q^2 + m_2^2)}\right) + \mathcal{O}(N_c^{-2}),\end{aligned} \tag{3.15}$$

using the soft wall rho meson trajectory $m_n^2 = 4\tilde{\kappa}^2(n + 1)$. Note that normalizing $F_1^{EM(\text{Dirac})}(0) = 1$ for the proton, fixes $1 + \mathcal{O}(N_c^{-2}) = 1$. In other words, the $1/N_c$ corrections to the EM form factors must vanish at $Q = 0$ due to the conservation of the electromagnetic current. Also note that (3.15) asymptotes a dipole form $\sim 1/Q^4$ which is consistent with the hard scattering rules [5].

2. Direct axial form factor: Dirac

The direct axial form factors are derived using the same reasoning, with $W_A^{\tilde{\alpha}\mu}(Q^2)$ (3.2) following from the pertinent variation of the bulk Dirac action

$$S^{(0,3)\text{Axial}}_{\text{Dirac}}[i,X]=\frac{1}{2g_5^2}\int dzd^4y\sqrt{g}e^{-\tilde{\kappa}^2z^2}A_N^{(0,3)}J_A^{(0,3)N},$$
$$S^{\pm\text{Axial}}_{\text{Dirac}}[i,X]=\frac{1}{2g_5^2}\frac{1}{\sqrt{2}}\int dzd^4y\sqrt{g}e^{-\tilde{\kappa}^2z^2}A_N^{\pm}J_A^{\mp N}, \tag{3.16}$$

or more explicitly for the chargeless component,

$$\begin{aligned}S^{(0,3)\text{Axial}}_{\text{Dirac}}[i,X]&=\frac{1}{2g_5^2}\int dzd^4y\sqrt{g}e^{-\tilde{\kappa}^2z^2}\frac{z}{R}(\bar{\Psi}_{1X}\gamma^N A_N^{(0,3)}T^{(0,3)}\Psi_{1i}-\bar{\Psi}_{2X}\gamma^N A_N^{(0,3)}T^{(0,3)}\Psi_{2i})\\&\approx(2\pi)^4\delta^4(P_X-p-q)\times F_X(P_X)\times F_N(p)\\&\quad\times\frac{1}{2g_5^2}\times 2g_5^2\times g^{(0,3)}_{A\text{nucleon}}\times\bar{u}_{s_X}(P_X)\not{\epsilon}(q)\gamma^5u_{s_i}(p)\times\frac{1}{2}[\mathcal{I}_R(n_X,\tilde{Q}^2)-\mathcal{I}_L(n_X,\tilde{Q}^2)],\end{aligned} \tag{3.17}$$

where the substitution (2.32) was used in the second line, i.e.,

$$\tilde{Q}^2=Q^2+\frac{1}{2}m_q^2\to Q^2+\tilde{m}_0^2-m_0^2. \tag{3.18}$$

Similarly, for the charged components

$$\begin{aligned}S^{\pm\text{Axial}}_{\text{Dirac}}[i,X]&\equiv\frac{1}{2g_5^2}\times\frac{1}{\sqrt{2}}\int dzd^4y\sqrt{g}e^{-\kappa^2z^2}\frac{z}{R}(\bar{\Psi}^{p/n}_{1X}\gamma^N A_N^{\pm}\Psi^{n/p}_{1i}-\bar{\Psi}^{p/n}_{2X}\gamma^N A_N^{\pm}\Psi^{n/p}_{2i}),\\&=(2\pi)^4\delta^4(P_X-p-q)\times F_X(P_X)\times F_N(p)\\&\quad\times\frac{1}{2g_5^2}\times 2g_5^2\times\frac{1}{\sqrt{2}}\times e^{\pm}_{W\text{nucleon}}\times\bar{u}_{s_X}(P_X)\not{\epsilon}^{\pm}(q)\gamma^5u_{s_i}(p)\times\frac{1}{2}[\mathcal{I}_R(n_X,\tilde{Q}^2)-\mathcal{I}_L(n_X,\tilde{Q}^2)].\end{aligned} \tag{3.19}$$

Here $\epsilon^{\pm}_{\mu}(q)$ is the polarization of the charged vectors. Following the normalization of the flavor generators T^a in (2.1), the axial and electroweak charges are

$$\begin{aligned}g^0_{A\text{nucleon}}&=g^0_{A\text{proton}}=g^0_{A\text{neutron}}=\frac{3}{2},\\g^3_{A\text{nucleon}}&=g^3_{A\text{proton}}=\frac{1}{2},\\g^3_{A\text{nucleon}}&=g^3_{A\text{neutron}}=-\frac{1}{2},\\e^{\pm}_{W\text{nucleon}}&=e^{\pm}_{W\text{proton}}=e^{\pm}_{W\text{neutron}}=1,\end{aligned} \tag{3.20}$$

Finally, the isoscalar axial form factor can be extracted from (3.17) using

$$\mathcal{W}^{\mu}_{A(\text{Dirac})}(Q^2)\equiv\mathcal{W}^{0\mu}_{A}(Q^2)=\bar{u}_{s'}(p')\gamma^{\mu}\gamma^5u_s(p)\times F_1^{0A(\text{Dirac})}(Q)=\frac{1}{F_N(p')F_N(p)}\frac{\delta S^{0\text{Axial}}_{\text{Dirac}}}{\delta\epsilon_{\mu}(q)}+\mathcal{O}(N_c^{-2}), \tag{3.21}$$

which yields the minimal Dirac contribution to the isoscalar axial form factor as

$$F_1^{0A(\text{Dirac})}(Q)\approx\frac{1}{2g_5^2}\times 2g_5^2\times g^0_{A\text{nucleon}}\times\frac{1}{2}[\mathcal{I}_R(n_X=0,\tilde{Q}^2)-\mathcal{I}_L(n_X=0,\tilde{Q}^2)]+\mathcal{O}(N_c^{-2}). \tag{3.22}$$

More explicitly, in the soft wall model we have

$$F_1^{0A(\text{Dirac})}(Q)\approx g^0_{A\text{nucleon}}\left(\frac{1}{(\frac{Q^2+\tilde{m}_0^2}{4\tilde{\kappa}^2})(\frac{Q^2+\tilde{m}_0^2}{4\tilde{\kappa}^2}+1)}-\frac{3}{(\frac{Q^2+\tilde{m}_0^2}{4\tilde{\kappa}^2})(\frac{Q^2+\tilde{m}_0^2}{4\tilde{\kappa}^2}+1)(\frac{Q^2+\tilde{m}_0^2}{4\tilde{\kappa}^2}+2)}\right)+\mathcal{O}(N_c^{-2}) \tag{3.23}$$

following (3.15). Equation (3.23) reduces to a dipole form factor asymptotically $\sim 1/Q^4$, which is consistent with the hard scattering rules [5]. Recall that the substitution (3.18) in the bulk-to-boundary axial-vector propagator is justified for $Qz_0 \gg 1$, as we noted in (2.43). For $Qz_0 \to 0$, (3.22)–(3.23) give

$$g_A^{3(\mathrm{Dirac})} = \frac{1}{3} g_A^{0(\mathrm{Dirac})} \approx \left[\frac{\tilde{m}_0^2}{m_0^2} - 1\right]\left[\left(\frac{\tilde{m}_0^2}{m_0^2}\right)\left(\frac{\tilde{m}_0^2}{m_0^2} + 1\right)\left(\frac{\tilde{m}_0^2}{m_0^2} + 2\right)\right]^{-1} \to \frac{1}{6}\left[\frac{\tilde{m}_0^2}{m_0^2} - 1\right] + \mathcal{O}((\sigma z_0^3)^3), \tag{3.24}$$

with the rightmost result corresponding to the leading perturbative correction as in (2.30) for $\sigma z_0^3 \ll 1$. Using the soft wall parameters in [14] (model A) yields $m_0 = 0.775$ GeV and $\tilde{m}_0 = 1.363$ GeV, resulting in a large Dirac leading perturbative contribution to the isovector axial charge of the nucleon $g_A^{3(\mathrm{Dirac})} \approx 1/3$. The near-boundary approximation is not justified in this limit, with the exact but numerical bulk-to-boundary axial-vector propagator required.

3. Pion pole

Finally, we note that the axial-vector form factor is characterized by two invariant form factors $F_A(q^2)$ and $H_A(q^2)$ in general, which are defined as

$$\langle p_1|J_A^{\mu a}(0)|p_2\rangle = \bar{u}(p_1)(\gamma^\mu\gamma^5 F_A(q^2) + q^\mu\gamma^5 H_A(q^2))T^a u(p_1), \tag{3.25}$$

with $q = p_2 - p_1$. In the chiral limit, the two form factors are tied by the conservation of the axial-vector current $H_A(q^2) = -2m_N F_A(q^2)/q^2$ with $H_A(q^2 \approx 0) \approx -2m_N g_A/q^2$ exhibiting the pion pole. The absence of this contribution in (3.32) can be traced back to the A_5 field which we have ignored. As we noted above, the A_5 mixes with the tachyon X. When taken into proper consideration, this mixing after gauge fixing locks A_5 with the phase Π of the tachyon, i.e., $X = X_0 e^{i\Pi}$, which is identified with the pion field. Careful considerations in bulk yield precisely $H_A(q^2)$ as expected from current conservation in the chiral limit [19]. Here we can just reinstate this contribution by inspection, with the full pion pole $q^2 \to q^2 - m_\pi^2$.

B. Transition form factors

In DIS scattering of neutrinos off nucleons, we will need the transition form factors of the left chargeless and charged currents. For that, we define the left vector transition form factor for the process $V, L + p \to X$

$$\mathcal{W}_{V,L}^\mu(Q^2) = \langle X|\tilde{J}_{V,L}^\mu(0)|p\rangle \tag{3.26}$$

with $Q^2 = (P_X - p)^2$. We first evaluate the $U(1)_L$ Dirac and Pauli contributions to the transition vector form factor (3.26) and then generalize them to the corresponding $U(1)_V^{\mathrm{EM}}, U(1)_L^{\pm} \subset U(2)_L$ contributions.

1. $U(1)_L$ contributions

The minimal Dirac interaction term between the bulk $U(1)_L$ gauge field L_N and the bulk fermionic field Ψ_1 in the action is

$$S_{\mathrm{Dirac}}^L[i, X] = \frac{1}{2g_5^2}\int dz d^4y \sqrt{g} e^{-\tilde{\kappa}^2 z^2}\frac{z}{R} L_N \bar{\Psi}_{1X}\gamma^N \Psi_{1i}, \tag{3.27}$$

following the canonical normalizations

$$\Psi \to \sqrt{2g_5^2}\Psi \quad L_N \to g_5 L_N, \tag{3.28}$$

which makes the couplings and power counting manifest in Witten diagrams. The explicit form of (3.27) in terms of the bulk fermions is

$$\tilde{S}_{\mathrm{Dirac}}^L[i, X] = (2\pi)^4\delta^4(P_X - p - q) \times F_X(P_X) \times F_N(p) \times \frac{1}{2g_5^2} \times 2g_5^2\left[\bar{u}_{s_X}(P_X)\not{\epsilon}(q)\left(\frac{1-\gamma^5}{2}\right)u_{s_i}(p)\mathcal{I}_L(n_x, Q^2) + \bar{u}_{s_X}(P_X)\not{\epsilon}(q)\left(\frac{1+\gamma^5}{2}\right)u_{s_i}(p)\mathcal{I}_R(n_x, Q^2)\right]. \tag{3.29}$$

The Dirac contribution to the $U(1)_L$ transition form factor reads explicitly

$$\begin{aligned}\mathcal{W}^{\mu}_{L,\mathrm{Dirac}}(q^2) &= \frac{1}{F_X(P_X)F_N(p)}\frac{\delta S^L_{\mathrm{Dirac}}}{\delta\epsilon_\mu(q)} + \mathcal{O}(N_c^{-2}),\\ &= \frac{1}{F_X(P_X)F_N(p)}\times\frac{1}{2g_5^2}\times\frac{1}{g_5}\times\frac{\delta\tilde{S}^L_{\mathrm{Dirac}}}{\delta\epsilon_\mu(q)} + \mathcal{O}(N_c^{-2}),\\ &= \frac{1}{2g_5^2}\times 2g_5^2\times\left[\bar{u}_{s_X}(P_X)\gamma^\mu\left(\frac{1-\gamma^5}{2}\right)u_{s_i}(p)\mathcal{I}_L(n_x,Q^2) + \bar{u}_{s_X}(P_X)\gamma^\mu\left(\frac{1+\gamma^5}{2}\right)u_{s_i}(p)\mathcal{I}_R(n_x,Q^2)\right] + \mathcal{O}(N_c^{-2}).\end{aligned} \tag{3.30}$$

2. $U(1)^{\pm}_L$ contributions

For neutrino and antineuutrino scattering, the pertinent left-handed hadronic transition form factor is

$$\mathcal{W}^{\mu}_{\pm}(Q^2) = \langle N(P_X)|\tilde{J}^{\pm\mu}_L(0)|N(p)\rangle, \tag{3.31}$$

which can be evaluated using the Dirac and Pauli contributions to the fermionic action. To illustrate the normalizations, consider for simplicity the contribution due to the Dirac part, which yields the interaction vertex

$$\begin{aligned}S^{\pm L}_{\mathrm{Dirac}}[i,X] &= \frac{1}{2g_5^2}\times\frac{1}{\sqrt{2}}\int dz d^4y\sqrt{g}e^{-\tilde{\kappa}^2z^2}L^{\pm}_N J^{\mp N}_L = \frac{1}{2g_5^2}\times\frac{1}{\sqrt{2}}\int dz d^4y\sqrt{g}e^{-\tilde{\kappa}^2z^2}\frac{z}{R}\bar{\Psi}^{p/n}_{1X}\gamma^N L^{\pm}_N\Psi^{n/p}_{1i}\\ &= (2\pi)^4\delta^4(P_X-p-q)\times\frac{1}{2g_5^2}\times 2g_5^2\times F_X(P_X)F_{p/n}(p)\\ &\quad\times\frac{1}{\sqrt{2}}\times e^{\pm}_{W\mathrm{nucleon}}\times\left[\bar{u}_{s_X}(P_X)\not{\epsilon}^{\pm}(q)\left(\frac{1-\gamma^5}{2}\right)u_{s_i}(p)\mathcal{I}_L(n_x,Q_L^2) + \bar{u}_{s_X}(P_X)\not{\epsilon}^{\pm}(q)\left(\frac{1+\gamma^5}{2}\right)u_{s_i}(p)\mathcal{I}_R(n_x,Q_L^2)\right],\end{aligned} \tag{3.32}$$

with the corresponding transition form factor

$$\begin{aligned}\mathcal{W}^{\pm\mu}_{L(\mathrm{Dirac})}(Q^2) &= \frac{1}{F_X(P_X)F_{p/n}(p)}\frac{1}{\frac{1}{2\sqrt{2}}}\frac{\delta S^{\pm L}_{\mathrm{Dirac}}}{\delta\epsilon^{\pm}_\mu(q)} + \mathcal{O}(N_c^{-2})\\ &= \frac{1}{2g_5^2}\times 2g_5^2\times e^{\pm}_{W\mathrm{nucleon}}\\ &\quad\times 2\left[\bar{u}_{s_X}(P_X)\gamma^\mu\left(\frac{1-\gamma^5}{2}\right)u_{s_i}(p)\mathcal{I}_L(n_x,Q_L^2) + \bar{u}_{s_X}(P_X)\gamma^\mu\left(\frac{1+\gamma^5}{2}\right)u_{s_i}(p)\mathcal{I}_R(n_x,Q_L^2)\right] + \mathcal{O}(N_c^{-2}),\\ &= \frac{1}{2g_5^2}\times 2g_5^2\times e^{\pm}_{W\mathrm{nucleon}}\\ &\quad\times(\bar{u}_{s_X}(P_X)\gamma^\mu u_{s_i}(p)[\mathcal{I}_R(n_x,Q_L^2)+\mathcal{I}_L(n_x,Q_L^2)] + \bar{u}_{s_X}(P_X)\gamma^\mu\gamma^5 u_{s_i}(p)[\mathcal{I}_R(n_x,Q_L^2)-\mathcal{I}_L(n_x,Q_L^2)])\\ &\quad+\mathcal{O}(N_c^{-2}).\end{aligned} \tag{3.33}$$

3. Charged transition form factor: Pauli

The minimal Dirac bulk interaction does not contribute to the neutron transition form factor. This contribution arises from the $U(1)_L$ part of the Pauli interaction in bulk [20]

$$S^{L,R}_{\mathrm{Pauli}}[i,X] = \frac{\eta}{2g_5^2}\int dz d^4y\sqrt{g}e^{-\tilde{\kappa}^2z^2}\frac{z^2}{R^2}(\bar{\Psi}_{1X}\sigma^{MN}L_{MN}\Psi_{1i} - \bar{\Psi}_{2X}\sigma^{MN}R_{MN}\Psi_{2i}). \tag{3.34}$$

The inclusion of this interaction is straightforward but tedious, with the final result for the charged currents

$$\begin{aligned}\mathcal{W}_L^{\pm\mu}(Q^2) = e^{\pm}_{W\text{nucleon}} & \\ & \times (\bar{u}_{s_X}(P_X)\gamma^\mu u_{s_i}(p)[\mathcal{I}_R(n_x,Q_L^2)+\mathcal{I}_L(n_x,Q_L^2)] \\ & \quad + \bar{u}_{s_X}(P_X)\gamma^\mu\gamma^5 u_{s_i}(p)[\mathcal{I}_R(n_x,Q_L^2)-\mathcal{I}_L(n_x,Q_L^2)]) \\ & + \eta^{\pm}(\bar{u}_{s_X}(P_X)\gamma^\mu u_{s_i}(p)[\mathcal{J}_R(n_x,Q_L^2)+\mathcal{J}_L(n_x,Q_L^2] \\ & \quad + \bar{u}_{s_X}(P_X)\gamma^\mu\gamma^5 u_{s_i}(p)[\mathcal{J}_R(n_x,Q_L^2)-\mathcal{J}_L(n_x,Q_L^2)]) \\ & + 2\eta^{\pm}(\bar{u}_{s_X}(P_X)\sigma^{\mu\nu} i q_\nu u_{s_i}(p)[\mathcal{I}_{LR}(n_x,Q_L^2)+\mathcal{I}_{RL}(n_x,Q_L^2)] \\ & \quad + \bar{u}_{s_X}(P_X)\sigma^{\mu\nu} i q_\nu\gamma^5 u_{s_i}(p)[\mathcal{I}_{LR}(n_x,Q_L^2)-\mathcal{I}_{RL}(n_x,Q_L^2)]) \\ & - \eta^{\pm}(\bar{u}_{s_X}(P_X) q^\mu \not{q} u_{s_i}(p)[\mathcal{K}_R(n_x,Q_L^2)+\mathcal{K}_L(n_x,Q_L^2)] \\ & \quad + \bar{u}_{s_X}(P_X) q^\mu \not{q}\gamma^5 u_{s_i}(p)[\mathcal{K}_R(n_x,Q_L^2)-\mathcal{K}_L(n_x,Q_L^2)]) + \mathcal{O}(N_c^{-2}),\end{aligned} \tag{3.35}$$

with

$$\sigma^{\mu\nu} = 2S^{\mu\nu} = \frac{i}{2}[\gamma^\mu,\gamma^\nu] = i(\gamma^\mu\gamma^\nu - \eta^{\mu\nu}), \tag{3.36}$$

and manifest current conservation, i.e., $q_\mu \mathcal{W}^{\pm\mu\nu} = 0$ for on shell spinors. The integrals

$$\mathcal{J}_L, \mathcal{K}_L(n_X,Q^2) \equiv \mathcal{J}, K(M+5/2,n_X,Q^2), \qquad \mathcal{J}_R, \mathcal{K}_R(n_X,Q^2) \equiv \mathcal{J}, K(M+3/2,n_X,Q^2) \tag{3.37}$$

are related to the general integrals of the type (3.10), namely

$$\begin{aligned}\mathcal{J}(\bar{m},n_X,Q^2) &= C(\bar{m},n_X)\Gamma(1+a)\int_0^\infty dw w^{\bar{m}-1}e^{-w}(w\mathcal{U}(1+a;2;w))' L_{n_X}^{\bar{m}-2}(w), \\ &= C(\bar{m},n_X)\Gamma(1+a)\int_0^\infty dw w^{\bar{m}-1}e^{-w}(-a\mathcal{U}(1+a;1;w)) L_{n_X}^{\bar{m}-2}(w), \\ &= C(\bar{m},n_X)\frac{\Gamma(\bar{m})\Gamma(\bar{m}+n_X-1)(n_X-a(\bar{m}-1))a\Gamma(a+n_X)}{\Gamma(n_X+1)\Gamma(a+\bar{m}+n_X+1)}, \\ &= \frac{-a(\bar{m}-1)+n_X}{a+\bar{m}+n_X}\times\mathcal{I}(\bar{m},n_X,Q^2), \\ \mathcal{K}(\bar{m},n_X,Q^2) &= \frac{1}{\tilde{\kappa}^2}\times\mathcal{J}(\bar{m},n_X,Q^2),\end{aligned} \tag{3.38}$$

with $a = Q^2/4\tilde{\kappa}^2$, and

$$\begin{aligned}\mathcal{I}_{LR}(n_X,Q^2) &= \frac{1}{\tilde{\kappa}}\times C(m+5/2,n_X)\Gamma(1+a)\int_0^\infty dw w^{m+1}e^{-w}\mathcal{U}\left(1+\frac{Q^2}{4\tilde{\kappa}^2};2;w\right)L_{n_X}^{m+\frac{1}{2}}(w), \\ \mathcal{I}_{RL}(n_X,Q^2) &= \frac{1}{\tilde{\kappa}}\times C(m+3/2,n_X)\Gamma(1+a)\int_0^\infty dw w^{m+2}e^{-w}\mathcal{U}\left(1+\frac{Q^2}{4\tilde{\kappa}^2};2;w\right)L_{n_X}^{m-\frac{1}{2}}(w).\end{aligned} \tag{3.39}$$

We have made use of the recursive relation between the confluent hypergeometric functions

$$w\partial_w\mathcal{U}(a,b,w) = (1-b)\mathcal{U}(a,b,w) - (1+a-b)\mathcal{U}(a,b-1,w), \tag{3.40}$$

together with their integral representation

$$\mathcal{U}(a,b,w) = \frac{1}{\Gamma(a)}\int_0^\infty dt t^{a-1}(t+1)^{-a+b-1}e^{-tw}, \tag{3.41}$$

and the property of the Laguerre polynomials

$$L_n^a(w) = \frac{\Gamma(a+1+n)}{\Gamma(a+1)\Gamma(n+1)}\,{}_1F_1(-n, a+1, w) \tag{3.42}$$

to evaluate the integrals.

4. $U(1)_V^{\rm EM} \subset U(2)_V$ contributions

The electromagnetic transition vector form factor $\mathcal{W}^\mu_{\rm EM}(Q^2)$ as defined through

$$\mathcal{W}^\mu_{\rm EM}(Q^2) = \langle N(P_X)|\tilde{J}^\mu_{\rm EM}(0)|N(p)\rangle = \langle N(P_X)|\frac{1}{3}\tilde{J}^{0\mu}_V(0) + \tilde{J}^{3\mu}_V(0)|N(p)\rangle \tag{3.43}$$

can be extracted from (3.8) with the inclusion of the Pauli contribution (3.34), using

$$\mathcal{W}^\mu_{EM(\rm Dirac)}(Q^2) = \frac{1}{F_X(P_X)F_N(p)}\frac{\delta S^{\rm EM}_{\rm Dirac+Pauli}}{\delta\epsilon_\mu(q)} + \mathcal{O}(N_c^{-2}). \tag{3.44}$$

The result is

$$\begin{aligned}\epsilon_\mu\mathcal{W}^\mu_{\rm EM}(Q^2) = \epsilon_\mu\Big(& e_{\rm nucleon}\times\bar{u}_{s_X}(P_X)\gamma^\mu u_{s_i}(p)\frac{1}{2}[\mathcal{I}_R(n_x,Q^2)+\mathcal{I}_L(n_x,Q^2)]\\ &+\eta^{p/n}\bar{u}_{s_X}(P_X)\gamma^\mu u_{s_i}(p)\frac{1}{2}[\mathcal{J}_R(n_x,Q^2)-\mathcal{J}_L(n_x,Q^2)]\\ &+\eta^{p/n}\bar{u}_{s_X}(P_X)\sigma^{\mu\nu}iq_\nu u_{s_i}(p)[\mathcal{I}_{LR}(n_x,Q^2)-\mathcal{I}_{RL}(n_x,Q^2)]\Big)+\mathcal{O}(N_c^{-2}).\end{aligned} \tag{3.45}$$

5. $U(1)_A \subset U(2)_A$ contributions

The chargeless axial transition form factor $\mathcal{W}^\mu_{0,3}(Q^2)$ as defined through

$$\mathcal{W}^{(0,3)\mu}_A(Q^2) = \langle N(P_X)|\tilde{J}^{(0,3)\mu}_A(0)|N(p)\rangle \tag{3.46}$$

follows the same reasoning, with the full result including the Dirac and Pauli contributions:

$$\begin{aligned}\epsilon^{(0,3)}_\mu\mathcal{W}^{(0,3)\mu}_A(Q^2) = \epsilon^{(0,3)}_\mu\Big(& g^{(0,3)}_{A\rm nucleon}\times\bar{u}_{s_X}(P_X)\gamma^\mu\gamma^5 u_{s_i}(p)\frac{1}{2}[\mathcal{I}_R(n_x,\tilde{Q}^2)-\mathcal{I}_L(n_x,\tilde{Q}^2)]\\ &+\eta^{(0,3)}\bar{u}_{s_X}(P_X)\gamma^\mu\gamma^5 u_{s_i}(p)\frac{1}{2}[\mathcal{J}_R(n_x,\tilde{Q}^2)+\mathcal{J}_L(n_x,\tilde{Q}^2)]\\ &+\eta^{(0,3)}\bar{u}_{s_X}(P_X)\sigma^{\mu\nu}iq_\nu\gamma^5 u_{s_i}(p)[\mathcal{I}_{LR}(n_x,\tilde{Q}^2)+\mathcal{I}_{RL}(n_x,\tilde{Q}^2)]\Big)+\mathcal{O}(N_c^{-2}).\end{aligned} \tag{3.47}$$

IV. NEUTRINO AND ANTINEUTRINO DIS SCATTERING IN QCD

In QCD lepton nucleon scattering follows from the contraction of the leptonic tensor and hadronic tensor through the exchange of neutral currents carried by γ, Z and charged currents carried by $W^\pm$. Some useful insights on standard neutrino DIS scattering on a nucleon can be found in [21]. In this section we briefly review the key definitions and characteristics of this scattering as a prelude to the holographic analysis, which will make use of the transition form factors established above for the s-wave contributions to DIS.

A. Structure functions for $\nu,\bar{\nu}$ scattering

An overall review of neutrino DIS scattering can be found in [21], so we will be brief in our presentation of the results for our ensuing analysis. For unpolarized nucleons, the hadronic tensor for neutrino (antineutrino) scattering can be organized under the strictures of Lorentz symmetry, parity, and current conservation in terms of three invariant structure functions

$$\begin{aligned} W_{\mu\nu}^{\nu,\bar{\nu}} &= \frac{1}{4\pi}\int d^4x e^{iq\cdot x}\langle P|[J_\mu^{\mp}(x), J_\nu^{\pm}(0)]|P\rangle, \\ &= \left(-\eta_{\mu\nu}+\frac{q_\mu q_\nu}{q^2}\right)F_1^{W^\pm}(x,q^2)+\left(P_\mu+\frac{q_\mu}{2x}\right)\left(P_\nu+\frac{q_\nu}{2x}\right)\frac{2x}{q^2}F_2^{W^\pm}(x,q^2)\mp i\epsilon_{\mu\nu\alpha\beta}q^\alpha P^\beta\frac{x}{q^2}F_3^{W^\pm}(x,q^2), \end{aligned} \tag{4.1}$$

where q_μ, P_μ, are the 4-momenta of the virtual current and nucleon, respectively. $x=-q^2/2P\cdot q$ is the Bjorken parameter which is kinematically bounded $0\le x\le 1$. $F_{1,2}$ refers to the symmetric structure functions, while F_3 refers to the antisymmetric one. The formers are parity preserving, while the latter is not for neutrino and antineutrino probes. In the DIS limit with $Q^2=-q^2\gg P^2$ and x fixed, the structure functions in QCD obey Bjorken scaling. In this limit, the parity even structure functions satisfy the Callan-Gross relation $F_2=2xF_1$. We note that analyticity allows to relate the hadronic DIS tensor (4.1) to the discontinuity of the forward Compton amplitude of a lepton on a nucleon

$$4\pi W_{\mu\nu}^{\nu,\bar{\nu}} = 2\pi\mathrm{Im}T_{\mu\nu}^{\nu,\bar{\nu}} \equiv 2\pi\mathrm{Im}i\int d^4x e^{iq\cdot x}\langle P|T^*(J_\mu^{\mp}(x)J_\nu^{\pm}(0))|P\rangle \tag{4.2}$$

To calculate the hadronic tensor (4.1) we use the completeness of the hadronic spectrum f

$$W_{\mu\nu}^{\nu,\bar{\nu}} = \frac{1}{2}\sum_{s,s_X}\sum_{M_X}\delta(M_X^2-(P+q)^2)\mathcal{W}_\mu^{\nu,\bar{\nu}*}\mathcal{W}_\nu^{\nu,\bar{\nu}} \equiv W_{\mu\nu}^{\nu,\bar{\nu}S}+iW_{\mu\nu}^{\nu,\bar{\nu}A} \tag{4.3}$$

with the transition current matrix element (3.26), for excited states of squared mass $M_X^2=Q^2(1/x-1)+m_N^2$, and $P^2=M_0^2=m_N^2$. For neutrino scattering the explicit form of the QCD quark (partonic) currents in (4.2) are given by

$$\begin{aligned} e\tilde{J}_{\mathrm{EM}}^\mu &= e\bar{q}Q\gamma^\mu q, \\ e_W\times 2\tilde{J}_L^{\pm\mu} &= e_W\bar{q}T^\pm\gamma^\mu\frac{1}{2}(1-\gamma^5)q, \\ e_W\tilde{J}_Z^\mu &= e_W\tilde{J}_L^\mu-2e_W\sin^2\theta_{\mathrm{W}}\tilde{J}_{\mathrm{EM}}^\mu = e_W\bar{q}\gamma^\mu\frac{1}{2}(1-\gamma^5)q-2e_W\sin 2\theta_{\mathrm{W}}\bar{q}Q\gamma^\mu q, \end{aligned} \tag{4.4}$$

with e, e_W the electric and electroweak charges, and $\sin\theta_{\mathrm{W}}=\frac{e}{e_W}$ with the Weinberg angle $\theta_W\approx\frac{\pi}{6}$.

$$Q=\begin{pmatrix}\frac{2}{3} & 0\\ 0 & -\frac{1}{3}\end{pmatrix}, \qquad T^+=(T^-)^\dagger=\begin{pmatrix}0 & 2\\ 0 & 0\end{pmatrix}. \tag{4.5}$$

The imaginary part in (4.2) receives contribution from the neutral $\gamma\gamma$, ZZ, γZ as they mix, and the charged $W^\mp W^\pm$ as they are conjugate.

B. Unpolarized parton distributions through charged currents

Neutrino and antineutrino scattering on a hadron through the charged currents yield very important information on the parton content of a hadron in the DIS limit. At weak coupling, the parton model gives a very simple descriptive of the structure functions in terms of the partonic distribution functions of the hadron. Assuming two flavors for simplicity and isospin symmetry, the partonic model for $\nu p\to l^-X$ through W^+ exchange gives

$$\begin{aligned} F_1^{W^+p}(x,Q) &= d(x,Q)+\bar{u}(x,Q), \\ F_2^{W^+p}(x,Q) &= 2x(d(x,Q)+\bar{u}(x,Q)), \\ F_3^{W^+p}(x,Q) &= 2(d(x,Q)-\bar{u}(x,Q)), \end{aligned} \tag{4.6}$$

while for $\bar{\nu}p\to l^+X$ through W^- exchange it gives

$$F_1^{W^- p}(x,Q) = u(x,Q) + \bar{d}(x,Q),$$
$$F_2^{W^- p}(x,Q) = 2x(u(x,Q) + \bar{d}(x,Q)),$$
$$F_3^{W^- p}(x,Q) = 2(u(x,Q) - \bar{d}(x,Q)), \tag{4.7}$$

with modulo e_W^2. The corresponding neutron structure functions follow by isospin symmetry. Equations (4.6)–(4.7) can be inverted to give the unpolarized valence and sea parton distributions in the proton. We now proceed to evaluate these unpolarized partonic distributions using the holographic dual of neutrino scattering.

V. NEUTRINO AND ANTINEUTRINO DIS IN HOLOGRAPHY

We now consider neutrino DIS scattering on a nucleon as a Dirac fermion in bulk using holography, in the double limit of a large number of colors and strong gauge coupling $\lambda = g^2 N_c$. Antineutrino DIS scattering follows from pertinent rearrangements. DIS scattering on a nucleon as a bulk dilatino using holography was first addressed in [5] and later by others [18,22–24]. At large x, DIS scattering using $U(1)_V$ probes follows from the direct and crossed Witten diagrams in bulk, and at small x it follows from Pomeron exchange in the form of a Reggeized and warped close string exchange in bulk. We now review the analysis for a $U(1)_V$ current and then extend it to the electromagnetic vector $U(1)_V^{\rm EM} \subset U(2)_V$, and the left-handed $U(1)_L^{\pm} \subset U(2)_L$ currents.

A. Structure functions: Baryonic exchange in the s channel

For unpolarized $U(1)_L$ scattering, the hadronic tensor is

$$W_L^{\mu\nu} = \frac{1}{4\pi}\sum_s \int d^4y e^{iq\cdot y}\langle P,s|[J_L^\mu(y), J_L^\nu(0)]|P,s\rangle, \tag{5.1}$$

with the spectral decomposition for the s-channel contributions

$$\begin{aligned} W_{L,s}^{\mu\nu} &= \frac{1}{4\pi}\sum_{s,s_X}\sum_{M_X}\int \frac{d^4P_X}{(2\pi)^4}\theta(P_X^0)(2\pi)\delta(P_X^2 - M_X^2)(2\pi)^4\delta^4(P+q-P_X)\langle P,s|J_L^\mu(0)|P_X,s_X\rangle\langle P_X,s_X|J_L^\nu(0)|P,s\rangle, \\ &= \frac{1}{2}\sum_{s,s_X}\sum_{M_X}\delta(M_X^2 - (P+q)^2)\langle P,s|J_L^\mu(0)|P+q,s_X\rangle\langle P+q,s_X|J_L^\nu(0)|P,s\rangle, \\ &= \frac{1}{2}\sum_{s,s_X}\sum_{M_X}\delta(M_X^2 - (P+q)^2)\mathcal{W}_L^\mu\mathcal{W}_L^{\nu *}. \end{aligned} \tag{5.2}$$

The t-channel Reggeized contributions will be addressed below.

B. Dirac contribution

Using the relations

$$\begin{aligned} \epsilon_\mu\langle P_X|\tilde{J}_{L,\rm Dirac}^\mu(q)|P\rangle &= (2\pi)^4\delta^4(P_X - P - q)\epsilon_\mu\langle P+q|J_{L,\rm Dirac}^\mu(0)|P\rangle = \mathcal{N}_L \times \frac{1}{g_5}\times \tilde{S}_{\rm int,Dirac}^L[i,X], \\ \epsilon_\mu\langle P|\tilde{J}_{L,\rm Dirac}^\mu(q)|P_X\rangle &= (2\pi)^4\delta^4(P_X - P - q)\epsilon_\mu\langle P|J_{L,\rm Dirac}^\mu(0)|P+q\rangle = \mathcal{N}_L \times \frac{1}{g_5}\times \tilde{S}_{\rm int,Dirac}^L[X,i], \end{aligned} \tag{5.3}$$

we can make explicit the contracted hadronic tensor

$$\begin{aligned} W_{L,s,\rm Dirac}^{\mu\nu} = \frac{1}{2}&\sum_{M_X}\delta(M_X^2 - (p+q)^2)\mathcal{N}_L^2 \\ &\times \sum_{s_i}\sum_{s_X}(\mathcal{I}_L\mathcal{I}_R(\bar{u}_{s_X}\gamma^\mu P_L u_{s_i}\bar{u}_{s_i}\gamma^\nu P_R u_{s_X} + \bar{u}_{s_X}\gamma^\mu P_R u_{s_i}\bar{u}_{s_i}\gamma^\nu P_L u_{s_X}) \\ &+ \mathcal{I}_L^2\bar{u}_{s_X}\gamma^\mu P_L u_{s_i}\bar{u}_{s_i}\gamma^\nu P_L u_{s_X} + \mathcal{I}_R^2\bar{u}_{s_X}\gamma^\mu P_R u_{s_i}\bar{u}_{s_i}\gamma^\nu P_R u_{s_X}). \end{aligned} \tag{5.4}$$

The additional normalization constant $\mathcal{N}_L = (1/2g_5^2)\times 2g_5^2 \times \tilde{\mathcal{N}}_L$ compensates for the missing higher spin-j and $\mathcal{O}(g_5^0)$ corrections in the s channel. Since $\sum_s (u_s)(p)(\bar{u}_s)(p) = \not{p} + M$, then the contracted hadronic tensor contributions from the s channel are

$$\epsilon_\mu \epsilon_\nu W^{\mu\nu}_{L,s,\text{Dirac}} = \sum_{M_X} \delta(M_X^2 - (p+q)^2)\mathcal{N}_L^2 \times 2\left(\mathcal{I}_R(n_x)\mathcal{I}_L(n_x) M_X M_0 \epsilon\cdot\epsilon + (\mathcal{I}_R^2(n_x) + \mathcal{I}_L^2(n_x))\left((p\cdot\epsilon)^2 - \frac{1}{2}(p^2 + p\cdot q)\epsilon\cdot\epsilon\right) + \frac{1}{2}(\mathcal{I}_R^2(n_x) - \mathcal{I}_L^2(n_x))(i\epsilon^{\mu\nu\alpha\beta} P_{X\alpha} p_\beta)\right). \tag{5.5}$$

By approximating the sum by an integral in a continuous state, i.e.,

$$\sum_{M_X} \delta(M_X^2 - (p+q)^2) \approx \frac{1}{4\tilde{\kappa}^2}\int dn \delta\left(\frac{s}{4\tilde{\kappa}^2} - \frac{M_n^2}{4\tilde{\kappa}^2}\right) = \frac{1}{4\tilde{\kappa}^2}, \tag{5.6}$$

we have

$$\epsilon_\mu \epsilon_\nu W^{\mu\nu}_{L,s,\text{Dirac}} \approx \frac{\mathcal{N}_L^2}{4\tilde{\kappa}^2} \times (2\mathcal{I}_L(n_x)\mathcal{I}_R(n_x) M_X M_0 \epsilon\cdot\epsilon + (\mathcal{I}_R^2(n_x) + \mathcal{I}_L^2(n_x))(2(p\cdot\epsilon)^2 - (p^2 + p\cdot q)\epsilon\cdot\epsilon) + (\mathcal{I}_R^2(n_x) - \mathcal{I}_L^2(n_x))(i\epsilon^{\mu\nu\alpha\beta} P_{X\alpha} p_\beta)). \tag{5.7}$$

The same contraction applied to the canonical hadronic tensor decomposition (4.1), for a neutrino, with a transverse polarization $\epsilon\cdot q = 0$ [which we have already used in deriving (5.7)], yields

$$\epsilon_\mu \epsilon_\nu W_L^{\mu\nu} = -\epsilon^2 F_1^L + \frac{2x}{q^2}(\epsilon\cdot p)^2 F_2^L - i\epsilon_\mu \epsilon_\nu \epsilon^{\mu\nu\alpha\beta} q_\alpha p_\beta \frac{x}{q^2} F_3^L(x, q^2). \tag{5.8}$$

A comparison of (5.8) to (5.7) allows for the extraction of the s-channel baryonic contributions to the DIS structure functions

$$\begin{aligned} F^L_{1s,\text{Dirac}} &= \frac{\mathcal{N}_L^2}{2\tilde{\kappa}^2}\left((\mathcal{I}_R^2(n_x) + \mathcal{I}_L^2(n_x))\left(\frac{M_0^2}{2} + \frac{Q^2}{4x}\right) - \mathcal{I}_R(n_x)\mathcal{I}_L(n_x) M_0\left(M_0^2 + Q^2\left(\frac{1}{x} - 1\right)\right)^{\frac{1}{2}}\right), \\ F^L_{2s,\text{Dirac}} &= \frac{\mathcal{N}_L^2}{4\tilde{\kappa}^2}(\mathcal{I}_R^2(n_x) + \mathcal{I}_L^2(n_x))\frac{Q^2}{x}, \\ F^L_{3s,\text{Dirac}} &= \frac{\mathcal{N}_L^2}{4\tilde{\kappa}^2}(\mathcal{I}_R^2(n_x) - \mathcal{I}_L^2(n_x))\frac{Q^2}{x}, \end{aligned} \tag{5.9}$$

with the DIS kinematics (3.12) subsumed. Similarly, using the transition form factor (3.44), we find

$$\begin{aligned} F^{\text{EM}}_{1s,\text{Dirac}} &= e^2_{\text{nucleon}} \times F^L_{1s,\text{Dirac}}, \\ F^{\text{EM}}_{2s,\text{Dirac}} &= e^2_{\text{nucleon}} \times F^L_{2s,\text{Dirac}}, \\ F^{\text{EM}}_{3s,\text{Dirac}} &= 0, \end{aligned} \tag{5.10}$$

while using the transition form factor (3.33), we find

$$\begin{aligned} F^{W^\pm}_{1s,\text{Dirac}} &= 4(e^\pm_{W\text{nucleon}})^2 \times F^L_{1s,\text{Dirac}} = \frac{4(e^\pm_{W\text{nucleon}})^2}{e^2_{\text{nucleon}}} \times F^{\text{EM}}_{1s,\text{Dirac}}, \\ F^{W^\pm}_{2s,\text{Dirac}} &= 4(e^\pm_{W\text{nucleon}})^2 \times F^L_{2s,\text{Dirac}} = \frac{4(e^\pm_{W\text{nucleon}})^2}{e^2_{\text{nucleon}}} \times F^{\text{EM}}_{2s,\text{Dirac}}, \\ F^{W^\pm}_{3s,\text{Dirac}} &= 4(e^\pm_{W\text{nucleon}})^2 \times F^L_{3s,\text{Dirac}}. \end{aligned} \tag{5.11}$$

C. Dirac plus Pauli contributions

The full left current vertex with the Pauli contribution is given in (3.35). A rerun of the preceding arguments yields the hadronic tensor for ν scattering in the untraced form ($\bar{\nu}$ scattering follows from $\nu \leftrightarrow \mu$)

$$\begin{aligned}
W_L^{+\mu\nu} = \frac{1}{16\pi\tilde{\kappa}^2}\Big[& 2M_0 M_X(\alpha_R^2 g^{\mu\nu} + (\beta_R^2 + 2\alpha_R\beta_R)q^\mu q^\nu + \lambda_R^2(g^{\mu\nu}q^2 - q^\mu q^\nu)) \\
& + 2M_0\lambda_R(\alpha_R g^{\mu\nu} q\cdot(P_X+p) + \beta_R q^\mu q^\nu q\cdot(P_X+p) - i\alpha_R\epsilon^{\nu\mu\alpha\beta}q_\alpha(P_X+p)_\beta) \\
& + 2(\alpha_R g^\mu_{\bar{\mu}} + \beta_R q^\mu q_{\bar{\mu}})(\alpha_R g^\nu_{\bar{\nu}} + \beta_R q^\nu q_{\bar{\nu}})(p^{\bar{\mu}}P_X^{\bar{\nu}} + p^{\bar{\nu}}P_X^{\bar{\mu}} - g^{\bar{\mu}\bar{\nu}}p\cdot P_X - i\epsilon^{\bar{\nu}\alpha\bar{\mu}\beta}P_{X\alpha}p_\beta) \\
& - \frac{1}{2}\lambda_R^2(3g^{\mu\nu}(2q\cdot p q\cdot P_X - q^2 p\cdot P_X) \\
& + 4(q^2(p^\mu P_X^\nu + p^\nu P_X^\mu) + q^\mu q^\nu p\cdot P_X - (q^\nu p^\mu + q^\mu p^\nu)q\cdot P_X - (q^\nu P_X^\mu + q^\mu P_X^\nu)q\cdot p)) \\
& + (R\to L, -i\to +i)\Big],
\end{aligned} \tag{5.12}$$

with $P_X = q + p$, $M_X^2 = M_0^2 + q^2(1 - 1/x)$, and

$$\alpha_R = 2(e_W^+\mathcal{I}_R + \eta\mathcal{J}_R), \qquad \beta_R = 4\eta\mathcal{I}_{LR}, \qquad \lambda_R = -2\eta\mathcal{K}_R, \tag{5.13}$$

$$\begin{aligned}
\epsilon_\mu^+\epsilon_\nu^{+*}W_{L,s}^{+\mu\nu} &= \frac{1}{2}\sum_{s,s_X}\sum_{M_X}\delta(M_X^2 - (P+q)^2)\epsilon_\mu^+\mathcal{W}_L^{+\mu}\epsilon_\nu^{+*}\mathcal{W}_L^{+*\nu} \\
&= \frac{(\mathcal{N}_L^+)^2}{8\tilde{\kappa}^2}\epsilon_\mu^+\epsilon_\nu^{+*}\times 8[2\tilde{\mathcal{I}}_{LR}(n_x)M_0 M_X\eta^{\mu\nu} + \tilde{\mathcal{I}}_+^2(n_x)(p^\mu P_X^\nu + p^\nu P_X^\mu - \eta^{\mu\nu}p\cdot P_X) + \tilde{\mathcal{I}}_-^2(n_x)(i\epsilon^{\mu\nu\alpha\beta}P_{X\alpha}p_\beta)]
\end{aligned} \tag{5.14}$$

where we have defined

$$\begin{aligned}
\tilde{\mathcal{I}}_{LR}(n_x) &\equiv \mathcal{I}_{\eta L}(n_x)\mathcal{I}_{\eta R}(n_x) + 4\eta^2 q^2\mathcal{I}_{RL}(n_x)\mathcal{I}_{LR}(n_x), \\
\tilde{\mathcal{I}}_+^2(n_x) &\equiv \mathcal{I}_{\eta R}^2(n_x) + \mathcal{I}_{\eta L}^2(n_x) - 4\eta^2 q^2(\mathcal{I}_{LR}^2(n_x) + \mathcal{I}_{RL}^2(n_x)), \\
\tilde{\mathcal{I}}_-^2(n_x) &\equiv \mathcal{I}_{\eta R}^2(n_x) - \mathcal{I}_{\eta L}^2(n_x), \\
\mathcal{I}_{\eta R}(n_x) &\equiv e_{W\text{nucleon}}^+\mathcal{I}_R(n_x) + \eta\mathcal{J}_R(n_x), \\
\mathcal{I}_{\eta L}(n_x) &\equiv e_{W\text{nucleon}}^+\mathcal{I}_L(n_x) + \eta\mathcal{J}_L(n_x),
\end{aligned} \tag{5.15}$$

and we have used $\epsilon^+\cdot q = 0$, $\epsilon^{+*}\cdot q = 0$, $q_{\bar{\nu}}q_{\bar{\mu}}\epsilon^{\bar{\nu}\beta\bar{\mu}\nu} = 0$, and $q_{\bar{\nu}}q_{\bar{\mu}}\epsilon^{\bar{\mu}\alpha\mu\bar{\nu}} = 0$.

Comparing (5.14) with the contraction of (4.1), for neutrino ν, i.e.,

$$\epsilon_\mu^+\epsilon_\nu^{+*}W_L^{+\mu\nu} = \epsilon_\mu^+\epsilon_\nu^{+*}W^{\nu,\mu\nu} = -\epsilon^+\cdot\epsilon^{+*}F_1^{W^+} + \frac{2x}{q^2}\epsilon^+\cdot p\epsilon^{+*}\cdot pF_2^{W^+} - i\epsilon_\mu^+\epsilon_\nu^{+*}\epsilon^{\mu\nu\alpha\beta}q_\alpha p_\beta\frac{x}{q^2}F_3^{W^+}(x,q^2), \tag{5.16}$$

allows for the extraction of the structure functions

$$\begin{aligned}
F_{1s}^{W^+} &= \frac{2(\mathcal{N}_L^+)^2}{\tilde{\kappa}^2}\left(\tilde{\mathcal{I}}_+^2(n_x)\left(\frac{M_0^2}{2} + \frac{Q^2}{4x}\right) - \tilde{\mathcal{I}}_{LR}(n_x)M_0\left(M_0^2 + Q^2\left(\frac{1}{x} - 1\right)\right)^{\frac{1}{2}}\right), \\
F_{2s}^{W^+} &= \frac{(\mathcal{N}_L^+)^2}{\tilde{\kappa}^2}\tilde{\mathcal{I}}_+^2(n_x)\frac{Q^2}{x}, \\
F_{3s}^{W^+} &= \frac{(\mathcal{N}_L^+)^2}{\tilde{\kappa}^2}\tilde{\mathcal{I}}_-^2(n_x)\frac{Q^2}{x},
\end{aligned} \tag{5.17}$$

where we have used $P_{X_\alpha} = p_\alpha + q_\alpha$, $p_\alpha p_\beta \epsilon^{\mu\nu\alpha\beta} = 0$, $\epsilon^+ \cdot q = 0$, $\epsilon^{+*} \cdot q = 0$, and $M_X^2 = M_0^2 + q^2(1 - 1/x)$. Strict bulk-to-boundary correspondence implies $\mathcal{N}_L^+ = 1$ in the double limit of a large number of colors N_c and strong gauge 't Hooft gauge coupling. Here we follow [18] and assume proportionality between the bulk and boundary structure functions with $\mathcal{N}_L^+$ an overall parameter that captures parts of the finite corrections to the strict double limit. It will be fixed by a point in the data. Similarly, we can find the structure functions for antineutrino $\tilde{\nu}$ scattering through W^- exchange as

$$\begin{aligned} F_{1s}^{W^-} &= F_{1s}^{W^+}(e^+_{W\text{nucleon}} \to e^-_{W\text{nucleon}}; \mathcal{N}_L^+ \to \mathcal{N}_L^-), \\ F_{2s}^{W^-} &= F_{2s}^{W^+}(e^+_{W\text{nucleon}} \to e^-_{W\text{nucleon}}; \mathcal{N}_L^+ \to \mathcal{N}_L^-), \\ F_{3s}^{W^-} &= F_{3s}^{W^+}(e^+_{W\text{nucleon}} \to e^-_{W\text{nucleon}}; \mathcal{N}_L^+ \to \mathcal{N}_L^-). \end{aligned} \tag{5.18}$$

D. Structure functions: Pomeron exchange in the t channel

DIS scattering at small x is dominated by Reggeon and Pomeron exchanges. In this section, we first consider DIS scattering using $U(1)_L$ currents in the Pomeron regime and then generalize our results to the electromagnetic vector $U(1)_V^{\text{EM}} \subset U(2)_V$, and the left-handed $U(1)_L^{\pm} \subset U(2)_L$ currents. The Pomeron is dual to a close string exchange or graviton in the t channel [22,23,25–27]. This is best obtained by recalling that the hadronic tensor ties to the forward scattering amplitude of a $U(1)_L$ current through

$$W_L^{\mu\nu} = \frac{1}{4\pi} \sum_s \int d^4y e^{iq\cdot y} \langle P, s | [J_L^\mu(y), J_L^\nu(0)] | P, s \rangle = 2\pi \text{Im} T_L^{\mu\nu}, \tag{5.19}$$

where the Compton scattering amplitude $T_L^{\mu\nu}$ is given by

$$\epsilon_\mu \epsilon_\nu T_{L,t}^{\mu\nu} \equiv \mathcal{A}^h_{Lp\to Lp}(s,t), \tag{5.20}$$

for massive graviton or glueball $h_{\mu\nu}$ exchange in the t channel, with the explicit result given in (D18). The Pomeron contribution as a graviton exchange to the t-channel structure functions $F^L_{1t,2t}(x,Q)$ follow from

$$\epsilon_\mu \epsilon_\nu W_{L,t}^{\mu\nu} = \epsilon^2 F_{1t}^L + \frac{2x}{q^2}(\epsilon \cdot p)^2 F_{2t}^L = 2\pi \text{Im} \mathcal{A}^{\text{tot}}_{Lp\to Lp}(s, t = -K^2 = 0), \tag{5.21}$$

for $\epsilon \cdot q = 0$. Inserting (D28) into (5.21) we obtain

$$\begin{aligned} 2xF_{1t}^L &= \frac{2\kappa^2}{g_5^2} \times \frac{\pi}{\sqrt{\lambda}} \times \left(\frac{Q}{\tilde{\kappa}}\right)^{2-2/\sqrt{\lambda}} \times \left(\frac{1}{x}\right)^{1-2/\sqrt{\lambda}} \\ &\times \exp\left[-\frac{\tilde{\xi}^2}{2} \frac{\sqrt{\lambda}}{\log[Q^2/\tilde{\kappa}^2] + \log[1/x]}\right] \times \left(\frac{\sqrt{\lambda}}{\log[Q^2/\tilde{\kappa}^2] + \log[1/x]}\right)^{3/2} \\ &\times (2\pi)^{1/2} \tilde{\xi} \left(1 + \mathcal{O}\left(\frac{\sqrt{\lambda}}{\log[Q^2/\tilde{\kappa}^2] + \log[1/x]}\right)\right) \times \mathcal{F}(j_0, K = 0) \times I_\xi^T(j_0, Q = Q'), \\ F_{2t}^L &= \frac{2\kappa^2}{g_5^2} \times \frac{\pi}{\sqrt{\lambda}} \times \left(\frac{Q}{\tilde{\kappa}}\right)^{2-2/\sqrt{\lambda}} \times \left(\frac{1}{x}\right)^{1-2/\sqrt{\lambda}} \\ &\times \exp\left[-\frac{\tilde{\xi}^2}{2} \frac{\sqrt{\lambda}}{\log[Q^2/\tilde{\kappa}^2] + \log[1/x]}\right] \times \left(\frac{\sqrt{\lambda}}{\log[Q^2/\tilde{\kappa}^2] + \log[1/x]}\right)^{3/2} \\ &\times (2\pi)^{1/2} \tilde{\xi} \left(1 + \mathcal{O}\left(\frac{\sqrt{\lambda}}{\log[Q^2/\tilde{\kappa}^2] + \log[1/x]}\right)\right) \times \mathcal{F}(j_0, K = 0) \times (I_\xi^T(j_0, Q = Q') + I_\xi^L(j_0, Q = Q')), \end{aligned} \tag{5.22}$$

with $\tilde{\xi} = \gamma + \pi/2$. The preexponents in (5.22) are commensurate with the expected Pomeron behavior $s^{\alpha_{\mathbb{P}}(0)-1}$ with the intercept $\alpha_{\mathbb{P}}(0) - 1 = 1\text{–}2/\sqrt{\lambda}$ after the identification $s \sim Q^2/x$ in the DIS limit. The additional overall factor of Q is the left over (longitudinal) polarization from the overlaping incoming-outgoing $U(1)_L$ wave functions. The exponents reflect

on the warped Gribov diffusion in $D_\perp = 3$, for $2_\perp$ spatial dimensions and $1_\perp$ holographic dimension. The result (5.22) extends to the SU(2) currents by introducing a normalization factor $\mathcal{N}_L^{a=\pm}$. More specifically, for the charged currents we have

$$\begin{aligned}
2xF_{1t}^{W^\pm} &= (\mathcal{N}_{Lt}^{\pm})^2 \frac{2\kappa^2}{g_5^2} \times \frac{\pi}{\sqrt{\lambda}} \times \left(\frac{Q}{\tilde{\kappa}}\right)^{2-2/\sqrt{\lambda}} \times \left(\frac{1}{x}\right)^{1-2/\sqrt{\lambda}} \\
&\times \exp\left[-\frac{\tilde{\xi}^2}{2} \frac{\sqrt{\lambda}}{\log[Q^2/\tilde{\kappa}^2] + \log[1/x]}\right] \times \left(\frac{\sqrt{\lambda}}{\log[Q^2/\tilde{\kappa}^2] + \log[1/x]}\right)^{3/2} \\
&\times (2\pi)^{1/2} \tilde{\xi} \left(1 + \mathcal{O}\left(\frac{\sqrt{\lambda}}{\log[Q^2/\tilde{\kappa}^2] + \log[1/x]}\right)\right) \times \mathcal{F}(j_0, K=0) \times I_\xi^T(j_0, Q=Q'), \\
F_{2t}^{W^\pm} &= (\mathcal{N}_{Lt}^{\pm})^2 \frac{2\kappa^2}{g_5^2} \times \frac{\pi}{\sqrt{\lambda}} \times \left(\frac{Q}{\tilde{\kappa}}\right)^{2-2/\sqrt{\lambda}} \times \left(\frac{1}{x}\right)^{1-2/\sqrt{\lambda}} \\
&\times \exp\left[-\frac{\tilde{\xi}^2}{2} \frac{\sqrt{\lambda}}{\log[Q^2/\tilde{\kappa}^2] + \log[1/x]}\right] \times \left(\frac{\sqrt{\lambda}}{\log[Q^2/\tilde{\kappa}^2] + \log[1/x]}\right)^{3/2} \\
&\times (2\pi)^{1/2} \tilde{\xi} \left(1 + \mathcal{O}\left(\frac{\sqrt{\lambda}}{\log[Q^2/\tilde{\kappa}^2] + \log[1/x]}\right)\right) \times \mathcal{F}(j_0, K=0) \times (I_\xi^T(j_0, Q=Q') + I_\xi^L(j_0, Q=Q')).
\end{aligned} \tag{5.23}$$

E. $F_{3t}^{W^\pm}$ structure functions: Reggeon exchange in the t channel

Reggeon exchange is also a t-channel contribution stemming from a spin-1 exchange induced by the Chern-Simons contribution in (4.1). The latter allows for the anomalous coupling of $W^-W^+\omega$ in bulk with ω_μ a spin-1 flavor singlet U(1) gauge field in bulk (the analog of the omega meson). In principle, the Reggeized spin-1 exchange in bulk contributes to the unpolarized and parity odd structure function F_3. A similar contribution was observed for the spin structure function in [23], following an earlier analysis in [22]. More specifically, the U(1) exchange of L_μ^0 in bulk stems from (2.17) and (2.15), with the vertices

$$\begin{aligned}
L\bar{\Psi}\Psi &: \int \frac{d^4p_2 d^4p_1 d^4k}{(2\pi)^{12}} (2\pi)^4 \delta^4(p_2 - k - p_1) S^k_{L\bar{\Psi}\Psi}, \\
LLL &: \int \frac{d^4q' d^4q d^4k}{(2\pi)^{12}} (2\pi)^4 \delta^4(q - k - q') S^k_{LLL},
\end{aligned} \tag{5.24}$$

where we have defined

$$\begin{aligned}
S^k_{L\bar{\Psi}\Psi} &= g_5^3 \kappa_{CS} \int dz [\epsilon^{\mu\sigma\nu\rho} \epsilon_\mu^+(q) \epsilon_\sigma^-(q') \partial_z L^+(q,z)(-ik_\nu) \epsilon_\rho^0(k) L^0(k,z) L^-(q',z) \\
&- \epsilon^{\sigma\mu\nu\rho} \epsilon_\sigma^+(q) \epsilon_\mu^-(q') \partial_z L^-(q',z)(-ik_\nu) \epsilon_\rho^0(k) L^0(k,z) L^+(q,z) \\
&+ \epsilon^{\mu\sigma\rho\nu} \epsilon_\mu^+(q) \epsilon_\sigma^-(q') \partial_z L^+(q,z) \epsilon_\rho^0(k) L^0(k,z)(-iq'_\nu) L^-(q',z) \\
&- \epsilon^{\sigma\mu\rho\nu} \epsilon_\sigma^+(q) \epsilon_\mu^-(q') \partial_z L^-(q',z) \epsilon_\rho^0(k) L^0(k,z)(iq_\nu) L^+(q,z) \\
&- \epsilon^{\sigma\rho\mu\nu} \epsilon_\sigma^+(q) \epsilon_\rho^-(q') \epsilon_\mu^0(k) \partial_z L^0(k,z)(-iq'_\nu) L^-(q',z) L^+(q,z) \\
&+ \epsilon^{\rho\sigma\mu\nu} \epsilon_\rho^+(q) \epsilon_\sigma^-(q') \epsilon_\mu^0(k) \partial_z L^0(k,z)(iq_\nu) L^+(q,z) L^-(q',z)], \\
&= g_5^3 \kappa_{CS} (-i) \epsilon^{\mu\sigma\nu\rho} \epsilon_\mu^+(q) \epsilon_\sigma^-(q')(q'_\nu + q_\nu) \epsilon_\rho^0(k) \\
&\times \int dz (\partial_z L^0(k,z) L(q',z) L(q,z) - \partial_z L(q,z) L^0(k,z) L(q',z),
\end{aligned} \tag{5.25}$$

with

$$L_\mu^+(x,z)=\epsilon_\mu^+(q)L^+(q,z)e^{iq\cdot x},\qquad L_\mu^-(x,z)=\epsilon_\mu^-(q')L^-(q',z)e^{-iq'\cdot x},\qquad L_\mu^0(x,z)=\epsilon_\mu^0(k)L^+(k,z)e^{-ik\cdot x}. \tag{5.26}$$

In the last line in (5.25), we have used the fact that $L^+(q,z)=L^-(q,z)=L(q,z)$.

Using the relation

$$\mathrm{Im}\mathcal{A}^{\mathrm{tot}}_{Lp\to Lp}(s,t=0)=\epsilon^{+\mu}\epsilon^{-\nu}W^\nu_{\mu\nu} \tag{5.27}$$

with $W^\nu_{\mu\nu}$ given by (4.1), and $\mathcal{A}^{\mathrm{tot}}_{Lp\to Lp}(s,t)$ given by (C32), we can extract the structure function $F_3^{W^\pm}(x,Q^2)$ in the t channel as

$$\begin{aligned}F_{3t}^{W^\pm}&=4\times4\times g_5\times\frac{1}{g_5^2}\times g_5^3\kappa_{CS}\times\left(\frac{Q}{\tilde\kappa}\right)^{2-j_0-\Delta(j_0)}\times\left(\frac{s}{\tilde\kappa^2}\right)^{j_0}\times\frac{e^{-\sqrt{\lambda}\tilde\xi^2/2\log[s/\tilde\kappa^2]}}{(\log[s/\tilde\kappa^2])^{3/2}}\\&\times(\sqrt{\lambda}/2\pi)^{1/2}\tilde\xi\left(1+\mathcal{O}\left(\frac{\sqrt{\lambda}}{\log[s/\tilde\kappa^2]}\right)\right)\times I_\xi(j_0,Q,Q'=Q)\times\mathcal{F}_1^{(LN)}(j_0,K=0),\\&=16\times g_5^2\kappa_{CS}\times\left(\frac{Q}{\tilde\kappa}\right)^{1-\frac{1}{\sqrt{\lambda}}}\times\left(\frac{1}{x}\right)^{1-\frac{1}{\sqrt{\lambda}}}\times\frac{e^{-\sqrt{\lambda}\tilde\xi^2/2(\log[Q^2/\tilde\kappa^2]+\log[1/x])}}{(\log[Q^2/\tilde\kappa^2]+\log[1/x])^{3/2}}\\&\times(\sqrt{\lambda}/2\pi)^{1/2}\tilde\xi\left(1+\mathcal{O}\left(\frac{\sqrt{\lambda}}{\log[Q^2/\tilde\kappa^2]+\log[1/x]}\right)\right)\times I_\xi(j_0,Q,Q'=Q)\times\mathcal{F}_1^{(LN)}(j_0,K=0).\end{aligned} \tag{5.28}$$

Here $s\approx\frac{Q^2}{x}$, $j_0=1-1/\sqrt{\lambda}$, $\Delta(j_0)=2$, and $\tilde\xi-\pi/2=\gamma=0.55772\ldots$ is Euler-Mascheroni constant.

VI. HOLOGRAPHIC RESULTS AND COMPARISON TO DATA

Equations (4.6)–(4.7) can be inverted to give the unpolarized valence and sea parton distributions in the proton, in terms of the pertinent holographic structure functions. The ones for the neutron follow by isospin symmetry. More specifically, we have for the unpolarized sea of the proton

$$\begin{aligned}x\bar u(x,Q)&=\frac14(F_2^{W^+p}(x,Q)-xF_3^{W^+p}(x,Q)),\\x\bar d(x,Q)&=\frac14(F_2^{W^-p}(x,Q)-xF_3^{W^-p}(x,Q)),\end{aligned} \tag{6.1}$$

and for the unpolarized valence contribution of the proton

$$\begin{aligned}xu_V(x,Q)&=x(u(x,Q)-\bar u(x,Q))=\frac14x(F_3^{W^-p}(x,Q)+F_3^{W^+p}(x,Q))\\&+\frac14(F_2^{W^-p}(x,Q)-F_2^{W^+p}(x,Q)),\\xd_V(x,Q)&=x(d(x,Q)-\bar d(x,Q))=\frac14x(F_3^{W^-p}(x,Q)+F_3^{W^+p}(x,Q))\\&-\frac14(F_2^{W^-p}(x,Q)-F_2^{W^+p}(x,Q)),\end{aligned} \tag{6.2}$$

with the structure functions receiving contributions from the s and t channels

$$\begin{aligned}F_2^{W^\pm p}(x,Q)&=F_{2s}^{W^\pm p}(x,Q)+F_{2t}^{W^\pm p}(x,Q),\\F_3^{W^\pm p}(x,Q)&=F_{3s}^{W^\pm p}(x,Q)+F_{3t}^{W^\pm p}(x,Q).\end{aligned} \tag{6.3}$$

The charged s-channel even-parity structure functions $F_{2s}^{W^\pm p}(x,Q)$ are given in (5.17) and (5.18), respectively, and the t-channel structure functions $F_{2t}^{W^\pm p}(x,Q)$ are given in (5.23). The charged s-channel odd-parity structure functions $F_{3s}^{W^\pm p}(x,Q)$ are given in (5.17) and (5.18), respectively. The charged t-channel odd parity structure functions $F_{3t}^{W^\pm p}(x,Q)$ are given in (5.28).

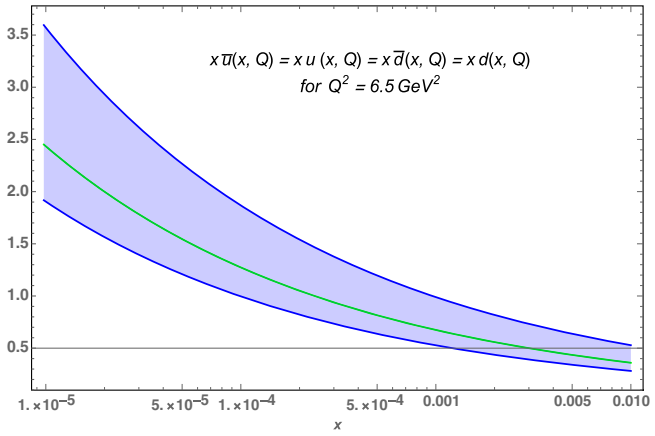

FIG. 1. Small-x holographic PDFs as given in (6.4) and (6.5) for: the normalization coefficient $\mathcal{N}^{\pm}_{Lt} = 0.309$ (the green curve), the normalization coefficient fixed between $\mathcal{N}^{\pm}_{Lt} = 0.274$ and $\mathcal{N}^{\pm}_{Lt} = 0.375$ (the blue band), 't Hooft coupling $\lambda = g^2_{\rm YM}N_c = 9.533$, the twist of proton $\tau = 3$ (fixed by the scaling of the electromagnetic form factor of proton in [20]), and soft-wall IR scale $\tilde{\kappa} = 0.350$ GeV (fixed by the mass of proton and ρ meson in [20]).

A. Results in the small-x regime

In the small-x regime, the results for the sea $\bar{u}$ and $\bar{d}$ distributions are solely due to the t-channel Pomeron exchange

$$\lim_{x\to 0} x\bar{u}(x,Q) = \frac{1}{4}F_{2t}^{W^+p}(x,Q),$$
$$\lim_{x\to 0} x\bar{d}(x,Q) = \frac{1}{4}F_{2t}^{W^-p}(x,Q), \tag{6.4}$$

with no Pomeron contribution to the tail of the valence distributions

$$\lim_{x\to 0} xu_V(x,Q) = 0,$$
$$\lim_{x\to 0} xd_V(x,Q) = 0. \tag{6.5}$$

Figure 1 shows the holographic Pomeron contribution at small x for the xu and xd distributions of the proton at a resolution $Q^2 = 6.5$ GeV^2, following from (6.4) and (6.5). The 't Hooft coupling is $\lambda = g^2_{\rm YM}N_c = 9.533$, the twist of proton is set to $\tau = 3$ (fixed by the scaling of the electromagnetic form factor of proton in [20]), and the soft-wall IR scale is fixed to $\tilde{\kappa} = 0.350$ GeV (to reproduce the mass of the proton and ρ meson as in [20]). The green curve uses the normalization coefficient $\mathcal{N}^{\pm}_{Lt} = 0.309$. The blue-band corresponds to the normalization coefficients fixed between $\mathcal{N}^{\pm}_{Lt} = 0.274$ and $\mathcal{N}^{\pm}_{Lt} = 0.375$.

B. Fixing the charged normalization $\mathcal{N}^{\pm}_{Lt}$ parameters

Throughout we will use the same 't Hooft coupling $\lambda = g^2_{\rm YM}N_c = 9.533$, which is within the standard choice in the most holographic constructions. The charged normalizations $\mathcal{N}^{\pm}_{Lt}$ are fixed between 0.274 and 0.375 and will be shown as a blue band in all results to follow. These normalizations are chosen for a best fit to the reduced noncharged (r, NC) and unpolarized deep inelastic $e^{\pm}p$ scattering cross section $\sigma^{\pm}_{r,NC}$ at low x. We recall, that $\sigma^{\pm}_{r,NC}$ is given by a linear combination of the generalised structure functions

$$\sigma^{\pm}_{r,NC} = \frac{{\rm d}^2\sigma^{e^{\pm}p}_{\rm NC}}{{\rm d}x_{\rm Bj}{\rm d}Q^2}\cdot\frac{Q^4 x_{\rm Bj}}{2\pi\alpha^2 Y_+} = \tilde{F}_2 \mp \frac{Y_-}{Y_+}x\tilde{F}_3 - \frac{y^2}{Y_+}\tilde{F}_L, \tag{6.6}$$

with $Y_\pm = 1 \pm (1-y)^2$. The overall structure functions, $\tilde{F}_2$, $\tilde{F}_{\rm L}$, and $x\tilde{F}_3$, are sums of structure functions, $F_{\rm X}$, $F^{\gamma Z}_{\rm X}$, and $F^{Z}_{\rm X}$, relating to photon exchange, photon-Z interference, and Z exchange, respectively, and depend on the electroweak parameters as

$$\tilde{F}_2 = F_2 - \kappa_Z v_e\cdot F_2^{\gamma Z} + \kappa_Z^2(v_e^2+a_e^2)\cdot F_2^Z,$$
$$\tilde{F}_{\rm L} = F_{\rm L} - \kappa_Z v_e\cdot F_{\rm L}^{\gamma Z} + \kappa_Z^2(v_e^2+a_e^2)\cdot F_{\rm L}^Z,$$
$$x\tilde{F}_3 = -\kappa_Z a_e\cdot xF_3^{\gamma Z} + \kappa_Z^2\cdot 2v_e a_e\cdot xF_3^Z.$$

Here v_e and a_e are the vector and axial-vector weak couplings of the electron to the Z boson, and $\kappa_Z(Q^2) = Q^2/[(Q^2+M_Z^2)(4\sin^2\theta_W\cos^2\theta_W)]$. The values of $\sin^2\theta_W = 0.23127$ and $M_Z = 91.1876$ GeV were used for the electroweak mixing angle and the Z-boson mass. In the quark-parton model where the kinematic variable $x_{\rm Bj}$ is equal to the fractional momentum of the struck quark, x, the structure functions are given in terms of the PDFs as

$$\begin{aligned}(F_2(x,Q),F_2^{\gamma Z}(x,Q),F_2^Z(x,Q)) \approx{}& [(e_u^2,2e_uv_u,v_u^2+a_u^2)(xu(x,Q)+x\bar{u}(x,Q))\\ &+(e_d^2,2e_dv_d,v_d^2+a_d^2)(xd(x,Q)+x\bar{d}(x,Q))],\\ (xF_3^{\gamma Z}(x,Q),xF_3^Z(x,Q)) \approx{}& 2[(e_ua_u,v_ua_u)(xu(x,Q)-x\bar{u}(x,Q))\\ &+(e_da_d,v_da_d)(xd(x,Q)-x\bar{d}(x,Q))],\\ (F_L(x,Q),F_L^{\gamma Z}(x,Q),F_L^Z(x,Q)) \approx{}& (0,0,0),\end{aligned} \tag{6.7}$$

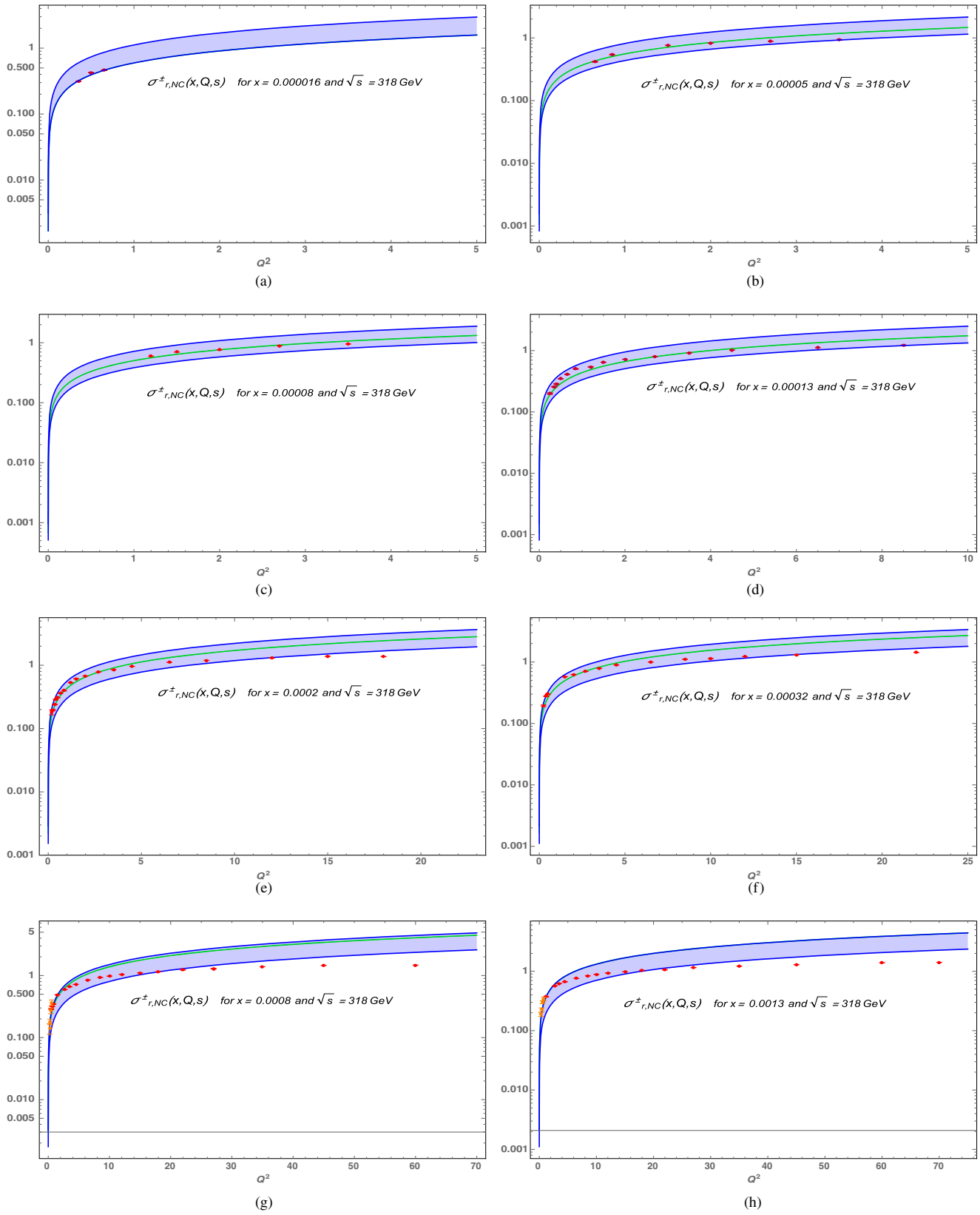

FIG. 2. The reduced noncharged and unpolarized deep inelastic $e^{\pm}p$ scattering cross section $\sigma^{\pm}_{r,NC}(x,Q,s)$ at low-x versus Q^2 as given in (6.6) for increasing x, at $\sqrt{s} = 318$ GeV. The middle green curve and the blue band are the holographic results for different charge normalizations $\mathcal{N}^{\pm}_{Lt}$. The red points are the H1 and ZEUS data [28], and the orange points at low Q^2 are the data from E665 [29]. See text.

with e_u and e_d denoting the electric charge of up- and down-type quarks, while $v_{u,d}$ and $a_{u,d}$ are the vector and axial-vector weak couplings of the up- and down-type quarks to the Z boson.

In Fig. 2 we show the measured $\sigma^{\pm}_{r,NC}(x,Q,s)$ versus Q^2 in GeV^2 at $\sqrt{s}=318$ GeV with increasing x resolution. Figure 2(a) follows from (6.6) for $x=0.000016$ using the small-x holographic PDF shown in Fig. 1. Figure 2(b) shows the same for $x=0.00005$. The middle green curve corresponds to $\mathcal{N}^{\pm}_{Lt}=0.309$. Figure 2(c) follows also from (6.6) for $x=0.00008$, with the middle green curve referring to $\mathcal{N}^{\pm}_{Lt}=0.314$. Figure 2(d) refers to $x=0.00013$ with the middle green curve referring to $\mathcal{N}^{\pm}_{Lt}=0.313$. Figure 2(e) follows again from (6.6) at $x=0.0002$ with the middle green curve $\mathcal{N}^{\pm}_{Lt}=0.329$. Figure 2(f) refers to $x=0.00032$ with the middle green curve referring to $\mathcal{N}^{\pm}_{Lt}=0.313$. Figure 2(f) refers to $x=0.0008$ with the middle green curve referring to $\mathcal{N}^{\pm}_{Lt}=0.335$. Figure 2(f) refers to $x=0.0013$ with the middle green curve referring to $\mathcal{N}^{\pm}_{Lt}=0.359$. The data from the H1 and ZEUS collaboration [28] are shown in red. The data shown in orange at very low Q^2 are from the E665 collaboration [29]. Note that we have reconstructed the orange data points for the cross section $\sigma^{\pm}_{r,NC}(x,Q,s)$ at $\sqrt{s}=318$ GeV from the E665 dataset for the structure function $F_2(x,Q)$ at $0.0008\leq x\leq 0.001$ using [30]

$$R(x,Q)=\frac{F_2}{2xF_1}\left(1+\frac{4M_p^2x^2}{Q^2}\right)-1=R^{1990}(x.Q). \quad (6.8)$$

As noted above, the blue-band follows from the normalization range fixed by $\mathcal{N}^{\pm}_{Lt}=0.274$ and $\mathcal{N}^{\pm}_{Lt}=0.375$. In Fig. 3, we show the structure functions constructed from our small-x holographic PDFs shown in Fig. 1.

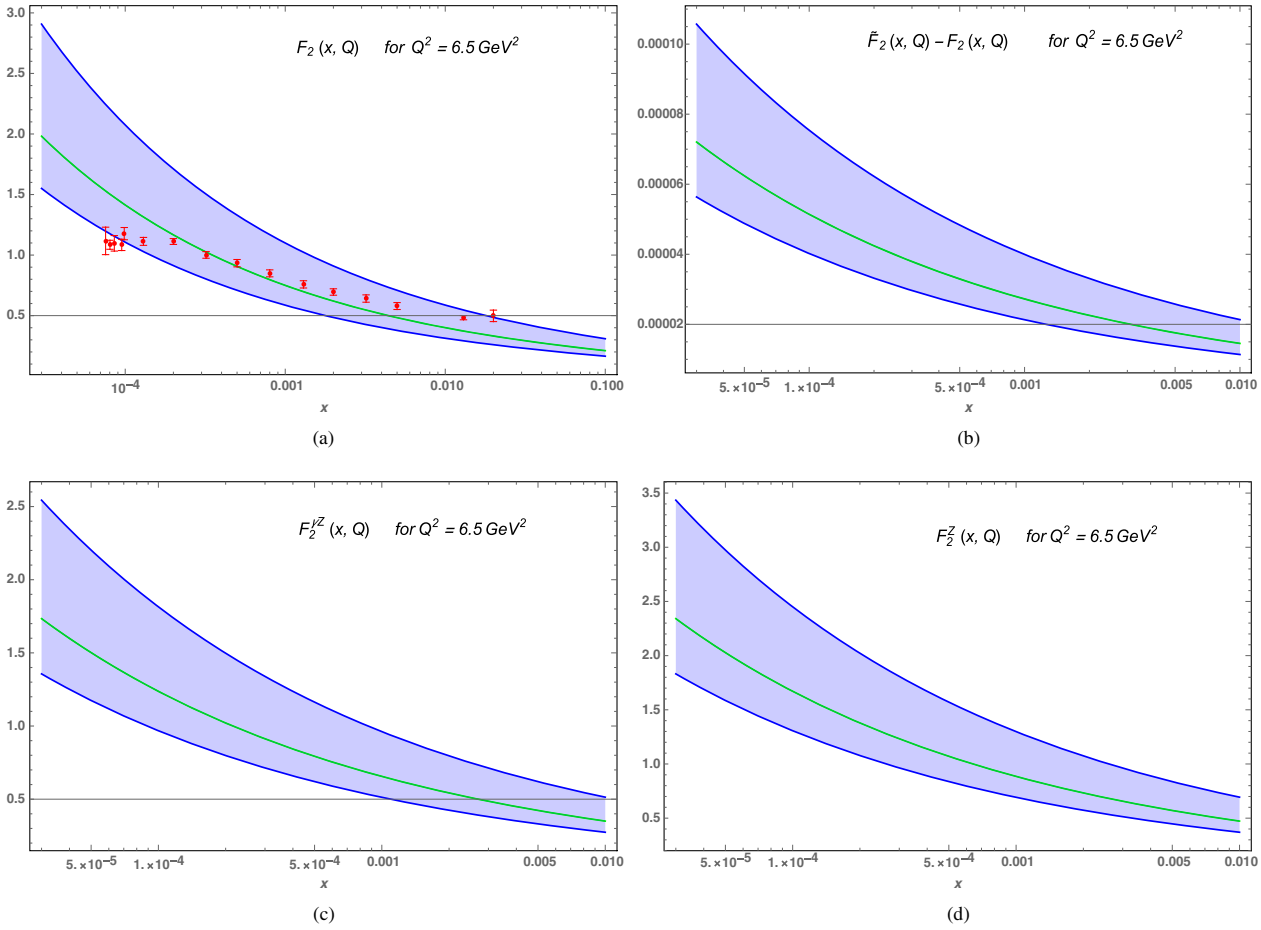

FIG. 3. (a) $F_2(x,Q)$ as given in (6.7) using the small-x holographic PDFs shown in Fig. 1. The red data points are from combined H1 and ZEUS collaborations [28] [reconstructed from their data for the cross section $\sigma^{\pm}_{r,NC}(x,Q,s)$ using our small-x holographic PDFs (6.4) and (6.5) shown in Fig. 1]. (b) $\tilde{F}_2(x,Q)-F_2(x,Q)$ as given in (6.7) using the small-x holographic PDFs shown in Fig. 1. (c) $F_2^{\gamma Z}(x,Q)$ as given in (6.7) using the small-x holographic PDFs shown in Fig. 1. d) $F_2^{Z}(x,Q)$ as given in (6.7) using the small-x holographic PDFs shown in Fig. 1.

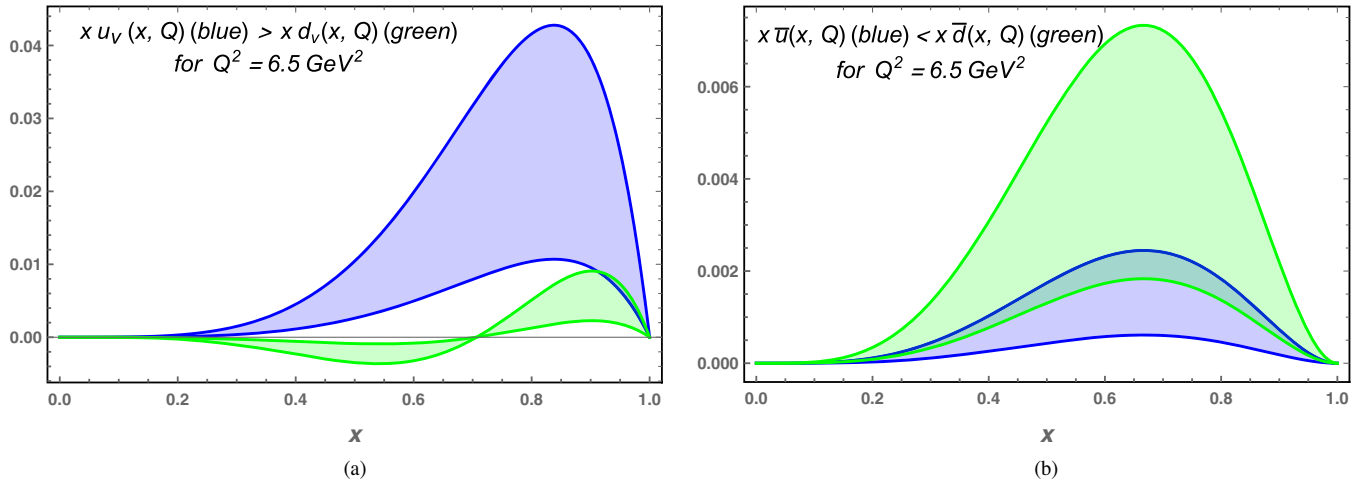

(a) (b)

FIG. 4. (a) Large-x holographic PDFs of the valence quarks in the proton as given in (6.10). (b) Large-x holographic PDFs of the sea quarks in the proton as given in (6.9). The bands follow from fixing $(\tilde{\tilde{\mathcal{N}}}_L^+, \tilde{\tilde{\mathcal{N}}}_L^-) = (17.715, 30.667)$ (green light band), and $(\tilde{\tilde{\mathcal{N}}}_L^+, \tilde{\tilde{\mathcal{N}}}_L^-) = (35.431, 61.335)$ (blue dark band). See text.

C. Results in the large-x regime

As we noted in the introduction, DIS scattering in holographic QCD at moderate values of partonic-x involves hadronic and not partonic constituents [5]. Indeed, in the large N_c limit, the leading single trace twist contributions acquire large anomalous dimensions and are suppressed. The dominant contributions stem from double-trace operators with mesonic quantum numbers. Another way to see this is to note that the large gauge coupling at the low renormalization point causes the color charges to undergo a rapid depletion into a cascade of even weaker charges, making them visible to hard probes only through double trace operators.

At large x, DIS scattering is almost off the entire hadron making the holographic approach pertinent. In this regime, the holographic limit enjoys approximate conformal symmetry, with the structure functions and form factors exhibiting various scaling laws including the parton-counting rules [5,6]. More specifically, we have for the sea contribution

$$\lim_{x\to 1}\lim_{\frac{\kappa^2}{Q^2}\to 0} x\bar{u}(x,Q) = \frac{1}{4}(F_{2s}^{W^+p}(x,Q) - xF_{3s}^{W^+p}(x,Q)),$$
$$\lim_{x\to 1}\lim_{\frac{\kappa^2}{Q^2}\to 0} x\bar{d}(x,Q) = \frac{1}{4}(F_{2s}^{W^-p}(x,Q) - xF_{3s}^{W^-p}(x,Q)), \quad (6.9)$$

and for the valence contribution

$$\lim_{x\to 1}\lim_{\frac{\kappa^2}{Q^2}\to 0} xu_V(x,Q) = \frac{1}{4}x(F_{3s}^{W^-p}(x,Q) + F_{3s}^{W^+p}(x,Q)) + \frac{1}{4}(F_{2s}^{W^-p}(x,Q) - F_{2s}^{W^+p}(x,Q)),$$
$$\lim_{x\to 1}\lim_{\frac{\kappa^2}{Q^2}\to 0} xd_V(x,Q) = \frac{1}{4}x(F_{3s}^{W^-p}(x,Q) + F_{3s}^{W^+p}(x,Q)) - \frac{1}{4}(F_{2s}^{W^-p}(x,Q) - F_{2s}^{W^+p}(x,Q)), \quad (6.10)$$

with the even and odd structure functions given, respectively, by

$$F_{2s}^{W^\pm p}(x,Q) = F_{2s,\mathrm{Dirac}}^{W^\pm p}(x,Q) + F_{2s,\mathrm{Pauli}}^{W^\pm p}(x,Q) + F_{2s,\mathrm{mixed}}^{W^\pm p}(x,Q),$$
$$F_{3s}^{W^\pm p}(x,Q) = F_{3s,\mathrm{Dirac}}^{W^\pm p}(x,Q) + F_{3s,\mathrm{Pauli}}^{W^\pm p}(x,Q) + F_{3s,\mathrm{mixed}}^{W^\pm p}(x,Q), \quad (6.11)$$

The large-x asymptotic of the Dirac + Pauli + Mixed structure functions following from (5.17), can be worked out in closed form. For the even-parity structure functions we have

$$F^{W^\pm p}_{2s,\text{Dirac}}(x,Q) = (\tilde{\mathcal{N}}^\pm_L)^2 \times (e^\pm_{W\text{nucleon}})^2 \times \left(\frac{\tilde{\kappa}^2}{Q^2}\right)^{\tau-1} x^{\tau+1}(1-x)^{\tau-2},$$
$$F^{W^\pm p}_{2s,\text{Pauli}}(x,Q) = (\tilde{\mathcal{N}}^\pm_L)^2 \times \eta^2 \times 4(\tau-1)^2 \times \left(\frac{\tilde{\kappa}^2}{Q^2}\right)^{\tau-1} x^{\tau+1}(1-x)^{\tau-2},$$
$$F^{W^\pm p}_{2s,\text{mixed}}(x,Q) = (\tilde{\mathcal{N}}^\pm_L)^2 \times e^\pm_{W\text{nucleon}} \times \eta \times 4(\tau-1) \times \left(\frac{\tilde{\kappa}^2}{Q^2}\right)^{\tau-1} x^{\tau+1}(1-x)^{\tau-2}, \tag{6.12}$$

in agreement with a recent analysis in [31] [see their Eqs. (88), (105), and (132)] and with the hard scattering rules [5].

For the odd-parity structure functions we also have

$$F^{W^\pm p}_{3s,\text{Dirac}}(x,Q) = (\tilde{\mathcal{N}}^\pm_L)^2 \times (e^\pm_{W\text{nucleon}})^2 \times \left(\frac{\tilde{\kappa}^2}{Q^2}\right)^{\tau-1} x^{\tau+1}(1-x)^{\tau-2},$$
$$F^{W^\pm p}_{3s,\text{Pauli}}(x,Q) = (\tilde{\mathcal{N}}^\pm_L)^2 \times \eta^2 \times 4(\tau-1)^2 \times \left(\frac{\tilde{\kappa}^2}{Q^2}\right)^{\tau-1} x^{\tau+1}(1-x)^{\tau-2},$$
$$F^{W^\pm p}_{3s,\text{mixed}}(x,Q) = (\tilde{\mathcal{N}}^\pm_L)^2 \times e^\pm_{W\text{nucleon}} \times \eta \times 4(\tau-1) \times \left(\frac{\tilde{\kappa}^2}{Q^2}\right)^{\tau-1} x^{\tau+1}(1-x)^{\tau-2}, \tag{6.13}$$

also in agreement with the recent results in [31] [see their Eqs. (88), (104), and (131)] and with the hard scattering rules [5]. Note that even though the Pauli vertex contribution involves an additional vierbein in comparison to the Dirac one, hence an *a priori* extra suppression with the z parameter and therefore Q^2 by duality, it is balanced by the extra z derivative in the magneticlike coupling $F_{\mu z}$, causing both contributions to scale identically with large Q^2 at large x.

Here $\tilde{\mathcal{N}}^\pm_L \equiv c(\tau) \times \mathcal{N}^\pm_L$ with $c(\tau)$ are undetermined coefficients, that can in principle be fixed rigorously in a specific model. As we noted earlier, strict bulk-to-boundary correspondence implies $\mathcal{N}^\pm_L = 1$ in the double and dual limit. Here we are assuming proportionality between the bulk and boundary structure functions, with $\mathcal{N}^\pm_L$ as overall parameters [18], that capture partially the finite corrections to the double limit. In the numerical analysis at large x to follow, we fit only the two parameters $\tilde{\tilde{\mathcal{N}}}^\pm_L$, which are defined as

$$\tilde{\tilde{\mathcal{N}}}^\pm_L \equiv (\tilde{\mathcal{N}}^\pm_L)^2 \times (e^\pm_{W\text{nucleon}})^2 + (\tilde{\mathcal{N}}^\pm_L)^2 \times \eta^2 \times 4(\tau-1)^2 + (\tilde{\mathcal{N}}^\pm_L)^2 \times e^\pm_{W\text{nucleon}} \times \eta \times 4(\tau-1). \tag{6.14}$$

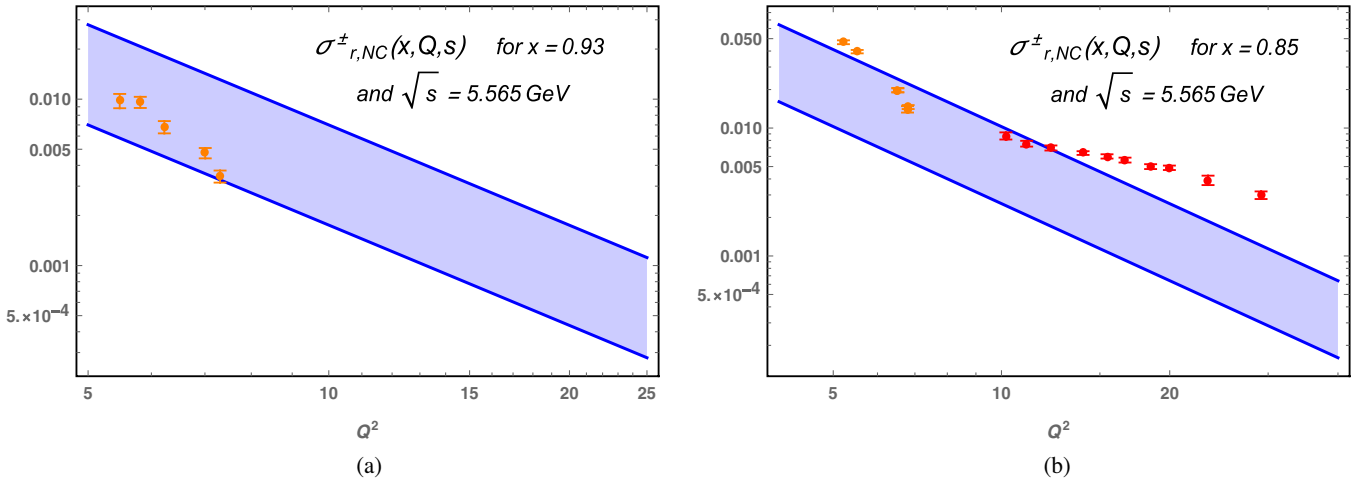

FIG. 5. (a) $\sigma^\pm_{r,NC}(x,Q,s)$ as given in (6.6) for $x = 0.93$, using the large-x holographic PDFs shown in Fig. 4, with the orange data points from JLAB [33]. (b) Same as in a for $x = 0.85$, with the red data points from the combined SLAC and BCDMS collaborations [30]. See text.

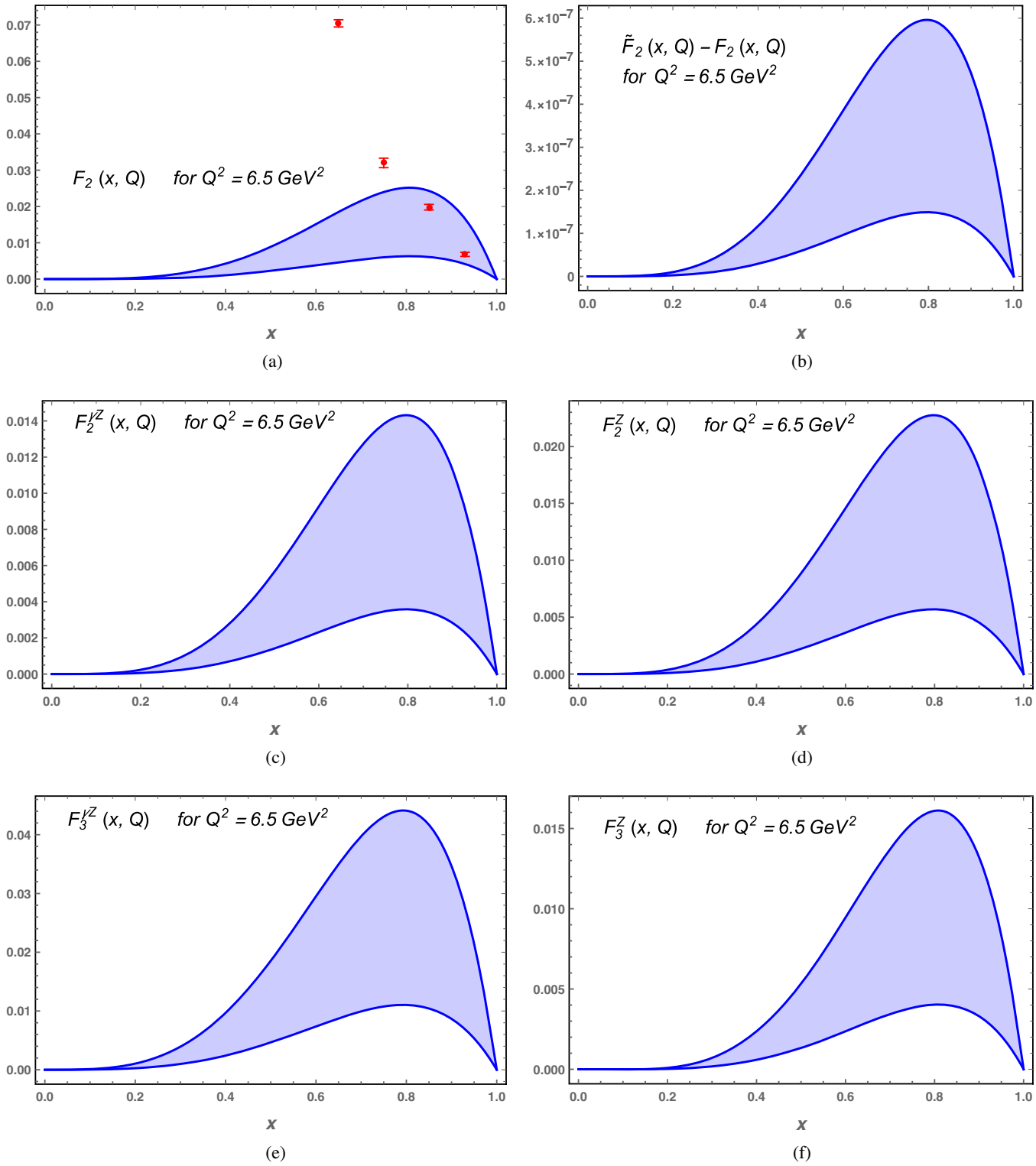

FIG. 6. (a)$F_2(x,Q)$ as given in (6.7) using the large-x holographic PDFs shown in Fig. 4. The red data points are from combined SLAC and BCDMS collaborations [30] for $x = 0.65$, $x = 0.75$, and $x = 0.85$. (b) $\tilde{F}_2(x,Q) - F_2(x,Q)$ as given in (6.7) using the large-x holographic PDFs shown in Fig. 4. (c) $F_2^{\gamma Z}(x,Q)$ as given in (6.7) using the large-x holographic PDFs shown in Fig. 4. (d) $F_2^{Z}(x,Q)$ as given in (6.7) using the large-x holographic PDFs shown in Fig. 4. (e) $F_3^{\gamma Z}(x,Q)$ as given in (6.7) using the large-x holographic PDFs shown in Fig. 4. (g) $F_3^{Z}(x,Q)$ as given in (6.7) using the large-x holographic PDFs shown in Fig. 4.

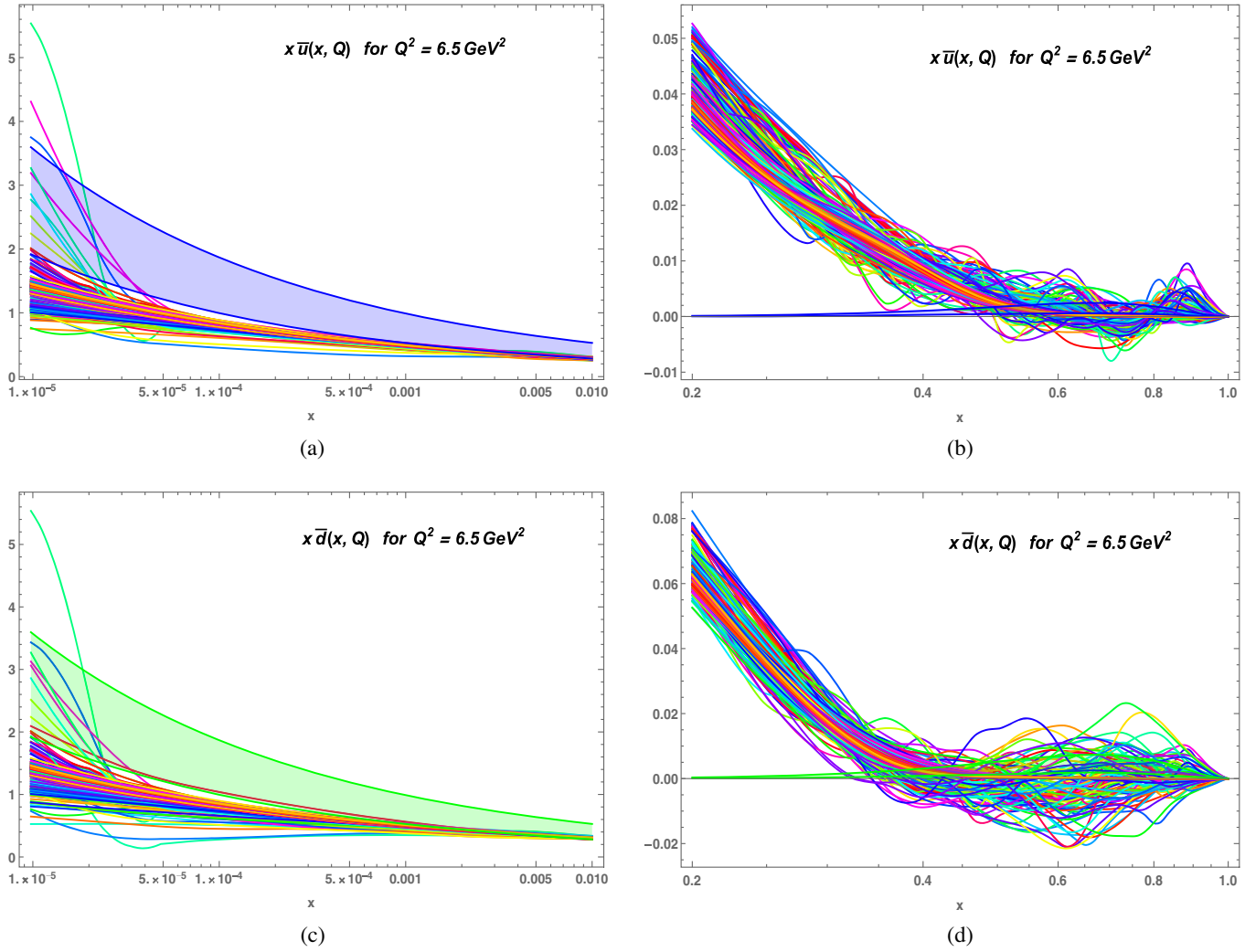

FIG. 7. (a),(b) Our holographic PDF sets (shown in blue band) compared to 292 PDF sets (shown in multiple solid lines) from CTEQ and LHAPDF projects incorporated within the ManeParse *Mathematica* package [35]. (c),(d) Our holographic PDF sets (shown in the green band) compared to 292 PDF sets (shown in multiple solid lines) from CTEQ and LHAPDF projects incorporated within the ManeParse *Mathematica* package [35].

In terms of (6.14), the structure functions (6.11) simplify

$$F_{2s}^{W^\pm p}(x,Q) = F_{3s}^{W^\pm p}(x,Q) = (\tilde{\tilde{\mathcal{N}}}_L^\pm)^2 \times \left(\frac{\tilde{\kappa}^2}{Q^2}\right)^{\tau-1} x^{\tau+1}(1-x)^{\tau-2}, \tag{6.15}$$

with $\tilde{\kappa} = 0.350$ GeV as fixed by the mass of the proton and ρ meson in [20].

Equation (6.15) scales as $(1/Q^2)^{\tau-1}$ asymptotically in agreement with the hard scaling laws expected from strong coupling [5], but vanishes as $(1-x)^{\tau-2}$ at large x in contrast to $(1-x)^{2\tau-3}$ suggested in [32]. The large-x behavior at strong coupling follows from the observation that for the virtual photon with amplitude $1/Q$ to scatter off the nucleon as a Dirac fermion, the latter has to shrink to a size $(1/Q)^\tau$, with a scattering probability $(1/Q^2)^{\tau-1}$. As a result, the structure function at large Q^2 but fixed $s \sim Q^2(1-x)$ scales as

$$F_2(x,Q) \sim Q^2 \left|\left(\frac{1}{Q^2}\right)^{\tau-1}\right|^2 (s = Q^2(1-x))^\alpha. \tag{6.16}$$

To reproduce the hard scaling law asymptotically requires $2\alpha + 6 - 4\tau = 2 - 2\tau$ or $\alpha = \tau - 2$, which is the large-x scaling in (6.15). To recover Bjorken scaling for the structure function requires $2\alpha + 6 - 4\tau = 0$ or $\alpha = 2\tau - 3$, which is the large-x scaling law suggested in [32]. We expect the latter to set in at very large Q^2.

In Fig. 4(a) we show the behavior the valence distributions $xu_V(x,Q)$ in the upper blue dark band, and $xd_V(x,Q)$ in the lower green light band at

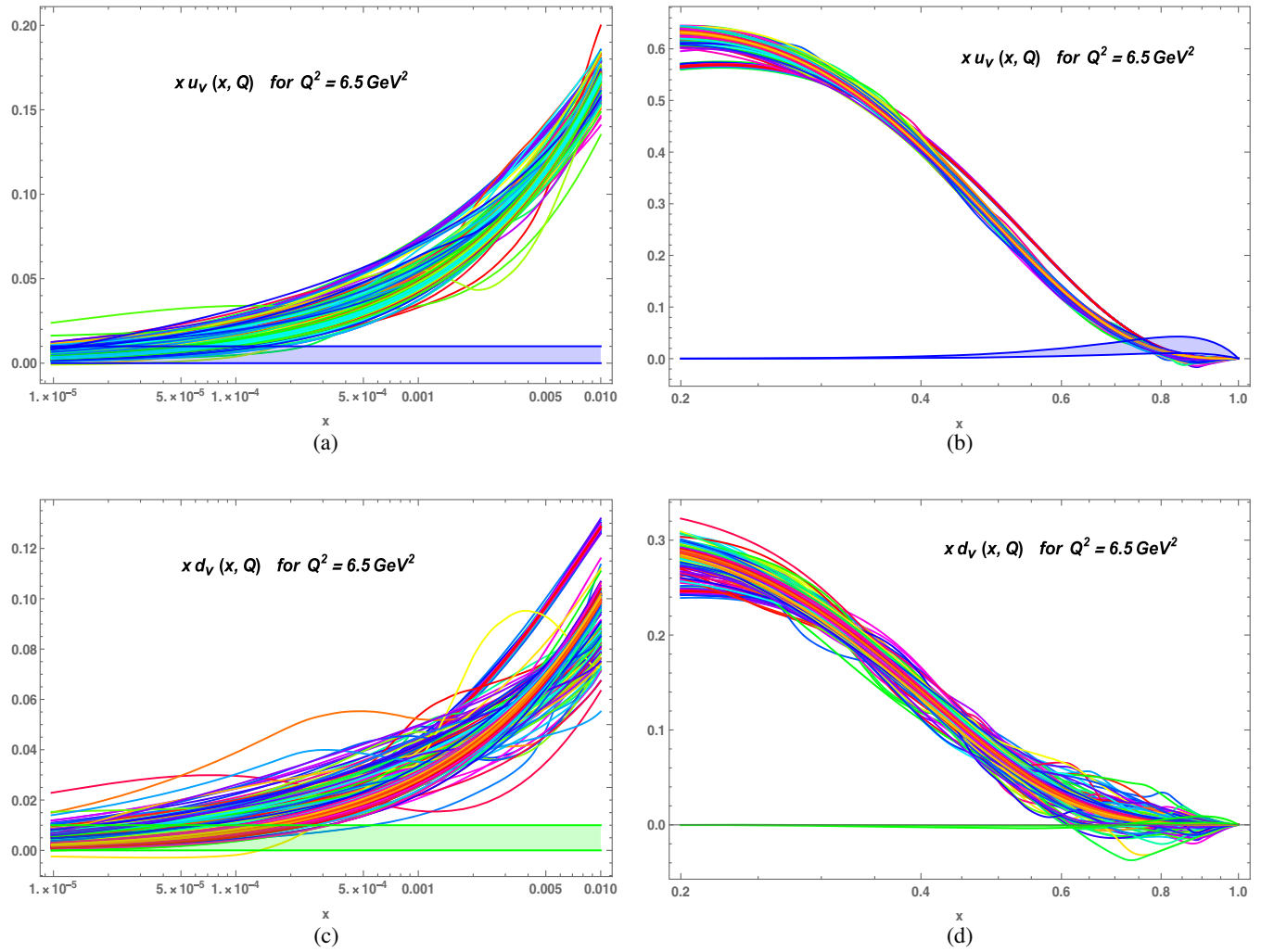

FIG. 8. (a),(b) Our holographic PDF sets (shown in blue band) compared to 292 PDF sets (shown in multiple solid lines) from CTEQ and LHAPDF projects incorporated within the ManeParse *Mathematica* package [35]. (c),(d) Our holographic PDF sets (shown in green band) compared to 292 PDF sets (shown in multiple solid lines) from CTEQ and LHAPDF projects incorporated within the ManeParse *Mathematica* package [35].

$Q^2 = 6.5$ GeV^2, following from (6.10). In Fig. 4(b) we show the behavior of the sea distributions $x\bar{u}(x,Q)$ in the lower blue dark band, and $x\bar{d}(x,Q)$ in the upper green light band at the same $Q^2 = 6.5$ GeV^2, following from (6.9). The normalization coefficients delimiting the bands are fixed to

$$(\tilde{\tilde{\mathcal{N}}}_L^+, \tilde{\tilde{\mathcal{N}}}_L^-) = (17.715, 30.667) \quad \text{(green light band: } d \text{ quark)},$$
$$(\tilde{\tilde{\mathcal{N}}}_L^+, \tilde{\tilde{\mathcal{N}}}_L^-) = (35.431, 61.335) \quad \text{(blue dark band: } u \text{ quark)}. \tag{6.17}$$

To assess the range of validity in parton x of the holographic results at large x, we reassess the reduced neutral charge $\sigma^{\pm}_{r,NC}(x,Q,s)$ as given in (6.6) solely in terms of the large-x holographic PDFs. The results are shown in Fig. 4 at low Q^2 for $\sqrt{s} = 5.565$ GeV. The orange data points are from JLAB [33]. The red data points are from the combined SLAC and BCDMS collaborations [30] (see Fig. 5.14 in [30]). Note that the $F_2(x,Q)$ data of [30] to $\sigma^{\pm}_{r,NC}(x,Q,s)$ where converted using (6.8). These results show that the range of validity of the holographic results at large x is limited to $0.75 \leq x \leq 1$ (see also below). Our results for the reported DIS $e^{\pm}p$ in Fig. 5 are consistent with the recent holographic results reported in [34] in the large-x regime (see Fig. 5 in [34]).

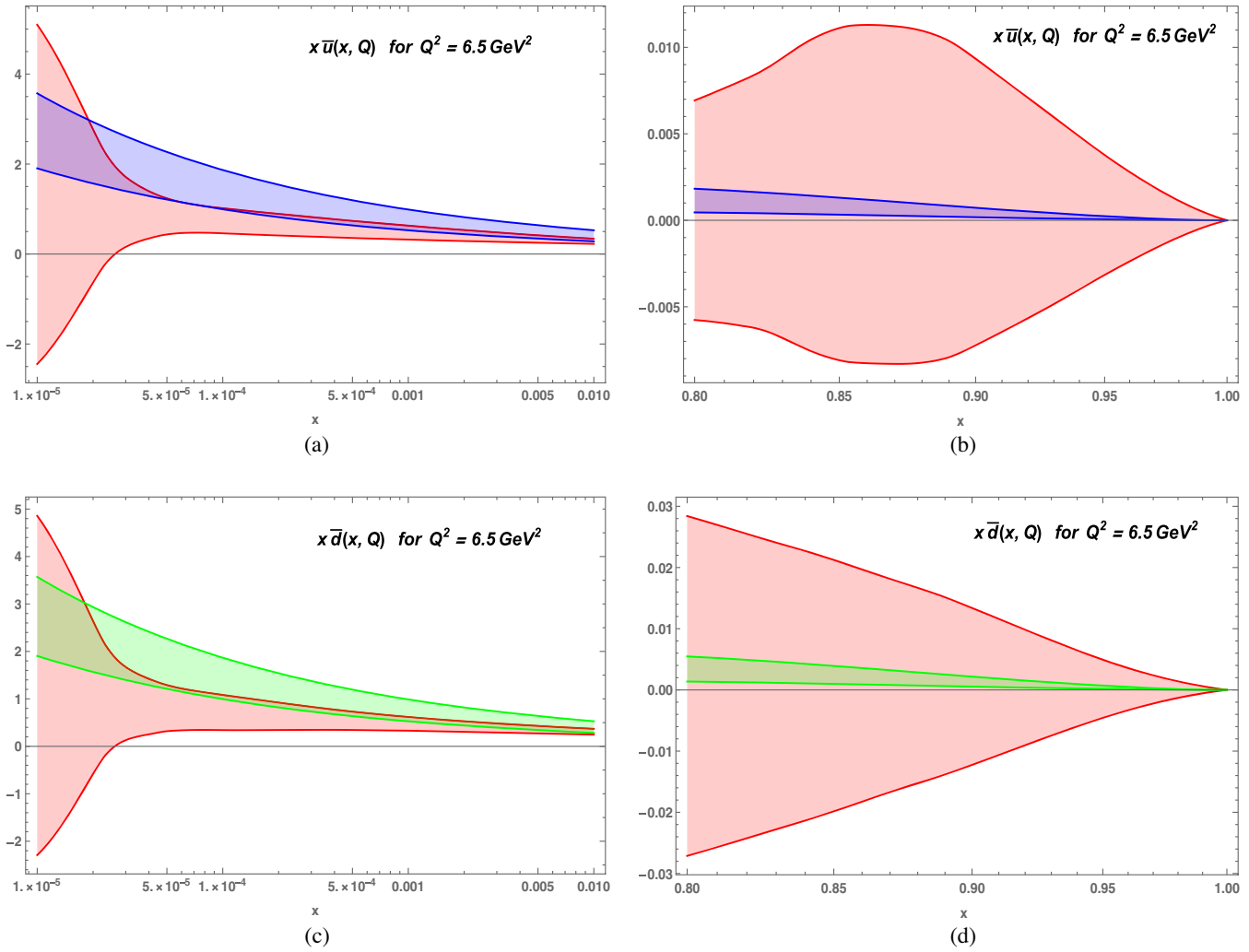

FIG. 9. (a),(b) Our holographic PDF sets (shown in blue band) compared to NNPDF collaboration PDF sets with error bars (shown in red band) from LHAPDF projects incorporated within the ManeParse *Mathematica* package [35]. (c),(d) Our holographic PDF sets (shown in green band) compared to NNPDF collaboration PDF sets with error bars (shown in red band) from LHAPDF projects incorporated within the ManeParse *Mathematica* package [35].

D. Structure functions at intermediate Q^2

To investigate further the range of validity of the holographic PDFs at intermediate Q^2 and large x, we show in Fig. 6(a) the holographic structure function $F_2(x)$ in (6.7) versus x at $Q^2 = 6.5$ GeV^2, evaluated using the results for the valence distributions shown in Fig. 4(a). The red data points are from the combined SLAC and BCDMS collaborations in [30] for $x = 0.65$, $x = 0.75$, and $x = 0.85$. In Fig. 6(b) we show the difference $\tilde{F}_2(x, Q) - F_2(x, Q)$ versus x as given in (6.7) for $Q^2 = 6.5$ GeV^2 using also the large-x holographic PDFs shown in Fig. 4. In Figs. 4(c)–4(f) we show, respectively, $F_2^{\gamma Z}(x, Q)$, $F_2^Z(x, Q)$, $F_3^{\gamma Z}(x, Q)$, and $F_3^Z(x, Q)$ versus large x for $Q^2 = 6.5$ GeV^2 using also the large-x holographic PDFs in Fig. 4. Figure 6(a) shows that the holographic results are compatible with the SLAC and BCDMS data [30] in the range $0.75 \leq x \leq 1$ for $Q^2 = 6.5$ GeV^2. Again, the normalization coefficients for the holographic valence PDFs setting the blue dark band are given in (6.17).

E. Comparison to the empirical CTEQ, LHAPDF, and NNPDF datasets

We have also compared our holographic PDF sets both for the small-x and large-x regimes for the valence and sea distributions, to 292 PDF sets from the CTEQ and LHAPDF projects incorporated within the ManeParse *Mathematica* package [35]. The global comparison is displayed in Figs. 7 and 8 for $Q^2 = 6.5$ GeV^2. Figures 8(a) and 8(c) show the 292 PDF sets in multiple solid lines from CTEQ and LHAPDF dataset [35], in comparison to our holographic PDF sets shown in blue light band for the up distributions, and in green light band for the

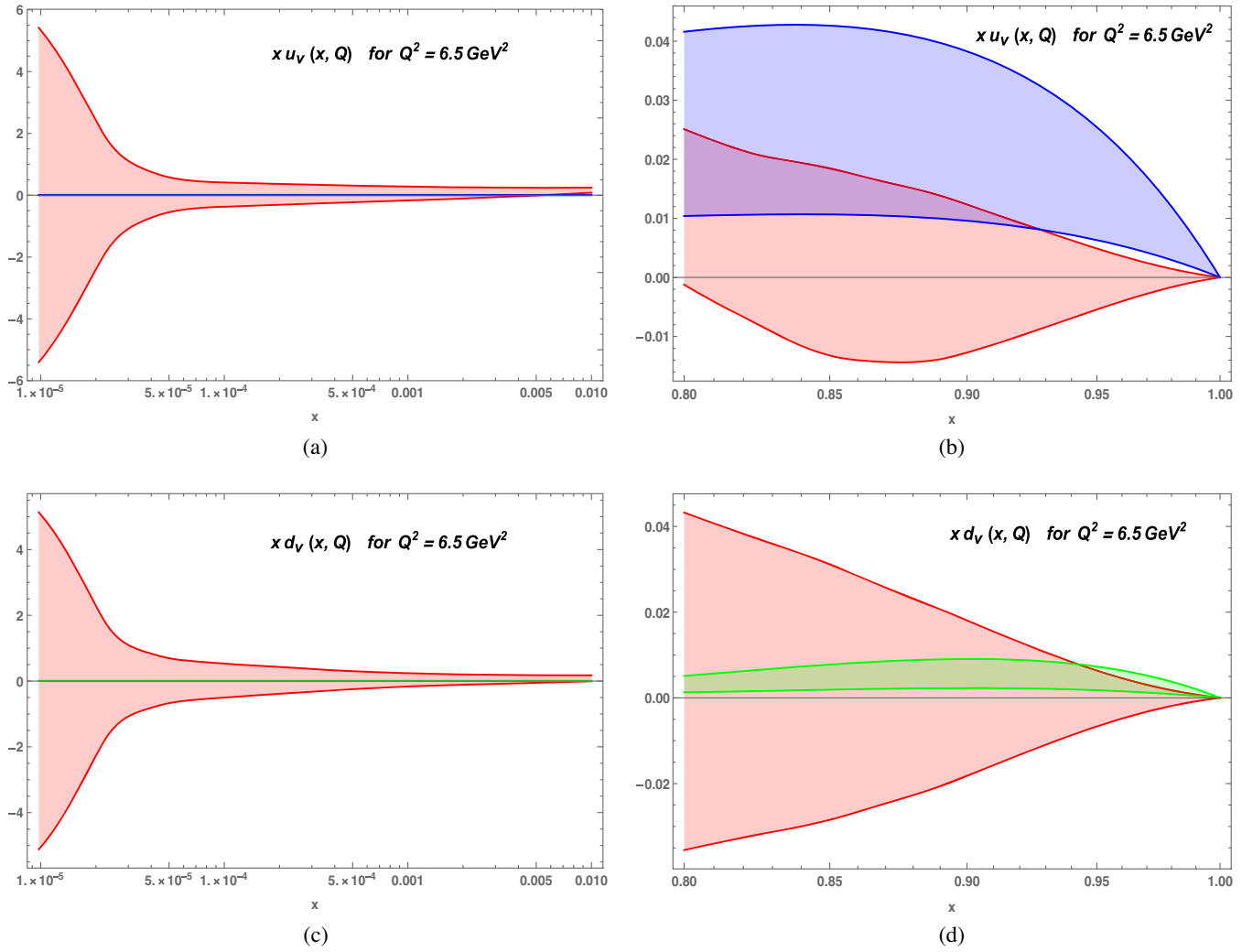

FIG. 10. (a),(b) Our holographic PDF sets (shown in green band) compared to NNPDF collaboration PDF sets with error bars (shown in red band) from LHAPDF projects incorporated within the ManeParse *Mathematica* package [35]. (c),(d) Our holographic PDF sets (shown in blue band) compared to NNPDF collaboration PDF sets with error bars (shown in red band) from LHAPDF projects incorporated within the ManeParse *Mathematica* package [35].

down distributions. The holographic growth at intermediate-x overcomes these datasets, but joins with a smaller subset of these data at very low x. Figures 8(b) and 8(d) show that the holographic sea at large x is relatively small but consistent overall with all the datasets in the expected applicability of our approach. A similar comparison for the holographic valence distributions is shown in Figs. 7(a) and 7(c) at low x and Figs. 8(b) and 8(d) at large x with consistency in both limits with the CTEQ and LHAPDF dataset [35].

In Fig. 9 we compare the holographic results for the sea distributions to the NNPDF collaboration PDF sets with error bars (shown in the red band) from the LHAPDF projects incorporated within the ManeParse *Mathematica* package [35]. Figures 9(a) and 9(c) show our results in blue dark band for the sea of up quarks, and in green light band for the sea of down quarks. Figures 9(b) and 9(d) show also our results for the sea of up and down quarks at large x. The growth of the holographic sea at low x is larger in the intermediate range but slower at very low x. At large x, our holographic results for the sea are relatively small but consistent with the reported dataset. In Fig. 10 the valence up and down distributions are compared to the same dataset with the same notations as for the sea. At low x, the holographic results are consistent with zero for the valence up and down quark distributions. At larger x, the holographic results are consistently larger for the up quark valence distribution in the region of validity of the holographic construction.

VII. CONCLUSIONS

We presented a comprehensive holographic derivation of DIS neutrino-nucleon scattering process using AdS/CFT duality formulated in a slice of AdS_5 with bulk U(2) valued

vector mesons to describe a tower of isovector and isoaxial particles, and a fermionic isodoublet to account for the even- and odd-parity proton and neutron excitations. To distinguish the vectors from the axials, chiral symmetry is broken either through a tachyon in the bifundamental representation both for the hard or soft wall model, or though boundary conditions for the hard wall. The Yukawa coupling of the bifundamental tachyon field between the even-odd bulk fermionic fields was ignored, since the DIS regime is mostly sensitive to the high lying part of the nuclon spectrum for which the effect is negligible.

Using Witten diagrams, we have derived the pertinent Dirac and Pauli form factors for both the direct or diagonal currents and the transition or off-diagonal currents. The results for the direct vector form factors are consistent with those in [20], and for the transition form factors they are consistent with those in [18]. To our knowledge, the results for the direct and transition axial form factors are new. We use them for a holographic estimate of the axial coupling g_A, which is directly sensitive to the explicit and implicit breaking of chiral symmetry.

We have used the transition form factors for the left currents to explicitly construct the s-channel contributions to neutrino and antineutrino DIS scattering through the pertinent Witten diagram. This has led to the explicit identification of the s-channel holographic contributions to the even- and odd-parity structure functions for both $W^{\pm}$ charged currents. The t-channel contributions stemming from the Reggeized Pomeron exchange is explicitly constructed and shown to dominate at low x the even-parity structure functions. The Reggeon exchange through the bulk Chern-Simons interaction is shown to dominate the low-x odd-parity structure function.

For intermediate values of Bjorken x, DIS scattering in holography is very different from QCD. The leading twist-2 operator in the operator product expansion (OPE) of the current-current (JJ) correlators acquire large anomalous dimension and are dwarfed by the double trace operators, which carry higher twists but are protected. In this regime, DIS scattering is off a poinlike hadron which is similar to scattering for $x \sim 1$. When $x \ll 1$, DIS scattering in QCD is dominated by Reggeon exchange and is dual to spin-2 or spin-1 Reggeized exchange in bulk. So lepton-nucleon scattering in holography allows us to probe the partonic content of the nucleon in the two regimes of $x \sim 1$ and $x \ll 1$.

We have carried explicit calculations and comparison to the available data both for the structure functions and PDFs from LHAPDF and CTEQ, in both of these regimes. Our results show consistency for large x for the intermediate range of $Q^2 < 10$ GeV^2 where scaling violations are still substantial. At low x our results show a somehow larger growth at intermediate but low x. The results at higher Q^2 resolution can be obtained through standard QCD evolution.

ACKNOWLEDGMENTS

K. M. is supported by the U.S. Department of Energy, Office of Science, Office of Nuclear Physics, Contract No. DEAC02-06CH11357, and an LDRD initiative at Argonne National Laboratory under Project No. 2020-0020. I. Z. is supported by the U.S. Department of Energy under Contract No. DE-FG-88ER40388.

APPENDIX A: $U_V(1)$ GAUGE FIELDS

The $U_V(1)$ gauge fields solves the equations of motion in bulk

$$\Box V^\mu + z e^{\tilde{\kappa}^2 z^2} \partial_z \left(e^{-\tilde{\kappa}^2 z^2} \frac{1}{z} \partial_z V^\mu \right) = 0,$$
$$\Box V_z - \partial_z (\partial_\mu V^\mu) = 0, \tag{A1}$$

subject to the gauge condition

$$\partial_\mu V^\mu + z e^{\kappa^2 z^2} \partial_z \left(e^{-\kappa^2 z^2} \frac{1}{z} V_z \right) = 0, \tag{A2}$$

and the boundary condition

$$V_\mu(z,y)|_{z\to 0} = \epsilon_\mu(q) e^{-iq\cdot y}, \tag{A3}$$

with polarization $\epsilon_\mu(q)$. The normalizable solutions in Kaluza-Klein (KK) modes are

$$V_\mu(z,y) = \epsilon_\mu(q) e^{-iq\cdot y} \Gamma\left(1+\frac{Q^2}{4\tilde{\kappa}^2}\right) \tilde{\kappa}^2 z^2 \mathcal{U}\left(1+\frac{Q^2}{4\tilde{\kappa}^2}; 2; \tilde{\kappa}^2 z^2\right),$$
$$V_z(z,y) = \frac{i}{2} \epsilon(q)\cdot q e^{-iq\cdot y} \Gamma\left(1+\frac{Q^2}{4\tilde{\kappa}^2}\right) z \mathcal{U}\left(1+\frac{Q^2}{4\tilde{\kappa}^2}; 1; \tilde{\kappa}^2 z^2\right), \tag{A4}$$

for $q^2 = Q^2 > 0$, where $\mathcal{U}(a;b;w)$ are the confluent hypergeometric functions of the second kind.

1. Bulk to boundary propagator

The non-normalizable wave function for the virtual photon is of the form $V_\mu(z,y) = \mathcal{V}(Q,z)\epsilon_\mu e^{-iq\cdot y}$, with $q^2 = -Q^2 < 0$ and

$$\mathcal{V}(Q,z) = g_5 \sum_n \frac{F_n \phi_n(z)}{Q^2 + m_n^2}. \tag{A5}$$

For the soft wall

$$\phi_n(z) = c_n \tilde{\kappa}^2 z^2 L_n^1(\tilde{\kappa}^2 z^2) \equiv J_A(m_n, z), \tag{A6}$$

with $c_n = \sqrt{2/n+1}$ fixed by the normalization condition

$$\int dz \sqrt{g} e^{-\phi} (g^{xx})^2 \phi_n(z) \phi_m(z) = \delta_{nm}. \tag{A7}$$

Also recall that $\mathcal{V}(Q,z)=\frac{1}{z}\partial_{z'}G(z,z')|_{z'=\epsilon}$, ties to the bulk to boundary propagator with

$$\mathcal{V}(Q,z)=\tilde{\kappa}^2z^2\Gamma\left(1+\frac{Q^2}{4\tilde{\kappa}^2}\right)\mathcal{U}\left(1+\frac{Q^2}{4\tilde{\kappa}^2};2;\tilde{\kappa}^2z^2\right)=\tilde{\kappa}^2z^2\int_0^1\frac{dx}{(1-x)^2}x^a\exp\left(-\frac{x}{1-x}\tilde{\kappa}^2z^2\right), \tag{A8}$$

and satisfies $\mathcal{V}(0,z)=\mathcal{V}(Q,0)=1$.

2. Bulk to bulk propagator

The bulk-to-bulk propagator for the massive mesons, for spacelike momenta ($q^2=-Q^2$), can be written as

$$G_{\mu\nu}(z,z')=i\mathcal{T}_{\mu\nu}G(z,z')=i\left(-\eta_{\mu\nu}+\frac{q_\mu q_\nu}{m_n^2}\right)G(z,z')=\sum_n J_V(m_n,z)\tilde{G}_{\mu\nu}(Q,m_n)J_V(m_n,z'), \tag{A9}$$

with

$$G(z,z')=-\sum_n\frac{\phi_n(z)\phi_n(z')}{Q^2+m_n^2}, \tag{A10}$$

and

$$J_V(m_n,z)=\phi_n(z),\qquad \tilde{G}_{\mu\nu}(Q,m_n)=\left(-\eta_{\mu\nu}+\frac{q_\mu q_\nu}{m_n^2}\right)\frac{-i}{Q^2+m_n^2}. \tag{A11}$$

Note that the bulk to boundary propagator follows by taking $z\to 0$, which simplifies (A10) as

$$G(z\to 0,z')\approx\left[-\frac{\phi_n(z\to 0)}{-g_5F_n}\right]\sum_n\frac{-g_5F_n\phi_n(z')}{Q^2+m_n^2}=\frac{z^2}{2}\sum_n\frac{g_5F_n\phi_n(z')}{Q^2+m_n^2}=\frac{z^2}{2}\mathcal{V}(Q,z'), \tag{A12}$$

where we used the fact that

$$F_n=\frac{1}{g_5}\left(-e^{-\phi}\frac{1}{z'}\partial_{z'}\phi_n(z')\right)_{z'=\epsilon}=-\frac{2}{g_5}c_n(n+1)\tilde{\kappa}^2, \tag{A13}$$

with $\phi_n(z\to 0)\approx c_n\tilde{\kappa}^2z^2(n+1)$. Note that the ratio in the bracket in (A12) is n independent! If we define the meson decay constant as $f_n=-F_n/m_n$, then we have

$$\phi_n(z)=\frac{f_n}{m_n}\times 2g_5\tilde{\kappa}^2z^2L_n^1(\tilde{\kappa}^2z^2), \tag{A14}$$

which is in line with vector meson dominance.

APPENDIX B: FERMIONIC FIELDS

We start by considering a general fermionic field in bulk AdS that solves the free Dirac equation in the presence of a soft wall. For that, we remove the dilaton field by rescaling

$$\Psi(y,z)=e^{+\tilde{\kappa}^2z^2/2}\tilde{\psi}(y,z), \tag{B1}$$

with the reduced field solving

$$\left[i\not{\partial}+\gamma^5\partial_z-\frac{2}{z}\gamma^5-\frac{1}{z}(M+\tilde{\kappa}^2z^2)\right]\tilde{\psi}(y,z)=0, \tag{B2}$$

where $\not{\partial}=\gamma^\mu\partial_\mu$. We now decompose the reduced field into two chiral copies

$$\tilde{\psi}(y,z) = \tilde{\psi}_L(y,z) + \tilde{\psi}_R(y,z), \qquad \tilde{\psi}_{L/R} = P_{L/R}\tilde{\psi}, \tag{B3}$$

with $(\gamma^5)^2 = 1$, and $P_{L/R} = P_{\mp} = \frac{1\mp\gamma^5}{2}$. The solution to (B2) follows by further reduction into L/R KK modes using

$$\tilde{\psi}_{L/R}(y,z) = e^{-iP\cdot y}\frac{1}{2}(1\mp\gamma^5)u_s(P)\frac{z^2}{R^2}\tilde{f}_{L/R}(z), \tag{B4}$$

with $u_s(P)$ a free Dirac spinor in four dimensions, and the L/R KK modes $\tilde{f}_{L/R}(z)$ now satisfying

$$\left[-\partial_z^2 + \tilde{\kappa}^4 z^2 + 2\tilde{\kappa}^2\left(M\mp\frac{1}{2}\right) + \frac{M(M\pm 1)}{z^2}\right]\tilde{f}_{L/R}(z) = P^2\tilde{f}_{L/R}(z). \tag{B5}$$

1. Spectrum and modes

The equation of motion (B5) has normalizable solutions only when P^2 has

$$P_n^2 = M_n^2 = 4\tilde{\kappa}^2\left(n + M + \frac{1}{2}\right), \tag{B6}$$

with $n = 0, 1, 2, \ldots$, which are

$$\begin{aligned}\tilde{f}_L^n(z) &= \sqrt{\frac{2\Gamma(n+1)}{\Gamma(n+M+3/2)}}\tilde{\kappa}^{M+3/2}z^{M+1}e^{-\tilde{\kappa}^2z^2/2}L_n^{M+1/2}(\tilde{\kappa}^2z^2),\\ \tilde{f}_R^n(z) &= \sqrt{\frac{2\Gamma(n+1)}{\Gamma(n+M+1/2)}}\tilde{\kappa}^{M+1/2}z^{M}e^{-\tilde{\kappa}^2z^2/2}L_n^{M-1/2}(\tilde{\kappa}^2z^2)\end{aligned} \tag{B7}$$

with the normalization condition

$$\int_0^\infty dz\tilde{f}_{L/R}^{n'}(z)\tilde{f}_{L/R}^{n}(z) = \delta_{n'n}. \tag{B8}$$

We can rewrite the normalized wave functions for the bulk Dirac fermion (or proton and neutron which correspond to the $n = 0$ states) as

$$\begin{aligned}\Psi(p,z) &= \psi_R(z)\Psi_R^0(p) + \psi_L(z)\Psi_L^0(p),\\ \bar{\Psi}(p,z) &= \psi_R(z)\bar{\Psi}_R^0(p) + \psi_L(z)\bar{\Psi}_L^0(p),\end{aligned} \tag{B9}$$

where for the soft wall

$$\begin{aligned}\psi_R(z) &= \frac{\tilde{n}_R}{\tilde{\kappa}^{\tau-2}}z^5\xi^{\frac{\tau-2}{2}}L_0^{(\tau-2)}(\xi),\\ \psi_L(z) &= \frac{\tilde{n}_L}{\tilde{\kappa}^{\tau-1}}z^5\xi^{\frac{\tau-1}{2}}L_0^{(\tau-1)}(\xi),\end{aligned} \tag{B10}$$

with $\xi = \tilde{\kappa}^2z^2$ and the generalized Laguerre polynomials $L_n^{(\alpha)}(\xi)$, $\tilde{n}_R = \tilde{n}_L\tilde{\kappa}^{-1}\sqrt{\tau-1}$, and $\tilde{n}_L = \tilde{\kappa}^\tau\sqrt{2/\Gamma(\tau)}$. The normalization of the bulk wave functions can also be rewritten as

$$\int_0^\infty dz\sqrt{g}e^{-\phi}e_a^\mu\psi_{R/L}^2(z) = \delta_a^\mu, \tag{B11}$$

with $\phi = \tilde{\kappa}^2 z^2$, and the inverse vielbein $e_a^\mu = \sqrt{|g^{\mu\mu}|}\delta_a^\mu$ (no summation intended in μ). The leading twist parameter is $\tau = 3$, and the free Weyl spinors $\Psi^0_{R/L}(p) = P_\pm u(p)$ and $\bar{\Psi}^0_{R/L}(p) = \bar{u}(p)P_\mp$ are tied to the free spinor normalization at the boundary

$$\bar{u}(p)u(p) = 2m_N, \qquad 2m_N \times \bar{u}(p')\gamma^\mu u(p) = \bar{u}(p')(p'+p)^\mu u(p). \tag{B12}$$

2. Bulk to boundary propagator

The bulk to boundary propagator (or the nonrenormalizable mode) of the bulk Dirac fermion is given by

$$\Psi(p,z) = \sum_n \frac{\sqrt{2g_5^2}F_n^R(p)\psi_n^R(z)}{p^2 - M_n^2} \times \Psi_R^0(p) + \sum_n \frac{\sqrt{2g_5^2}F_n^L(p)\psi_n^L(z)}{p^2 - M_n^2} \times \Psi_L^0(p), \tag{B13}$$

where the fermionic decay functions are defined as

$$\begin{aligned} F_n^R(p) &= \frac{1}{\sqrt{2g_5^2}} \times p\tilde{\kappa}\sqrt{\frac{2\Gamma(\tau-1+n)}{\Gamma(\tau-1)\Gamma(n+1)}}, \\ F_n^L(p) &= \frac{1}{\sqrt{2g_5^2}} \times M_n\tilde{\kappa}\sqrt{\frac{2\Gamma(\tau-1+n)}{\Gamma(\tau-1)\Gamma(n+1)}}. \end{aligned} \tag{B14}$$

Note that the on shell bulk Dirac fermions are just the residues at the poles $p^2 - m_n^2$ in (B13). The in-out baryonic states used in our DIS analysis throughout are

$$\begin{aligned} \Psi_i &= e^{-ip\cdot y}e^{+\tilde{\kappa}^2 z^2/2}\frac{z^2}{R^2}\left[\left(\frac{1-\gamma^5}{2}\right)u_{s_i}(p)\tilde{f}_L^0(z) + \left(\frac{1+\gamma^5}{2}\right)u_{s_i}(p)\tilde{f}_R^0(z)\right] \times \sqrt{2g_5^2} \times F_N(p), \\ \Psi_X &= e^{-iP_X\cdot y}e^{+\tilde{\kappa}^2 z^2/2}\frac{z^2}{R^2}\left[\left(\frac{1-\gamma^5}{2}\right)u_{s_X}(P_X)\tilde{f}_L^{n_X}(z) + \left(\frac{1+\gamma^5}{2}\right)u_{s_X}(P_X)\tilde{f}_R^{n_X}(z)\right] \times \sqrt{2g_5^2} \times F_X(P_X), \end{aligned} \tag{B15}$$

where s_i and s_X label the in-out spin, and identified $F_0^R = F_0^L = F_N(p)$ (ground state) and $F_n^R = F_n^L = F_X(P_X)$ (excited state).

3. Yukawa coupling through the tachyon

The inclusion of a bi-fundamental tachyon field $X(x,z)$ in bulk to lift the degeneracy between the vector and axial-vector mesons, would also imply a Yukawa coupling between the even-odd bulk fermionic fields $\Psi_{1,2}$ which we have not considered here. More specifically [12]

$$\mathcal{S}_{12,X} = \frac{1}{2g_5^2}\frac{g_X}{2}\int d^5x\sqrt{g}(\bar{\Psi}_1(x,z)X(x,z)\Psi_2(x,z) + \bar{\Psi}_2(x,z)X^\dagger(x,z)\Psi_1(x,z)), \tag{B16}$$

which would mix 1,2 and lifts the degeneracy of the low-lying even and odd parity states in the nucleon sector, $(\Psi_1 \pm \Psi_2)/\sqrt{2}$. A first order estimate in perturbation theory gives for the nucleon ground state with $n = 0$

$$\Delta M_\pm = \mp\frac{g_X}{4}\int\frac{dz}{z}X_0(z)(|\tilde{f}_L^0(z)|^2 - |\tilde{f}_R^0(z)|^2) = \mp\frac{g_X\sigma}{8\tilde{\kappa}^2}, \tag{B17}$$

with $X_0(z)$ given in (2.21). (B16) through the expansion around the vev, $X(x,z) \approx X_0(z)e^{i\Pi(x,z)}$, would also generate a contribution to the pion-nucleon coupling and also the axial charge of the direct and transition axial form factors [12]. Since our central interest is neutrino DIS scattering we can neglect this coupling and its effects on our results, as most of our

analysis involves the behavior near the UV boundary where the effects of σ is negligible both in the nucleonic wave functions and the spectrum.

APPENDIX C: DETAILS OF THE REGGEON EXCHANGE

The bulk gauge field $L^0_\mu(k,z)$ exchange contribution to the diffractive Compton scattering amplitude in the t channel is given by

$$\begin{aligned} i\mathcal{A}^L_{Lp\to Lp}(s,t) &= \sum_n i\tilde{\mathcal{A}}^L_{Lp\to Lp}(m_n,s,t),\\ i\tilde{\mathcal{A}}^L_{Lp\to Lp}(m_n,s,t) &= (-i)V^\mu_{LLL}(q,q',k,m_n)\times\tilde{G}_{\mu\nu}(m_n,t)\times(-i)V^\nu_{L\bar\Psi\Psi}(p_1,p_2,k,m_n), \end{aligned} \tag{C1}$$

with the bulk vertices ($k=p_2-p_1=q-q'$)

$$\begin{aligned} V^\mu_{LLL}(q,q',k,m_n) &\equiv \left(\frac{\delta S^k_{LLL}}{\delta(\epsilon^0_\mu\partial_z L^0(k,z))}\right)J_L(m_n,z)+\left(\frac{\delta S^k_{LLL}}{\delta(\epsilon^0_\mu L^0(k,z))}\right)J_L(m_n,z),\\ &= g_5^3\kappa_{CS}B^\mu(q,q',\epsilon^\pm)\int dz(\mathcal{V}(Q,z)\mathcal{V}(Q',z)\partial_z J_L(m_n,z)-\partial_z\mathcal{V}(Q,z)\mathcal{V}(Q',z)J_L(m_n,z)),\\ V^\nu_{L\bar\Psi\Psi}(p_1,p_2,k,m_n) &\equiv \left(\frac{\delta S^k_{L\bar\Psi\Psi}}{\delta(\epsilon^0_\nu L^0(k,z))}\right)J_L(m_n,z)=g_5\int dz\sqrt{g}e^{-\phi}z\bar\Psi(p_2,z)\gamma^\nu\Psi(p_1,z)J_L(m_n,z). \end{aligned} \tag{C2}$$

We have defined $p=(p_1+p_2)/2$, $t=-K^2$, $\mathcal{V}(Q,z)\equiv L(q=\sqrt{-Q^2},z)$ as given in (A8), and used the bulk-to-bulk gauge field propagator (A9) with the substitutions $q\to k$, $Q\to K$, and $V\to L$. We have also used the vertices in (5.24), and defined

$$B^\mu(q,q',\epsilon^\pm)\equiv(-i)\epsilon^{\rho\sigma\nu\mu}\epsilon^+_\rho(q)\epsilon^-_\sigma(q')(q'_\nu+q_\nu). \tag{C3}$$

For $z'\to 0$, we can use (A12) and simplify (C1) as

$$i\mathcal{A}^L_{Lp\to Lp}(s,t)\approx(-i)\mathcal{V}^\mu_{LLL}(q_1,q_2,k_z)\times(-i\eta_{\mu\nu})\times(-i)\mathcal{V}^\nu_{L\bar\Psi\Psi}(p_1,p_2,k_z), \tag{C4}$$

with

$$\begin{aligned} \mathcal{V}^\mu_{LLL}(q_1,q_2,k_z) &= g_5^3\kappa_{CS}B^\mu(q,q',\epsilon^\pm)\int dz\left(\mathcal{V}(Q,z)\mathcal{V}(Q',z)z-\partial_z\mathcal{V}(Q,z)\mathcal{V}(Q',z)\frac{z^2}{2}\right),\\ \mathcal{V}^\nu_{L\bar\Psi\Psi}(p_1,p_2,k_z) &= g_5\times\frac{3}{2}\times\int dz\sqrt{g}e^{-\phi}z\bar\Psi(p_2,z)\gamma^\nu\Psi(p_1,z)\mathcal{V}(K,z)=g_5F_1^{(LN)}(K), \end{aligned} \tag{C5}$$

where $\mathcal{V}(K,z)\equiv L^0(k=\sqrt{-K^2},z)$, and $F_1^{(LN)}(K)$ is the form factor of the nucleon due to L^0_μ.

The Reggeization of the bulk spin-1 gauge field $L^0_\mu(k,z)$ exchange can be obtained, in a similar way to the Reggezation of the spin-2 graviton exchange, through the substitution

$$J_L(m_n(j),z)\to z^{-(j-1)}\phi_n(j,z)=z^{-(j-1)}\frac{\tilde\phi_n(j,z)}{z} \tag{C6}$$

followed by the summation over all spin-j meson exchanges using the Sommerfeld-Watson formula

$$\frac{1}{2}\sum_{j\geq 1}(s^{j-1}+(-s)^{j-1})\to-\frac{\pi}{2}\int_{\mathbb{C}}\frac{dj}{2\pi i}\left(\frac{s^{j-1}+(-s)^{j-1}}{\sin\pi j}\right). \tag{C7}$$

The contour $\mathbb{C}$ is to the left of all odd poles $j=1,3,\ldots$ (in contrast to the Reggeized graviton where the contour is chosen to the left of the even poles), and requires the analytical continuation of the exchanged amplitudes to the complex j plane.

The spin-j normalized meson wave functions $J_L(m_n(j),z)$ (C6) are expressed in terms of the wave functions of massive scalar fields $\tilde{\phi}_n(j,z)$ which are given, for the soft wall model, in terms of the generalized Laguerre polynomials as

$$\tilde{\phi}_n(j,z) = c_n(j) z^{\Delta(j)} L_n^{\Delta(j)-2}(w), \tag{C8}$$

with $w=\tilde{\kappa}^2 z^2$. The normalization coefficients are

$$c_n(j) = \left(\frac{2\tilde{\kappa}^{2(\Delta(j)-1)}\Gamma(n+1)}{\Gamma(n+\Delta(j)-1)}\right)^{\frac{1}{2}}, \tag{C9}$$

and the dimension of the massive scalar fields (with an additional mass coming from the massive open string states attached to the D9- or D7-branes) $\Delta(j)$ is given by

$$\begin{aligned}\Delta(j) &= 2+\sqrt{4+m^2R^2+\frac{R^2}{\alpha'}(j-1)},\\ &= 2+\sqrt{\sqrt{\lambda}(j-j_0)},\end{aligned} \tag{C10}$$

where, in the last line, we have used the fact that $m^2R^2=-3$. The spin-1 transverse bulk gauge field defined as $zL_\mu^0(m_n,z)$ obeys the same bulk equation of motion as a bulk massive scalar field $\tilde{\phi}_n(j=1,z)$ with $m^2R^2=-3$ which is manifest in (E10). We have also used the open string quantized mass spectrum $m_j^2R^2=(j-1)(R^2/\alpha')=\sqrt{\lambda}(j-1)$ for open strings attached to the D9- or D7-branes in bulk, and we have defined $j_0=1-1/\sqrt{\lambda}$.

We now recall that the non-normalized bulk-to-boundary propagators of massive scalar fields are given in terms of Kummer's (confluent hypergeometric) function of the second kind, and their integral representations are (for spacelike momenta $k^2=-K^2$)

$$\begin{aligned}\tilde{\mathcal{V}}(j,K,z) &= z^{\Delta(j)}U\left(a_K+\frac{\Delta(j)}{2},\Delta(j)-1;w\right) = z^{\Delta(j)}w^{2-\Delta(j)}U(\tilde{a}(j),\tilde{b}(j);w),\\ &= z^{\Delta(j)}w^{2-\Delta(j)}\frac{1}{\Gamma(\tilde{a}(j))}\int_0^1 dx x^{\tilde{a}(j)-1}(1-x)^{-\tilde{b}(j)}\exp\left(-\frac{x}{1-x}w\right),\end{aligned} \tag{C11}$$

with $w=\tilde{\kappa}^2z^2$

$$a_K = a = \frac{K^2}{4\tilde{\kappa}^2}, \qquad \tilde{a}(j) = a_K+2-\frac{\Delta(j)}{2}, \qquad \tilde{b}(j)=3-\Delta(j), \tag{C12}$$

after using the identity $U(m,n;y)=y^{1-n}U(1+m-n,2-n,y)$. Therefore, the bulk-to-bulk propagator of spin-j mesons

$$J_L(m_n(j),z)G(j,z,z')J_L(m_n(j),z') = z^{-(j-1)}G(j,z,z')z'^{-(j-1)} \tag{C13}$$

can be approximated at the boundary as (for spacelike momenta $k^2=-K^2$)

$$\begin{aligned}G(j,z\to 0,z') &\approx -\left[\frac{\phi_n(j,z\to 0)}{-g_5\mathcal{F}_n(j)}\right]\times\sum_n\frac{-g_5\mathcal{F}_n(j)\phi_n(j,z')}{K^2+m_n^2(j)},\\ &= (\tilde{\kappa}^2)^{\Delta(j)-2}\frac{z^{\Delta(j)-1}}{\Delta(j)-1}\frac{\Gamma(\Delta(j)-2+a)}{\Gamma(\Delta(j)-2)}\mathcal{V}(j,K,z'),\end{aligned} \tag{C14}$$

where $\phi_n(j,z\to 0)=\frac{1}{z}\tilde{\phi}_n(j,z\to 0)$. We have defined the non-normalized bulk-to-boundary propagator of spin-j mesons

$$\mathcal{V}(j,K,z') = \sum_n\frac{-g_5\mathcal{F}_n(j)\phi_n(j,z')}{K^2+m_n^2(j)} = \frac{1}{z}\tilde{\mathcal{V}}(j,K,z')\Big|_{a+\frac{\Delta(j)}{2}\to a+1+(\Delta(j)-3)}, \tag{C15}$$

with the shift $a+\frac{\Delta(j)}{2}\to a+1+(\Delta(j)-3)$ defined in such a way that the mass spectrum of massive scalar fields $m_n^2=4\tilde{\kappa}^2(n+\frac{\Delta(j=1)}{2})$ and the mass spectrum of spin-1 gauge fields $m_n^2=4\tilde{\kappa}^2(n+1)$ match, i.e., we shift $n+\frac{\Delta(j=1)}{2}\to n+1+(\Delta(j=1)-3)$, giving the mass spectrum of spin-j mesons

$$m_n^2(j)=4\tilde{\kappa}^2(n+1+(\Delta(j)-3)). \tag{C16}$$

We have also used

$$\begin{aligned}\mathcal{F}_n(j)&=\frac{\mathcal{C}(j,K,\epsilon)}{g_5}(-\sqrt{g}e^{-\phi}(g^{xx})^2\partial_{z'}\phi_n(j,z'))_{z'=\epsilon},\\ \mathcal{C}(j,K,\epsilon)&=\mathcal{V}(j,K,\epsilon),\end{aligned} \tag{C17}$$

and the substitution $\phi_n(j,z\to 0)=\frac{1}{z}\tilde{\phi}_n(j,z\to 0)\approx c_n(j)z^{\Delta(j)-1}L_n^{\Delta(j)-2}(0)$ for the soft wall model.

After the Reggeization, the scattering amplitude for the spin-j meson exchange becomes

$$i\mathcal{A}^L_{Lp\to Lp}(j,s,t)\approx(-i)\mathcal{V}^{\mu}_{LLL}(j,q_1,q_2,k_z)\times(-i\eta_{\mu\nu})\times(-i)\mathcal{V}^{\nu}_{L\bar{\Psi}\Psi}(j,p_1,p_2,k_z), \tag{C18}$$

with

$$\begin{aligned}\mathcal{V}^{\mu}_{LLL}(j,q_1,q_2,k_z)&=\frac{1}{g_5^2}\times g_5^3\kappa_{CS}B^{\mu}(q,q',\epsilon^{\pm})\int dz z^{2(j-1)}\\&\quad\times\left(\mathcal{V}(Q,z)\mathcal{V}(Q',z)\times\frac{(\Delta(j)-1-(j-1))z^{\Delta(j)-1-(j-1)-1}}{\Delta(j)-1}\right.\\&\quad\left.-\partial_z\mathcal{V}(Q,z)\mathcal{V}(Q',z)\times\frac{z^{\Delta(j)-1-(j-1)}}{\Delta(j)-1}\right)\times(\tilde{\kappa}^2)^{\Delta(j)-2}\frac{\Gamma(\Delta(j)-2+a)}{\Gamma(\Delta(j)-2)},\\&=\mathcal{V}_{LLL}(j,Q,Q')\times B^{\mu}(q,q',\epsilon^{\pm}),\\\mathcal{V}^{\nu}_{L\bar{\Psi}\Psi}(p_1,p_2,k_z)&=g_5\times\frac{3}{2}\times\int dz\sqrt{g}e^{-\phi}z^{1+2(j-1)}\bar{\Psi}(p_2,z)\gamma^{\nu}\Psi(p_1,z)z^{-(j-1)}\mathcal{V}(j,K,z),\\&=g_5F_1^{(LN)}(j,K)\times\bar{u}(p_2)\gamma^{\nu}u(p_1).\end{aligned} \tag{C19}$$

We have defined

$$\begin{aligned}\mathcal{V}_{LLL}(j,Q,Q')&=\frac{1}{g_5^2}\times g_5^3\kappa_{CS}\int dz\, z^{2(j-1)}\\&\quad\times\left(\mathcal{V}(Q,z)\mathcal{V}(Q',z)\times\frac{(\Delta(j)-1-(j-1))z^{\Delta(j)-1-(j-1)-1}}{\Delta(j)-1}\right.\\&\quad\left.-\partial_z\mathcal{V}(Q,z)\mathcal{V}(Q',z)\times\frac{z^{\Delta(j)-1-(j-1)}}{\Delta(j)-1}\right)(\tilde{\kappa}^2)^{\Delta(j)-2}\frac{\Gamma(\Delta(j)-2+a)}{\Gamma(\Delta(j)-2)},\\&=\frac{1}{g_5^2}\times g_5^3\kappa_{CS}\times Q^{2-j-\Delta(j)}\times I_{\xi}(j,Q,Q')\times\tilde{\kappa}^{2\Delta(j)-4}\times\frac{\Gamma(\Delta(j)-2+a)}{\Gamma(\Delta(j)-2)}\times\frac{1}{\Delta(j)-1},\end{aligned} \tag{C20}$$

with

$$I_\xi(j,Q,Q') = \int d\xi \xi^{j-2+\Delta(j)}(\mathcal{V}(\xi)\mathcal{V}(\xi Q'/Q)\times(\Delta(j)-1-(j-1))\xi^{-1} - \partial_\xi \mathcal{V}(\xi)\mathcal{V}(\xi Q'/Q)),$$
$$\approx (\Delta(j)-1-(j-1))\times 2^{\Delta(j)+j-3}\frac{Q'}{Q}G^{2,2}_{2,2}\left(\frac{Q^2}{Q'^2}\middle|\begin{matrix}\frac{1}{2},\frac{3}{2}\\ \frac{1}{2}(j+\Delta(j)-1),\frac{1}{2}(j+\Delta(j)+1)\end{matrix}\right)$$
$$+ 2^{\Delta(j)+j-2}\frac{Q'}{Q}G^{2,2}_{2,2}\left(\frac{Q^2}{Q'^2}\middle|\begin{matrix}\frac{1}{2},\frac{3}{2}\\ \frac{1}{2}(j+\Delta(j)+1),\frac{1}{2}(j+\Delta(j)+1)\end{matrix}\right), \tag{C21}$$

where $G^{m,n}_{p,q}(z|\begin{smallmatrix}a_1,\ldots,a_p\\ b_1,\ldots,b_q\end{smallmatrix})$ is the Meijer G function. We have used the identities

$$\lim_{\frac{Q}{\tilde\kappa}\to\infty}\mathcal{V}(\xi) = \xi K_1(\xi) \quad \text{and} \quad \partial_\xi(\xi^\nu K_\nu(\xi)) = -\xi^\nu K_{\nu-1}(\xi) \tag{C22}$$

to evaluate the integrals with $\xi = Qz$. The function $F_1^{(LN)}(j,K)$ in (C19) admits the integral representation

$$F_1^{(LN)}(j,K) = \frac{3}{2}\times\frac{1}{2}\frac{\tilde\kappa^{-(j-1)-\Delta(j)-1}}{\Gamma(a)}\int_0^1 dx\, x^{a-1}(1-x)^{-\tilde b(j)}$$
$$\times\left(\left(\frac{\tilde n_R}{\tilde\kappa^{\tau-1}}\right)^2\times\Gamma(c(j))\left(\frac{1}{1-x}\right)^{-c(j)} + \left(\frac{\tilde n_L}{\tilde\kappa^{\tau}}\right)^2\times\Gamma(c(j)+1)\left(\frac{1}{1-x}\right)^{-(c(j)+1)}\right),$$
$$= \frac{3}{2}\times\frac{1}{2}\tilde\kappa^{-(j-1)-\Delta(j)-1}$$
$$\times\left(\left(\frac{\tilde n_R}{\tilde\kappa^{\tau-1}}\right)^2\times\frac{\Gamma(c(j))\Gamma(1-\tilde b(j)+c(j))}{\Gamma(1-\tilde b(j)+c(j)+a)} + \left(\frac{\tilde n_L}{\tilde\kappa^{\tau}}\right)^2\times\frac{\Gamma(c(j)+1)\Gamma(2-\tilde b(j)+c(j))}{\Gamma(2-\tilde b(j)+c(j)+a)}\right), \tag{C23}$$

where

$$\tilde b(j) = 3-\Delta(j), \qquad c(j) = (\tau+1)+\frac{j-1}{2}-\frac{\Delta(j)}{2}-\frac{1}{2}. \tag{C24}$$

After summing over all contributions from the spin-j mesons, the total amplitude $\mathcal{A}^{\rm tot}_{Lp\to Lp}(s,t)$ is given by

$$\mathcal{A}^{\rm tot}_{Lp\to Lp}(s,t) = -\int_{\mathbb{C}}\frac{dj}{2\pi i}\left(\frac{s^{j-1}+(-s)^{j-1}}{\sin\pi j}\right)\mathcal{A}^{L}_{Lp\to Lp}(j,s,t),$$
$$\mathcal{A}^{L}_{Lp\to Lp}(j,s,t) = \mathcal{V}_{LLL}(j,Q,Q')\times B^\mu(q,q',\epsilon^\pm)\times g_5 F_1^{(LN)}(j,K)\times\bar u(p_2)\gamma_\mu u(p_1), \tag{C25}$$

The contour $\mathbb{C}$ is at the rightmost of the branch point of $F_1^{LN}(j,K)$ and the leftmost of $j=1,3,\ldots$. From (C25), we determine the single Reggeon amplitude (total amplitude) in momentum space, after wrapping the j-plane contour $\mathbb{C}$ to the left,

$$\mathcal{A}^{\rm tot}_{Lp\to Lp}(s,t) = -s^{j_0-1}\int_{-\infty}^{j_0}\frac{dj}{\pi}\left(\frac{1+e^{-i\pi}}{\sin\pi j}\right)s^{j-j_0}\mathrm{Im}[\mathcal{A}^{L}_{Lp\to Lp}(j,s,t)]. \tag{C26}$$

The imaginary part follows from the discontinuity of the Γ function

$$\mathrm{Im}[\mathcal{A}^{L}_{Lp\to Lp}(j,s,t)] \approx (\Gamma(\Delta(j)-2)\mathcal{V}_{LLL}(j,Q,Q')\times B^\mu(q,q',\epsilon^\pm)\times g_5 F_1^{(LN)}(j,K)\times\bar u(p_2)\gamma_\mu u(p_1))|_{j\to j_0,\Delta(j)\to 2}$$
$$\times\,\mathrm{Im}\left[\frac{1}{\Gamma(\tilde\Delta(j))}\right], \tag{C27}$$

with the complex argument

$$\tilde{\Delta}(j) = \Delta(j) - 2 = i\sqrt{\sqrt{\lambda}(j_0 - j)} \equiv iy \tag{C28}$$

and $j_0 = 1 - 1/\sqrt{\lambda}$. For $y \to 0$, we may approximate $1/\Gamma(iy) \approx iye^{iy\gamma}$, with the Euler-Mascheroni constant $\gamma = 0.55772\ldots$. The single Reggeon amplitude (total amplitude) in momentum space (C25) can now be cast in block form

$$\mathcal{A}^{\rm tot}_{Lp\to Lp}(s,t) = I(j_0,s) \times G_5(j_0,s,t), \tag{C29}$$

with

$$I(j_0,s) = -\tilde{s}^{j_0}\int_{-\infty}^{j_0}\frac{dj}{\pi}\left(\frac{1+e^{-i\pi}}{\sin\pi j}\right)\tilde{s}^{j-j_0}\sin\left[\tilde{\xi}\sqrt{\sqrt{\lambda}(j_0-j)}\right],$$
$$G_5(j_0,s,t) = \frac{1}{\tilde{s}}(\tilde{\kappa}^{2(j-1)}\Gamma(\Delta(j)-2)\mathcal{V}_{LLL}(j,Q,Q') \times B^{\mu}(q,q',\epsilon^{\pm}) \times g_5 F_1^{(LN)}(j,K) \times \bar{u}(p_2)\gamma_{\mu}u(p_1))|_{j\to j_0,\Delta(j)\to 2}, \tag{C30}$$

We have set $\tilde{s} \equiv s/\tilde{\kappa}^2$, and $\tilde{\xi} - \pi/2 = \gamma = 0.55772\ldots$ is Euler-Mascheroni constant. We note that the apparent pole in the Gamma function at the Reggeon intercept, cancels out in the combination $\Gamma(\Delta(j_0)-2)\mathcal{V}_{LLL}(j_0,Q,Q')$.

In the block form (C29), the spin-j integral $I(j_0,s)$ is similar to the spin-j integral in [27] [see Eq. (4.19)], with the identifications $\mathcal{K}(s,b^{\perp},z,z') \leftrightarrow \mathcal{A}^{\rm tot}_{Lp\to Lp}(s,t)$, $(zz'/R^4)G_3(j_0,v) \leftrightarrow G_5(j_0,s,t)$, $\xi(v) \leftrightarrow \tilde{\xi}$, and $\hat{s} \leftrightarrow \tilde{s}$. We then follow [27] to evaluate the spin-j integral by closing the j-contour appropriately. In the high energy limit $\sqrt{\lambda}/\tilde{\tau} \to 0$ ($\tilde{\tau} \equiv \log\tilde{s}$), the single Reggeon contribution to the amplitude is

$$\mathcal{A}^{\rm tot}_{Lp\to Lp}(s,t) \simeq e^{j_0\tilde{\tau}}[(\sqrt{\lambda}/\pi)+i](\sqrt{\lambda}/2\pi)^{1/2}\tilde{\xi}\frac{e^{-\sqrt{\lambda}\tilde{\xi}^2/2\tilde{\tau}}}{\tilde{\tau}^{3/2}}\left(1+\mathcal{O}\left(\frac{\sqrt{\lambda}}{\tilde{\tau}}\right)\right) \times G_5(j_0,s,t). \tag{C31}$$

We can rewrite the amplitude (C31) as

$$\mathcal{A}^{\rm tot}_{Lp\to Lp}(s,t) \simeq 4\times 4\times g_5 \times \frac{1}{g_5^2}\times g_5^3\kappa_{CS}\times\left(\frac{Q}{\tilde{\kappa}}\right)^{2-j_0-\Delta(j_0)}\times\left(\frac{s}{\tilde{\kappa}^2}\right)^{j_0}\times\frac{e^{-\sqrt{\lambda}\tilde{\xi}^2/2\log[s/\tilde{\kappa}^2]}}{(\log[s/\tilde{\kappa}^2])^{3/2}}$$
$$\times[(\sqrt{\lambda}/\pi)+i]\times(\sqrt{\lambda}/2\pi)^{1/2}\tilde{\xi}\left(1+\mathcal{O}\left(\frac{\sqrt{\lambda}}{\log[s/\tilde{\kappa}^2]}\right)\right)\times\tilde{G}_5(j_0,t,Q,Q'), \tag{C32}$$

where

$$\tilde{G}_5(j_0,s,t) \equiv \frac{1}{4}\times\frac{1}{4}\times\frac{1}{g_5}\times\frac{1}{\frac{1}{g_5^2}\times g_5^3\kappa_{CS}}\times\frac{1}{\tilde{\kappa}^2}\times\frac{1}{Q^{2-j-\Delta(j)}}\times\frac{1}{\kappa^{2\Delta(j)-4}}\times\frac{1}{\tilde{\kappa}^{-(j-1)-\Delta(j)-1}}\times\frac{1}{\tilde{\kappa}^{2(j-1)}}\times G_5(j_0,s,t),$$
$$= I_{\xi}(j_0,Q,Q')\times\mathcal{F}_1^{(LN)}(j_0,K)\times s^{-1}\times\frac{1}{4}\times B^{\mu}(q,q',\epsilon^{\pm})\times\frac{1}{4}\times\bar{u}(p_2)\gamma_{\mu}u(p_1), \tag{C33}$$

with

$$\mathcal{F}_1^{(LN)}(j_0,K) \equiv \frac{\Gamma(\Delta(j_0)-2+a)}{\Delta(j_0)-1}\times\frac{1}{\tilde{\kappa}^{-(j_0-1)-\Delta(j_0)-1}}\times F_1^{(LN)}(j_0,K). \tag{C34}$$

APPENDIX D: DETAILS OF THE POMERON EXCHANGE

The transverse and traceless part of the graviton ($\eta_{\mu\nu} \to \eta_{\mu\nu} + h_{\mu\nu}$) follows from the quadratic part of the Einstein-Hilbert action in de Donder gauge,

$$S = \int d^5x\sqrt{g}e^{-2\phi}\mathcal{L}_h,$$
$$\mathcal{L}_h = -\frac{1}{4\tilde{g}_5^2} g^{\mu\nu}\eta^{\lambda\rho}\eta^{\sigma\tau}\partial_\mu h_{\lambda\sigma}\partial_\nu h_{\rho\tau}, \tag{D1}$$

with Newton constant $16\pi G_N = 8\pi^2/N_c^2 = \tilde{g}_5^2 = 2\kappa^2$. The massive glueball spectrum is determined by solving the equation of motion for $h_{\mu\nu}$ following from (D1), with for spin-2 glueballs

$$m_n^2 = 8\tilde{\kappa}_N^2(n+1), \qquad \tilde{g}_5 f_n = 2\tilde{\kappa}_N \tag{D2}$$

1. Graviton coupling in bulk

For the graviton in the axial gauge $h_{\mu z} = h_{zz} = 0$. Using $\eta_{\mu\nu} \to \eta_{\mu\nu} + h_{\mu\nu}$ in the linearized bulk action gives

$$h\bar{\Psi}\Psi\colon -\frac{\sqrt{2\kappa^2}}{2}\int d^5x\sqrt{g}h_{\mu\nu}T_F^{\mu\nu},$$
$$hLL\colon -\frac{\sqrt{2\kappa^2}}{2}\int d^5x\sqrt{g}h_{\mu\nu}T_L^{\mu\nu}, \tag{D3}$$

with the energy-momentum tensors for the fermions and left gauge fields

$$T_F^{\mu\nu} = e^{-\phi}\frac{i}{2}z\bar{\Psi}\gamma^\mu\overleftrightarrow{\partial^\nu}\Psi - \eta^{\mu\nu}\mathcal{L}_F,$$
$$T_L^{\mu\nu} = -e^{-\phi}(z^4\eta^{\rho\sigma}\eta^{\mu\beta}\eta^{\nu\gamma}F^L_{\beta\rho}F^L_{\gamma\sigma} - z^4\eta^{\mu\beta}\eta^{\nu\gamma}F^L_{\beta z}F^L_{\gamma z}) - \eta^{\mu\nu}\mathcal{L}_L, \tag{D4}$$

and the rescaling

$$\Psi \to \sqrt{2g_5^2}\Psi, \qquad L_N \to g_5 L_N, \qquad h_{\mu\nu} \to \sqrt{2\kappa^2}h_{\mu\nu}. \tag{D5}$$

Evaluating the couplings or the vertices (D3) on the solutions, Fourier transforming the fields to momentum space, and integrating by part the trace-full part for the fermions, we find for the couplings to the fermions ($h\bar{\Psi}\Psi$) to the left gauge fields (hLL)

$$h\bar{\Psi}\Psi\colon \int \frac{d^4p_2d^4p_1d^4k}{(2\pi)^{12}}(2\pi)^4\delta^4(p_2 - k - p_1)(S^k_{h\bar{\Psi}\Psi}),$$
$$hLL\colon \int \frac{d^4q'd^4qd^4k}{(2\pi)^{12}}(2\pi)^4\delta^4(q - k - q')(S^k_{hLL}), \tag{D6}$$

with

$$S^k_{h\bar{\Psi}\Psi} = -\frac{\sqrt{2\kappa^2}}{2}\int dz\sqrt{g}e^{-\phi}z\epsilon^{TT}_{\mu\nu}h(k,z)\bar{\Psi}(p_2,z)\gamma^\mu p^\nu\Psi(p_1,z),$$
$$S^k_{hLL} = \sqrt{2\kappa^2}\int dz\sqrt{g}e^{-\phi}z^4\epsilon^{TT}_{\mu\nu}h(k,z)K^{\mu\nu}(q,q',\epsilon,\epsilon',z). \tag{D7}$$

We have set $h_{\mu\nu} = \epsilon^{TT}_{\mu\nu}h(k,z)$ (where $\epsilon^{TT}_{\mu\nu}$ is transverse and traceless polarization tensor), $q^2 = -Q^2$, $q'^2 = -Q'^2$ for spacelike momenta, and defined

$$K^{\mu\nu}(q,q',\epsilon,\epsilon',z) \equiv B_1^{\mu\nu}\mathcal{V}(Q,z)\mathcal{V}(Q',z) - B_0^{\mu\nu}\partial_z\mathcal{V}(Q,z)\partial_z\mathcal{V}(Q',z),$$
$$B_0^{\mu\nu}(\epsilon,\epsilon') \equiv \epsilon^\mu\epsilon'^\nu,$$
$$B_1^{\mu\nu}(q,q',\epsilon,\epsilon') \equiv \epsilon\cdot\epsilon' q^\mu q'^\nu - q\cdot\epsilon'\epsilon^\mu q'^\nu - q'\cdot\epsilon q^\mu\epsilon'^\nu + q\cdot q'\epsilon^\mu\epsilon'^\nu, \tag{D8}$$

with $B_{1,0} = \eta_{\mu\nu}B_{1,0}^{\mu\nu}$, $K = \eta_{\mu\nu}K^{\mu\nu}$, and the non-normalizable wave function for the virtual photon $\mathcal{V}(Q,z)$ given in (A4).

2. Scattering amplitude

The t channel Compton exchange of a spin-2 glueball of mass m_n in AdS reads

$$i\mathcal{A}^h_{Lp\to Lp}(s,t) = \sum_n i\tilde{\mathcal{A}}^h_{Lp\to Lp}(m_n,s,t),$$
$$i\tilde{\mathcal{A}}^h_{Lp\to Lp}(m_n,s,t) = (-i)V^{\mu\nu(TT)}_{hLL}(q,q',k,m_n)\times\tilde{G}^{TT}_{\mu\nu\alpha\beta}(m_n,t)\times(-i)V^{\alpha\beta(TT)}_{h\bar{\Psi}\Psi}(p_1,p_2,k,m_n), \tag{D9}$$

with the bulk vertices ($k = p_2 - p_1 = q - q'$)

$$V^{\mu\nu(TT)}_{hLL}(q,q',k,m_n) \equiv \left(\frac{\delta S^k_{hLL}}{\delta(\epsilon^{TT}_{\mu\nu}h(k,z))}\right)J_h(m_n,z) = \sqrt{2\kappa^2}\times\frac{1}{2}\int dz\sqrt{g}e^{-\phi}z^4K^{\mu\nu}(q,q',\epsilon,\epsilon',z)J_h(m_n,z),$$
$$V^{\alpha\beta(TT)}_{h\bar{\Psi}\Psi}(p_1,p_2,k,m_n) \equiv \left(\frac{\delta S^k_{h\bar{\Psi}\Psi}}{\delta(\epsilon^{TT}_{\alpha\beta}h(k,z))}\right)J_h(m_n,z) = -\sqrt{2\kappa^2}\times\int dz\sqrt{g}e^{-\phi}z\bar{\Psi}(p_2,z)\gamma^\alpha p^\beta\Psi(p_1,z)J_h(m_n,z), \tag{D10}$$

with $p = (p_1+p_2)/2$. The bulk-to-bulk transverse and traceless graviton propagator $G_{\mu\nu\alpha\beta} = G^{TT}_{\mu\nu\alpha\beta}$ for the 2^{++} glueball is [36,37]

$$G^{TT}_{\mu\nu\alpha\beta}(m_n,t,z,z') = J_h(m_n,z)\tilde{G}^{TT}_{\mu\nu\alpha\beta}(m_n,t)J_h(m_n,z'),$$
$$\tilde{G}^{TT}_{\mu\nu\alpha\beta}(m_n,t) = \frac{1}{2}\left(\mathcal{T}_{\mu\alpha}\mathcal{T}_{\nu\beta} + \mathcal{T}_{\mu\beta}\mathcal{T}_{\nu\alpha} - \frac{2}{3}\mathcal{T}_{\mu\nu}\mathcal{T}_{\alpha\beta}\right)\frac{i}{t-m_n^2+i\epsilon},$$

with

$$\mathcal{T}_{\mu\nu} = -\eta_{\mu\nu} + k_\mu k_\nu/m_n^2,$$
$$J_h(m_n,z) \equiv \psi_n(z) = c_n z^4 L_n^{\Delta(j)-2}(2\xi), \tag{D11}$$

and

$$c_n = \left(\frac{2^4\tilde{\kappa}_N^6\Gamma(n+1)}{\Gamma(n+3)}\right)^{\frac{1}{2}}, \tag{D12}$$

normalized according to

$$\int dz\sqrt{g}e^{-\phi}|g^{xx}|\psi_n(z)\psi_m(z) = \delta_{nm}. \tag{D13}$$

For $z'\to 0$, we can simplify (D9) as ($t = -K^2$),

$$i\mathcal{A}^h_{Lp\to Lp}(s,t) \approx (-i)\mathcal{V}^{\mu\nu(TT)}_{hLL}(q_1,q_2,k_z)\times\left(\frac{i}{2}\eta_{\mu\alpha}\eta_{\nu\beta}\right)\times(-i)\mathcal{V}^{\alpha\beta(TT)}_{h\bar{\Psi}\Psi}(p_1,p_2,k_z), \tag{D14}$$

with

$$\mathcal{V}^{\mu\nu(TT)}_{hLL}(q_1,q_2,k_z)=\sqrt{2\kappa^2}\times\frac{1}{2}\int dz\sqrt{g}e^{-\phi}z^4K^{\mu\nu}(q,q',\epsilon,\epsilon',z)\frac{z^4}{4},$$
$$\mathcal{V}^{\alpha\beta(TT)}_{h\bar{\Psi}\Psi}(p_1,p_2,k_z)=-\sqrt{2\kappa^2}\times\int dz\sqrt{g}e^{-\phi}z\bar{\Psi}(p_2,z)\gamma^\mu p^\nu\Psi(p_1,z)\mathcal{H}(K,z), \tag{D15}$$

where

$$\begin{aligned}\mathcal{H}(K,z)&=\sum_n\frac{\sqrt{2}\kappa F_n\psi_n(z')}{K^2+m_n^2},\\&=4z^4\Gamma(a_K+2)U(a_K+2,3;2\xi)=\Gamma(a_K+2)U(a_K,-1;2\xi),\\&=\frac{\Gamma(a_K+2)}{\Gamma(a_K)}\int_0^1dx\,x^{a_K-1}(1-x)\exp\left(-\frac{x}{1-x}(2\xi)\right),\end{aligned} \tag{D16}$$

with $a_K=a/2=K^2/8\tilde{\kappa}_N^2$,

$$F_n=\frac{1}{\sqrt{2}\kappa}\left(-\frac{1}{z'^3}\partial_{z'}\psi_n(z')\right)_{z'=\epsilon}=-\frac{4}{\sqrt{2}\kappa}c_nL_n^2(0), \tag{D17}$$

We have used the transformation $U(m,n;y)=y^{1-n}U(1+m-n,2-n,y)$ in the second line of (D16).

3. High energy limit

In the high energy limit $\sqrt{\lambda}/\tilde{\tau}\to 0$ with $\tilde{\tau}\equiv\log\tilde{s}=\log[s/\tilde{\kappa}_N^2]$, the single Pomeron (or spin-j glueballs) contribution to the Compton scattering amplitude has been evaluated in [24], with the result

$$\mathcal{A}^{\rm tot}_{Lp\to Lp}(s,t)\simeq e^{j_0\tilde{\tau}}[(\sqrt{\lambda}/\pi)+i](\sqrt{\lambda}/2\pi)^{1/2}\tilde{\xi}\frac{e^{-\sqrt{\lambda}\tilde{\xi}^2/2\tilde{\tau}}}{\tilde{\tau}^{3/2}}\left(1+\mathcal{O}\left(\frac{\sqrt{\lambda}}{\tilde{\tau}}\right)\right)\times G_5(j_0,s,t,Q) \tag{D18}$$

with $\tilde{\xi}-\pi/2=\gamma=0.55772.....$ is Euler-Mascheroni constant, and

$$\begin{aligned}G_5(j_0,s,t,Q)=&\left(\frac{\tilde{\kappa}_N}{\tilde{\kappa}_V}\right)^{4-\Delta(j)+j-2}\\&\times\frac{1}{s^2}\left(\frac{1}{2}\tilde{\kappa}_V^{4-\Delta(j)+j-2}\Gamma(\Delta(j)-2)(\mathcal{V}^T_{hLL}(j,Q,Q')\times B_1^{\alpha\beta}-\mathcal{V}^L_{hLL}(j,Q,Q')\times B_0^{\alpha\beta})\right.\\&\left.\times\frac{\sqrt{2\kappa^2}}{g_5^2}\times\tilde{\kappa}_N^{j-2+\Delta(j)}A(j,K)\bar{u}(p_2)\gamma_\alpha p_\beta u(p_1)\right)\Big|_{j\to j_0,\Delta(j)\to 2},\end{aligned} \tag{D19}$$

with, $Qz=\xi$,

$$\begin{aligned}\mathcal{V}^T_{hLL}(j,Q,Q')&=\frac{\sqrt{2\kappa^2}}{2}\int_0^\infty dz\sqrt{g}e^{-z^2\tilde{\kappa}_V^2}z^{4+2(j-2)}\times\mathcal{V}(Q,z)\times\mathcal{V}(Q',z)\times C(j)\times z^{\Delta(j)-(j-2)},\\&=Q^{4-(j+\Delta(j))}\times\frac{\sqrt{2\kappa^2}}{2}\int_0^\infty d\xi e^{-\xi^2\frac{\tilde{\kappa}_V^2}{Q^2}}\xi^{4+2(j-2)}\times\mathcal{V}(\xi)\times\mathcal{V}(\xi Q'/Q)\times C(j)\times\xi^{\Delta(j)-(j-2)},\\\mathcal{V}^L_{hLL}(j,Q,Q')&=\frac{\sqrt{2\kappa^2}}{2}\int_0^\infty dz\sqrt{g}e^{-z^2\tilde{\kappa}_V^2}z^{4+2(j-2)}\times\partial_z\mathcal{V}(Q,z)\times\partial_z\mathcal{V}(Q',z)\times C(j)\times z^{\Delta(j)-(j-2)},\\&=Q^{6-(j+\Delta(j))}\times\frac{\sqrt{2\kappa^2}}{2}\int_0^\infty d\xi e^{-\xi^2\frac{\tilde{\kappa}_V^2}{Q^2}}\xi^{4+2(j-2)}\times\partial_\xi\mathcal{V}(\xi)\times\partial_\xi\mathcal{V}(\xi Q'/Q)\times C(j)\times\xi^{\Delta(j)-(j-2)},\end{aligned} \tag{D20}$$

and

$$A(j,K)=\frac{\tilde{\kappa}_N^{-(j-2)-\Delta(j)}}{2}\frac{\Gamma(c)\Gamma(1-\tilde{b}+c)}{\Gamma(1-\tilde{b}+c+\tilde{a})}\times\left(\left(\frac{\tilde{n}_R}{\tilde{\kappa}_N^{\tau-1}}\right)^2{}_2F_1(\tilde{a},c+1,1-\tilde{b}+c+\tilde{a},-1)+\left(\frac{\tilde{n}_L}{\tilde{\kappa}_N^{\tau}}\right)^2\frac{c(1-\tilde{b}+c)}{1-\tilde{b}+c+\tilde{a}}{}_2F_1(\tilde{a}+1,c+1,2-\tilde{b}+c+\tilde{a},-1)\right). \tag{D21}$$

The parameters are fixed as

$$\begin{aligned}1-\tilde{b}+c&=(\tau-1)+\frac{j-2}{2}+\frac{\Delta(j)}{2},\\ 1-\tilde{b}+c+\tilde{a}&=(\tau+1)+\frac{j-2}{2}+a_K,\\ c&=(\tau+1)+\frac{j-2}{2}-\frac{\Delta(j)}{2},\\ \tilde{n}_R&=\tilde{n}_L\tilde{\kappa}_N^{-1}\sqrt{\tau-1},\qquad \tilde{n}_L=\tilde{\kappa}_N^{\tau}\sqrt{2/\Gamma(\tau)},\end{aligned} \tag{D22}$$

and

$$\begin{aligned}C(j)&=\tilde{\kappa}_V^{2\Delta(j)-4}\times\frac{1}{\Delta(j)}\frac{2^{\Delta(j)-2}\Gamma(a_K+\frac{\Delta(j)}{2})}{\Gamma(\Delta(j)-2)},\\ \Delta(j)&=2+\sqrt{2\sqrt{\lambda}(j-j_0)}\quad\text{and}\quad a_K=\frac{a}{2}=\frac{K^2}{8\tilde{\kappa}^2}\quad\text{and}\quad j_0=2-\frac{2}{\sqrt{\lambda}}.\end{aligned} \tag{D23}$$

We can rewrite $G_5(j_0,s,t,Q,Q')$ of (D19) more compactly as

$$G_5(j_0,s,t,Q,Q')=\frac{2\kappa^2}{g_5^2}\times\left(\frac{Q}{\tilde{\kappa}}\right)^{2-(j+\Delta(j))}\times\frac{1}{s^2}\mathcal{F}(j,K)(I_\xi^T(j,Q,Q')\times B_1^{\alpha\beta}p_\alpha p_\beta-I_\xi^L(j,Q,Q')\times B_0^{\alpha\beta}p_\alpha p_\beta Q^2)|_{j\to j_0,\Delta(j)\to 2}, \tag{D24}$$

where we have set $\tilde{\kappa}_V=\tilde{\kappa}_N=\tilde{\kappa}$, and defined the dimensionless functions

$$\begin{aligned}\mathcal{F}(j,K)&\equiv\tilde{\kappa}^{j+2-\Delta(j)}\times\Gamma(\Delta(j)-2)\times C(j,K)\times A(j,K),\\ I_\xi^T(j,Q,Q')&\equiv\frac{1}{2}\int_0^\infty d\xi\, e^{-\xi^2\frac{\tilde{\kappa}_V^2}{Q^2}}\xi^{\Delta(j)+j+2}\times\mathcal{V}(\xi)\times\mathcal{V}(\xi Q'/Q),\\ &\approx\frac{1}{2}\times 2^{\Delta(j)+j+2}\frac{Q'}{Q}G^{2,2}_{2,2}\left(\frac{Q^2}{Q'^2}\middle|\begin{matrix}\frac{1}{2},\frac{3}{2}\\ \frac{1}{2}(j+\Delta(j)+4),\frac{1}{2}(j+\Delta(j)+6)\end{matrix}\right),\\ I_\xi^L(j,Q,Q')&\equiv\frac{1}{2}\int_0^\infty d\xi e^{-\xi^2\frac{\tilde{\kappa}_V^2}{Q^2}}\xi^{\Delta(j)+j+2}\times\partial_\xi\mathcal{V}(\xi)\times\partial_\xi\mathcal{V}(\xi Q'/Q),\\ &\approx\frac{1}{2}\times 2^{\Delta(j)+j+2}\frac{Q'^2}{Q^2}G^{2,2}_{2,2}\left(\frac{Q^2}{Q'^2}\middle|\begin{matrix}1,1\\ \frac{1}{2}(j+\Delta(j)+5),\frac{1}{2}(j+\Delta(j)+5)\end{matrix}\right),\end{aligned} \tag{D25}$$

using the identities (C22).

We can also rewrite the amplitude (D18) as

$$\mathcal{A}^{\rm tot}_{Lp\to Lp}(s,t) \simeq \frac{2\kappa^2}{g_5^2}\times\left(\frac{Q}{\tilde\kappa}\right)^{2+2/\sqrt{\lambda}}\times\left(\frac{s}{\tilde\kappa^2}\right)^{-2/\sqrt{\lambda}}\times\frac{e^{-\sqrt{\lambda}\tilde\xi^2/2\log[s/\tilde\kappa^2]}}{(\log[s/\tilde\kappa^2])^{3/2}} \times[(\sqrt{\lambda}/\pi)+i]\times(\sqrt{\lambda}/2\pi)^{1/2}\tilde\xi\left(1+\mathcal{O}\left(\frac{\sqrt{\lambda}}{\log[s/\tilde\kappa^2]}\right)\right)\times\tilde G_5(j_0,t,Q,Q') \tag{D26}$$

where we have explicitly used $\tilde\tau=\log[s/\tilde\kappa^2]$, $j_0=2-\frac{2}{\sqrt{\lambda}}$, $\Delta(j_0)=2$, $\tilde\xi-\pi/2=\gamma=0.55772\ldots..$ is a Euler-Mascheroni constant, and defined

$$\tilde G_5(j_0,s,t,Q,Q')\equiv\frac{1}{Q^4}\times\frac{g_5^2}{2\kappa^2}\times\left(\frac{\tilde\kappa}{Q}\right)^{2-(j_0+\Delta(j_0))}\times s^2\times G_5(j_0,s,t,Q,Q') \tag{D27}$$

For small x, we have $s\simeq Q^2/x$, we can rewrite the amplitude (D26) in terms of x as

$$\mathcal{A}^{\rm tot}_{Lp\to Lp}(x,Q,t) \simeq \frac{1}{2}\times\frac{2\kappa^2}{g_5^2}\times\left(\frac{Q}{\tilde\kappa}\right)^{2-2/\sqrt{\lambda}}\times\left(\frac{1}{x}\right)^{1-2/\sqrt{\lambda}}\times\frac{e^{-\sqrt{\lambda}\tilde\xi^2/2(\log[Q^2/\tilde\kappa^2]+\log[1/x])}}{(\log[Q^2/\tilde\kappa^2]+\log[1/x])^{3/2}} \times[(\sqrt{\lambda}/\pi)+i]\times(\sqrt{\lambda}/2\pi)^{1/2}\tilde\xi\left(1+\mathcal{O}\left(\frac{\sqrt{\lambda}}{\log[Q^2/\tilde\kappa^2]+\log[1/x]}\right)\right)\times\tilde{\tilde G}_5(j_0,x,t,Q,Q'), \tag{D28}$$

where we have defined $\tilde{\tilde G}_5(j_0,x,t,Q,Q')\equiv 2x\tilde G_5(j_0,s,t,Q,Q')$ with $(\epsilon\cdot q=0)$

$$\tilde{\tilde G}_5(j_0,x,t,Q,Q')=\mathcal{F}(j,K)\left(I^T_\xi(j,Q,Q')\times\left(\frac{1}{2x}\epsilon^2-\frac{2x}{Q^2}(\epsilon\cdot p)^2\right)-I^L_\xi(j,Q,Q')\times\frac{2x}{Q^2}(\epsilon\cdot p)^2\right)\Big|_{j\to j_0,\Delta(j)\to 2}, \tag{D29}$$

APPENDIX E: OPERATOR PRODUCT EXPANSION

The parton model emerges in QCD through a leading twist contribution to the structure functions. The twist expansion follows from the OPE of the JJ currents. We now illustrate this expansion to leading order for the charged current contributions in T-ordered product in (4.2). Specifically, we have as $x\to 0$

$$T^*(J^{W^-}_\mu(x)J^{W^+}_\nu(0))\approx e_W^2\left(\bar q(x)T^-T^+\gamma_\mu\frac{1}{2}(1-\gamma_5)S(x)\gamma_\nu\frac{1}{2}(1-\gamma_5)q(0)+\bar q(0)T^+T^-\gamma_\nu\frac{1}{2}(1-\gamma_5)S(-x)\gamma_\mu\frac{1}{2}(1-\gamma_5)q(x)\right), \tag{E1}$$

with $S(x)=2i\gamma\cdot x/(2\pi x^2)^2$. With the help of the identity

$$\gamma_\mu\gamma\cdot x\gamma_\nu=(S_{\mu\nu\alpha\beta}+i\epsilon_{\mu\nu\alpha\beta}\gamma_5)x^\alpha\gamma^\beta, \tag{E2}$$

with the symmetric tensor

$$S_{\mu\nu\alpha\beta}=\eta_{\mu\alpha}\eta_{\nu\beta}+\eta_{\mu\beta}\eta\nu\alpha-\eta_{\mu\nu}\eta_{\alpha\beta}, \tag{E3}$$

in (E1), the short distance contribution to the T-ordered product in (4.2) is

$$T^{-+}_{\mu\nu}\approx 2e_W^2\frac{q^\alpha}{q^2}\langle P|(S_{\mu\nu\alpha\beta}\bar q(0)\tau^3\gamma^\beta(1-\gamma_5)q(0)-i\epsilon_{\mu\nu\alpha\beta}\bar q(0)\gamma^\beta(1-\gamma_5)q(0))|P\rangle. \tag{E4}$$

For unpolarized scattering, a comparison of (E4) to (4.2) suggests that the parity odd structure function F_3 can be identified with the antisymmetric tensor contribution,

$$F_3(x,Q^2)P^\beta \approx (2e_W)^2 \mathrm{Im}\left(\frac{1}{x}\langle P|\bar{q}\gamma^\beta(1-\gamma_5)q|P\rangle\right), \tag{E5}$$

(E5) is suggestive of a $j=1$ exchange through the left singlet current, since $s^{j=1} \leftrightarrow 1/x$.

Although the twist-2 contribution to the OPE is real, it provides the relevant starting point for the Reggeization by summing over higher spin-j states in holography [22]. For that, we first note that the holographic dual of the singlet current form factor is

$$\begin{aligned}\langle P_X|\bar{q}\gamma^\beta(1-\gamma_5)q|P\rangle &= [e_N\bar{u}_N(P_X)\gamma^\beta(1-\gamma^5)u_N(P)] \\ &\times \int dz\sqrt{g}e^{-\phi}\mathcal{V}(Q,z)\frac{z}{R}\left[\frac{1}{2}\left(\frac{z^2}{R^2}\right)^2\tilde{f}_L^{n_x}(z)\tilde{f}_L^0(z)+\frac{1}{2}\left(\frac{z^2}{R^2}\right)^2\tilde{f}_R^{n_x}(z)\tilde{f}_R^0(z)\right].\end{aligned} \tag{E6}$$

The bulk-to-boundary propagator $\mathcal{V}(Q,z')$ relates to the bulk-to-bulk propagator $G(Q,z,z')$ through

$$\lim_{z\to 0}\frac{2}{z'^2}G_1(Q,z',z)=\mathcal{V}(Q,z). \tag{E7}$$

Using (E7) into (E6) gives

$$\begin{aligned}\langle P_X|\bar{q}\gamma^\beta(1-\gamma_5)q|P\rangle &= [e_N\bar{u}_N(P_X)\gamma^\beta(1-\gamma^5)u_N(P)] \\ &\times \lim_{z'\to 0}\frac{2}{z'^2}\int dz\sqrt{g}e^{-\phi}G_1(Q,z',z) \\ &\times \frac{z}{R}\left[\frac{1}{2}\left(\frac{z^2}{R^2}\right)^2\tilde{f}_L^{n_x}(z)\tilde{f}_L^0(z)+\frac{1}{2}\left(\frac{z^2}{R^2}\right)^2\tilde{f}_R^{n_x}(z)\tilde{f}_R^0(z)\right].\end{aligned} \tag{E8}$$

1. Hard wall

For the hard wall model with $\phi=0$, the bulk-to-bulk propagator can be readily constructed

$$G_1(Q,z',z)=zz'(I_0(Qz_0)K_1(Qz_>)+K_0(Qz_0)I_1(Qz_>))\frac{I_1(Qz_<)}{I_0(Qz_0)} \tag{E9}$$

and (E7) explicitly checked. However, for the Reggeization it is more useful to recall that the bulk-to-bulk propagator for the $U_L(1)$ vector field, obeys the Green's equation in warped space ($Q^2=-q^2$)

$$((\Delta_{j=1}-z^2Q^2+m_{j=1}^2)=(-z^2(\partial_z^2+Q^2)+z\partial_z))G_{j=1}(Q,z',z)=\frac{\delta(z-z')}{\sqrt{g}}, \tag{E10}$$

with $m_{j=1}^2=-3$. Using the open-string Regge trajectory

$$j=1+\alpha'(m_j^2-m_1^2) \quad \text{with} \quad \alpha'=l_s^2=1/\sqrt{\lambda} \tag{E11}$$

(E10) generalizes to spin j

$$(\Delta_j-z^2Q^2+m_j^2)G_j(Q,z',z)=\frac{\delta(z-z')}{\sqrt{g}} \tag{E12}$$

with the recursive relation for the warped Laplacian-like

$$\Delta_j=z^{1-j}\Delta_1 z^{j-1}. \tag{E13}$$

Equation (E12) can be formally inverted

$$\sqrt{g}G_j(Q,z',z)=\frac{1}{(\Delta_j-z^2Q^2+m_j^2)}\delta(z-z')=z^{2-j}\frac{1}{(\Delta_2-z^2Q^2+m_j^2)}z^{j-2}\delta(z-z'). \tag{E14}$$

Changing to the conformal variable $z^2=e^{-\rho}$, noting that $\Delta_2=-4\partial_\rho^2+4$ and using the plane-wave identity

$$z'\delta(z-z')=\left(\frac{z'}{z}\right)^{j-2}\int\frac{d\nu}{\pi}e^{i\nu(\rho-\rho')}, \tag{E15}$$

we can recast (E14) in the form

$$\sqrt{g}G_j(0,z',z)=\sqrt{g'}(g'^{xx})^j(zz')^{2-j}\int\frac{d\nu}{\pi}\frac{1}{4\nu^2+4+m_j^2}e^{i\nu(\rho-\rho')} \tag{E16}$$

for $Q=0$. The Reggeized form of the spin-j and twist-2 extension of (E8) is

$$\begin{aligned}\sum_j\frac{1}{x^j}\langle P|\bar{q}\gamma^\beta\partial^{j-1}(1-\gamma_5)q|P\rangle=&\int_{\mathbb{C}}\frac{dj}{4i}\frac{1-e^{-i\pi j}}{\sin\pi j}\frac{1}{x^j}[e_N\bar{u}_N(P)\gamma^\beta\partial^{j-1}(1-\gamma^5)u_N(P)]\\&\times\lim_{z'\to0}\frac{2}{z'^2}\int dz\sqrt{g'}(g'^{xx})^j(zz')^{2-j}\int\frac{d\nu}{\pi}\frac{1}{4\nu^2+1+\sqrt{\lambda}(j-1)}e^{i\nu(\rho-\rho')}\frac{z}{R}\\&\times\left[\frac{1}{2}\psi_L^2(z)+\frac{1}{2}\psi_R^2(z)\right]\end{aligned} \tag{E17}$$

using the open string Regge trajectory (E11) in the forward limit ($Q=0$). Here $\psi_L(z)$ is the lowest left-chirality bulk fermionic wave function for the hard wall. The contour $\mathbb{C}$ is to the leftmost of the poles $j=1,3,\ldots$ and to the right of the pole $j_0=1-1/\sqrt{\lambda}$. Undoing the contour integration $\mathbb{C}$ by closing to the left and picking the single pole j_0, and then performing the ν integration yield

$$\begin{aligned}\mathrm{Im}\sum_j^{\mathrm{odd}}\frac{1}{x^j}\langle P|\bar{q}\gamma^\beta\partial^{j-1}(1-\gamma_5)q|P\rangle=&\frac{1}{x^{j_0}}[e_N\bar{u}_N(P)\gamma^\beta\partial^{j_0-1}(1-\gamma^5)u_N(P)]\\&\times\frac{\pi}{2\sqrt{\lambda}}\lim_{z'\to0}\frac{2}{z'^2}\int dz\sqrt{g'}(g'^{xx})^{j_L}(zz')^{2-j_0}\frac{e^{-(\rho-\rho')/4D\chi}}{\sqrt{\pi D\chi}}\frac{z}{R}\left[\frac{1}{2}\psi_L^2(z)+\frac{1}{2}\psi_R^2(z)\right].\end{aligned} \tag{E18}$$

The Gribov time is $\chi=\ln(1/x)$ and the diffusion constant of the Reggeon is $D=4/\sqrt{\lambda}$. Equation (E18) fixes the odd structure function in (E5) in the forward direction using this semiquantitative OPE argument,

$$F_3(0,x)\approx\frac{1}{x^{j_0}}\approx\frac{1}{x^{1-1/\sqrt{\lambda}}}. \tag{E19}$$

2. Soft wall

For the soft-wall model, the Reggeized current form factor is given by

$$\begin{aligned}&\sum_j^{\mathrm{odd}}\frac{1}{x^j}\langle P|\bar{q}\gamma^\beta\partial^{j-1}(1-\gamma_5)q|P\rangle\\&=-x^{j_0}\int_{-\infty}^{j_0}\frac{dj}{\pi}\left(\frac{1+e^{-i\pi}}{\sin\pi j}\right)x^{j-j_0}\mathrm{Im}\left[2\times\frac{2}{3}\times\tilde{\kappa}^{(j-1)+\Delta(j)+1}\times\frac{\Gamma(\Delta(j)-2+a)}{\Gamma(\Delta(j)-2)}\times\frac{1}{g_5}\times\mathcal{V}^\beta_{L\bar{\Psi}\Psi}(p_1=p_2=p,k_z=0)\right]\\&=-x^{j_0}\int_{-\infty}^{j_0}\frac{dj}{\pi}\left(\frac{1+e^{-i\pi}}{\sin\pi j}\right)x^{j-j_0}\mathrm{Im}\left[2\times\frac{2}{3}\times\tilde{\kappa}^{(j-1)+\Delta(j)+1}\times\frac{\Gamma(\Delta(j)-2+a)}{\Gamma(\Delta(j)-2)}\times\frac{1}{g_5}\times g_5F_1^{(LN)}(j,K=0)\times\bar{u}(p)\gamma^\beta u(p)\right],\end{aligned} \tag{E20}$$

where $\mathcal{V}^{\beta}_{L\bar{\Psi}\Psi}(p_1,p_2,k_z)$ is given by (C19), and $F_1^{(LN)}(j,K)$ is given by (C23). Note that the bracket

$$\left[2\times\frac{2}{3}\times\tilde{\kappa}^{(j-1)+\Delta(j)+1}\times\frac{\Gamma(\Delta(j)-2+a)}{\Gamma(\Delta(j)-2)}\times\frac{1}{g_5}\times g_5F_1^{(LN)}(j,K)\right] \tag{E21}$$

is the spin-j form factor which reduces to the spin-1 form factor for $j=1$, for the current operator $2\times\tilde{J}^{\beta}_L(0)=\bar{q}\gamma^{\beta}(1-\gamma_5)q$ sourced by $\frac{1}{2}\times\frac{3}{2}\times L^0_{\beta}(K,z\to 0)$ at the boundary. Also note that the momentum transfer is $k_z\equiv q_z$ and that $-k^2=K^2\equiv Q^2$ with $a=K^2/4\tilde{\kappa}^2\equiv Q^2/4\tilde{\kappa}^2$. The momentum of the incoming nucleon is $p_1=p$, and the momentum of the outgoing nucleon is $p_2=p$, with $k=p_2-p_1\equiv q$.

Following the reasoning in Appendix C, we can evaluate the integral in (E20) with the result

$$\mathrm{Im}\sum_j^{\mathrm{odd}}\frac{1}{x^j}\langle P|\bar{q}\gamma^{\beta}\partial^{j-1}(1-\gamma_5)q|P\rangle\simeq e^{j_0\tau_x}[0\times(\sqrt{\lambda}/\pi)+i/i](\sqrt{\lambda}/2\pi)^{1/2}\tilde{\xi}\frac{e^{-\sqrt{\lambda}\tilde{\xi}^2/2\tau_x}}{\tau_x^{3/2}}\left(1+\mathcal{O}\left(\frac{\sqrt{\lambda}}{\tau_x}\right)\right)\times\mathcal{G}_5(j_0,x,Q=0), \tag{E22}$$

with

$$\mathcal{G}_5(j_0,x,Q=0)=\left(\Gamma(\Delta(j)-2)\times 2\times\frac{2}{3}\times\tilde{\kappa}^{(j-1)+\Delta(j)+1}\times\frac{\Gamma(\Delta(j)-2+a)}{\Gamma(\Delta(j)-2)}\times\frac{1}{g_5}\times g_5F_1^{(LN)}(j,Q)\times 2P^{\beta}\right)\Big|_{j\to j_0,\Delta(j)\to 2,Q\to 0}. \tag{E23}$$

Again, $j_0=1-\frac{1}{\sqrt{\lambda}}$, $\tau_x=\log[1/x]$, $\bar{u}(p)\gamma^{\beta}u(p)=2p^{\beta}=2P^{\beta}$, and $\tilde{\xi}-\pi/2=\gamma=0.55772\ldots..$ is the Euler-Mascheroni constant. Finally, comparing (E22) to (E5), we find

$$F_3(0,x)\approx\frac{1}{x^{1-1/\sqrt{\lambda}}}\times(\sqrt{\lambda}/2\pi)^{1/2}\tilde{\xi}\frac{e^{-\sqrt{\lambda}\tilde{\xi}^2/2\tau_x}}{\tau_x^{3/2}}\left(1+\mathcal{O}\left(\frac{\sqrt{\lambda}}{\tau_x}\right)\right)\times\tilde{\mathcal{G}}_5(j_0,x,0), \tag{E24}$$

with

$$\tilde{\mathcal{G}}_5(j_0,x,0)=\left(\Gamma(\Delta(j)-2)\times 2\times\frac{2}{3}\times\tilde{\kappa}^{(j-1)+\Delta(j)+1}\times\frac{\Gamma(\Delta(j)-2+a)}{\Gamma(\Delta(j)-2)}\times\frac{1}{g_5}\times g_5F_1^{(LN)}(j,Q)\right)\Big|_{j\to j_0,\Delta(j)\to 2,Q\to 0}. \tag{E25}$$

APPENDIX F: TRACE OF GAMMA MATRICES

Note that the Dirac traces do not depend on the specific form of the $\gamma^0,\gamma^1,\gamma^2,\gamma^3$ matrices but are completely determined by the Clifford algebra

$$\{\gamma^{\mu},\gamma^{\nu}\}\equiv\gamma^{\mu}\gamma^{\nu}+\gamma^{\nu}\gamma^{\mu}=2\eta^{\mu\nu}, \tag{F1}$$

and some useful identities for carrying some of the Dirac traces of gamma matrices above, are given by (note that $\gamma^5=i\gamma^0\gamma^1\gamma^2\gamma^3$ and it satisfies $\gamma^5\gamma^{\mu}=-\gamma^{\mu}\gamma^5$)

$$\mathrm{tr}(\gamma^{\mu}\gamma^{\nu})=4\eta^{\mu\nu}, \tag{F2}$$

$$\mathrm{tr}(\gamma^{\mu}\gamma^{\nu}\gamma^5)=0, \tag{F3}$$

$$\mathrm{tr}(\gamma^{\alpha}\gamma^{\mu}\gamma^{\beta}\gamma^{\nu})=4\eta^{\alpha\mu}\eta^{\beta\nu}-4\eta^{\alpha\beta}\eta^{\mu\nu}+4\eta^{\alpha\nu}\eta^{\mu\beta}, \tag{F4}$$

$$\mathrm{tr}(\gamma^{\alpha}\gamma^{\mu}\gamma^{\beta}\gamma^{\nu}\gamma^5)=-4i\epsilon^{\alpha\mu\beta\nu}, \tag{F5}$$

$$\begin{aligned}\mathrm{tr}(\gamma^\alpha\gamma^\mu\gamma^{\tilde{\nu}}\gamma^\beta\gamma^{\tilde{\mu}}\gamma^\nu) &= 4\eta^{\alpha\mu}\times(\eta^{\tilde{\nu}\beta}\eta^{\tilde{\mu}\nu}-\eta^{\tilde{\nu}\,\tilde{\mu}}\eta^{\beta\nu}+\eta^{\tilde{\nu}\nu}\eta^{\beta\tilde{\mu}})-4\eta^{\alpha\tilde{\nu}}\times(\eta^{\mu\beta}\eta^{\tilde{\mu}\nu}-\eta^{\mu\tilde{\mu}}\eta^{\beta\nu}+\eta^{\mu\nu}\eta^{\beta\tilde{\mu}})\\ &+4\eta^{\alpha\beta}\times(\eta^{\mu\tilde{\nu}}\eta^{\tilde{\mu}\nu}-\eta^{\mu\tilde{\mu}}\eta^{\tilde{\nu}\nu}+\eta^{\mu\nu}\eta^{\tilde{\nu}\,\tilde{\mu}})-4\eta^{\alpha\tilde{\mu}}\times(\eta^{\mu\tilde{\nu}}\eta^{\beta\nu}-\eta^{\mu\beta}\eta^{\tilde{\nu}\nu}+\eta^{\mu\nu}\eta^{\tilde{\nu}\beta})\\ &+4\eta^{\alpha\nu}\times(\eta^{\mu\tilde{\nu}}\eta^{\beta\tilde{\mu}}-\eta^{\mu\beta}\eta^{\tilde{\nu}\,\tilde{\mu}}+\eta^{\mu\tilde{\mu}}\eta^{\tilde{\nu}\beta}),\end{aligned}\tag{F6}$$

$$\mathrm{tr}(\gamma^\alpha\gamma^\mu\gamma^{\tilde{\nu}}\gamma^\beta\gamma^{\tilde{\mu}}\gamma^\nu\gamma^5) = -4i(\eta^{\alpha\mu}\epsilon^{\tilde{\nu}\beta\tilde{\mu}\nu}-\eta^{\alpha\tilde{\nu}}\epsilon^{\mu\beta\tilde{\mu}\nu}+\eta^{\tilde{\nu}\mu}\epsilon^{\alpha\beta\tilde{\mu}\nu}-\eta^{\tilde{\mu}\nu}\epsilon^{\beta\alpha\mu\tilde{\nu}}+\eta^{\beta\nu}\epsilon^{\tilde{\mu}\alpha\mu\tilde{\nu}}-\eta^{\beta\tilde{\mu}}\epsilon^{\nu\alpha\mu\tilde{\nu}}),\tag{F7}$$

and

$$\begin{aligned}\mathrm{tr}(\gamma^{\nu_1}\cdots\gamma^{\nu_n}\gamma^5) &= 0 \quad \forall\ \text{odd } n,\\ \mathrm{tr}(\gamma^{\nu_1}\cdots\gamma^{\nu_n}) &= 0 \quad \forall\ \text{odd } n.\end{aligned}\tag{F8}$$

[1] C. Adloff *et al.* (H1 Collaboration), Eur. Phys. J. C **13**, 609 (2000); Phys. Lett. B **520**, 183 (2001); Eur. Phys. J. C **21**, 33 (2001).

[2] S. Chekanov *et al.* (ZEUS Collaboration), Eur. Phys. J. C **21**, 443 (2001).

[3] K. J. Golec-Biernat and M. Wusthoff, Phys. Rev. D **59**, 014017 (1998).

[4] I. Balitsky, Nucl. Phys. **B463**, 99 (1996); Y. V. Kovchegov, Phys. Rev. D **60**, 034008 (1999).

[5] J. Polchinski and M. J. Strassler, J. High Energy Phys. 05 (2003) 012.

[6] S. J. Brodsky and G. R. Farrar, Phys. Rev. Lett. **31**, 1153 (1973).

[7] Y. Hatta, E. Iancu, and A. H. Mueller, J. High Energy Phys. 01 (2008) 063.

[8] K. A. Mamo and I. Zahed, Phys. Rev. D **100**, 046015 (2019); **101**, 066014 (2020).

[9] J. Hirn and V. Sanz, J. High Energy Phys. 12 (2005) 030.

[10] S. K. Domokos, H. R. Grigoryan, and J. A. Harvey, Phys. Rev. D **80**, 115018 (2009).

[11] A. Cherman, T. D. Cohen, and E. S. Werbos, Phys. Rev. C **79**, 045203 (2009).

[12] D. K. Hong, T. Inami, and H. U. Yee, Phys. Lett. B **646**, 165 (2007).

[13] T. Gutsche, V. E. Lyubovitskij, I. Schmidt, and A. Vega, Phys. Rev. D **86**, 036007 (2012).

[14] J. Erlich, E. Katz, D. T. Son, and M. A. Stephanov, Phys. Rev. Lett. **95**, 261602 (2005).

[15] T. Sakai and S. Sugimoto, Prog. Theor. Phys. **113**, 843 (2005).

[16] C. Alexandrou, M. Constantinou, K. Hadjiyiannakou, K. Jansen, C. Kallidonis, G. Koutsou, and A. V. Aviles-Casco, Phys. Rev. D **96**, 054507 (2017).

[17] N. Tsutsui *et al.* (CP-PACS and JLQCD Collaborations), Phys. Rev. D **70**, 111501 (2004).

[18] N. R. F. Braga and A. Vega, Eur. Phys. J. C **72**, 2236 (2012); C. A. Ballon Bayona, H. Boschi-Filho, and N. R. F. Braga, J. High Energy Phys. 03 (2008) 064.

[19] Z. Abidin and P. T. P. Hutauruk, Phys. Rev. D **100**, 054026 (2019).

[20] Z. Abidin and C. E. Carlson, Phys. Rev. D **79**, 115003 (2009).

[21] J. M. Conrad, M. H. Shaevitz, and T. Bolton, Rev. Mod. Phys. **70**, 1341 (1998).

[22] Y. Hatta, T. Ueda, and B. W. Xiao, J. High Energy Phys. 08 (2009) 007.

[23] N. Kovensky, G. Michalski, and M. Schvellinger, J. High Energy Phys. 10 (2018) 084.

[24] K. A. Mamo and I. Zahed, Phys. Rev. D **101**, 086003 (2020).

[25] M. Rho, S. J. Sin, and I. Zahed, Phys. Lett. B **466**, 199 (1999); G. Basar, D. E. Kharzeev, H. U. Yee, and I. Zahed, Phys. Rev. D **85**, 105005 (2012); A. Stoffers and I. Zahed, Phys. Rev. D **87**, 075023 (2013); arXiv:1210.3724; Phys. Rev. D **88**, 025038 (2013).

[26] R. A. Janik and R. B. Peschanski, Nucl. Phys. **B586**, 163 (2000).

[27] R. C. Brower, J. Polchinski, M. J. Strassler, and C. I. Tan, J. High Energy Phys. 12 (2007) 005; R. C. Brower, M. J. Strassler, and C. I. Tan, J. High Energy Phys. 03 (2009) 092; R. C. Brower, M. S. Costa, M. Djuric, T. Raben, and C. I. Tan, J. High Energy Phys. 02 (2015) 104; A. Ballon-Bayona, R. C. Quevedo, M. S. Costa, and M. Djuric, Phys. Rev. D **93**, 035005 (2016).

[28] H. Abramowicz *et al.* (H1 and ZEUS Collaborations), Eur. Phys. J. C **75**, 580 (2015).

[29] M. R. Adams *et al.* (E665 Collaboration), Phys. Rev. D **54**, 3006 (1996).

[30] L. W. Whitlow, Deep inelastic structure functions from electron scattering on hydrogen, deuterium, and iron at 0.6-GeV$^2 \leq Q^2 \leq$ 30-GeV^2, Report No. SLAC-0357.

[31] D. Jorrin, G. Michalski, and M. Schvellinger, J. High Energy Phys. 06 (2020) 063.
[32] S. D. Drell and T. Yan, Phys. Rev. Lett. **24**, 181 (1970).
[33] S. P. Malace *et al.* (Jefferson Lab E00-115 Collaboration), Phys. Rev. C **80**, 035207 (2009).
[34] E. F. Capossoli, M. A. M. Contreras, D. Li, A. Vega, and H. Boschi-Filho, Phys. Rev. D **102**, 086004 (2020).
[35] D. B. Clark, E. Godat, and F. I. Olness, Comput. Phys. Commun. **216**, 126 (2017).
[36] S. Raju, Phys. Rev. D **83**, 126002 (2011).
[37] E. D'Hoker, D. Z. Freedman, S. D. Mathur, A. Matusis, and L. Rastelli, Nucl. Phys. **B562**, 330 (1999).